

198

OAK RIDGE NATIONAL LABORATORY LIBRARY



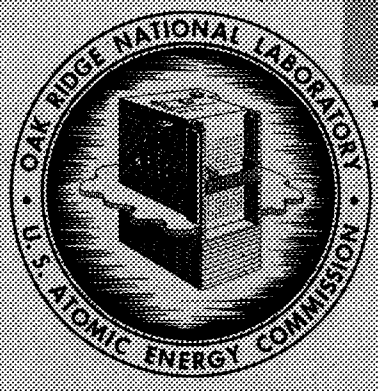
3 4456 0022561 9

CENTRAL RESEARCH LIBRARY
DOCUMENT COLLECTION

ORNL-3015
UC-81 - Reactors-Power

GAS-COOLED REACTOR PROJECT
QUARTERLY PROGRESS REPORT
FOR PERIOD ENDING SEPTEMBER 30, 1960

**CENTRAL RESEARCH LIBRARY
DOCUMENT COLLECTION
LIBRARY LOAN COPY**
DO NOT TRANSFER TO ANOTHER PERSON
If you wish someone else to see this
document, send to us with document
and the library will arrange a loan.



OAK RIDGE NATIONAL LABORATORY
operated by
UNION CARBIDE CORPORATION
for the
U.S. ATOMIC ENERGY COMMISSION

ORNL-3015

Reactors - Power
TID-4500 (15th ed.)

Contract No. W-7405-eng-26

GAS-COOLED REACTOR PROJECT
QUARTERLY PROGRESS REPORT
For Period Ending September 30, 1960

Staff
Oak Ridge National Laboratory

DATE ISSUED

NOV 7 1960

OAK RIDGE NATIONAL LABORATORY
Oak Ridge, Tennessee
operated by
UNION CARBIDE CORPORATION
for the
U. S. ATOMIC ENERGY COMMISSION



3 4456 0022561 9



CONTENTS

| | |
|---------------|-----|
| SUMMARY | vii |
|---------------|-----|

PART 1. DESIGN INVESTIGATIONS

| | |
|--|----|
| 1. REACTOR PHYSICS | 3 |
| Suggested Operating Program for EGCR Control Rods | 3 |
| Heat Deposition in the EGCR Control Rods | 11 |
| Gamma-Ray Heat Deposition in the EGCR Core | 14 |
| 2. REACTOR DESIGN STUDIES | 21 |
| EGCR Fuel Assemblies | 21 |
| Hot-Channel Factors | 21 |
| Failure Criteria | 25 |
| Fission-Gas Release | 26 |
| Pressure Drop | 31 |
| EGCR Control Rods | 32 |
| Stress Analysis of EGCR Pressure Vessel | 35 |
| Experimental Results | 35 |
| Comparison of Analytical and Experimental Results | 42 |
| 3. EXPERIMENTAL INVESTIGATIONS OF HEAT TRANSFER AND FLUID FLOW | 48 |
| Resistance-Heated-Tube Heat Transfer Experiment | 48 |
| Mass-Transfer Measurements | 53 |
| Velocity Distribution in Septafoil Channels | 63 |

PART 2. MATERIALS RESEARCH AND TESTING

| | |
|--|----|
| 4. MATERIALS DEVELOPMENT | 71 |
| Fuel and Moderator Materials Development | 71 |
| Development of UO ₂ Fabrication Processes | 71 |
| Fabrication of UO ₂ for Experimental Assemblies | 71 |
| Development of Apparatus for Bulk-Density Measurements | 71 |
| Fission-Product-Release Studies | 72 |
| Fabrication of Fueled Graphite | 74 |

| | |
|---|-----|
| Reactions of UO ₂ with Graphite | 75 |
| Determination of the Elastic Constants of AGOT Graphite | 76 |
| Mechanical Property Tests on EGCR Graphite Sleeves | 78 |
| Evaluation of Graphite Coatings | 79 |
| Evolution of Lithium from BeO | 81 |
| Fabrication of Swaged-Rod Irradiation Capsules | 81 |
| Structural Materials Evaluation | 82 |
| Reactions of Type 304 Stainless Steel with CO-CO ₂ Mixtures | 82 |
| Creep Buckling and Collapse of Stainless Steel Tubes | 83 |
| Tube-Burst Tests of Stainless Steel | 84 |
| Mechanical Properties of AISI-Type 502 Steel for EGCR Top Grid Structure | 84 |
| Studies of Pressure Vessel Steels | 86 |
| Compatibility of Molybdenum with Coolant Impurities | 87 |
| Manufacturing and Inspection Methods Development | 91 |
| Fuel Element Fabrication | 91 |
| High-Temperature Thermocouple Development | 92 |
| Graphite Sleeve Inspection | 93 |
| Welding of EGCR Loop Through Tubes | 94 |
| Welding of Dissimilar Metals | 95 |
| Beryllium Investigations | 96 |
| Compatibility of Beryllium with Coolant Impurities | 96 |
| Procurement of Beryllium Tubing | 100 |
| Fabrication of Tubing | 100 |
| Beryllium Tubing Evaluation | 101 |
| Beryllium Joining | 102 |
| 5. IN-PILE TESTING OF COMPONENTS AND MATERIALS | 107 |
| Fuel Element Irradiation Program | 107 |
| Full-Diameter Prototype EGCR Fuel Capsules | 107 |
| Beryllium Cladding and UO ₂ Grain-Size Studies | 107 |
| Miniature Capsule Fission-Gas-Release Experiments | 112 |
| Advanced Fuel Element Testing | 113 |
| Examination of Irradiated Capsules | 114 |

| | |
|---|-----|
| LITER-Irradiated Miniature Capsules | 114 |
| ORR-Irradiated Prototype Capsules | 117 |
| Measurement of Fission-Gas Pressure in Prototype Capsule at EGCR Operating Temperature | 117 |
| ORR Closed-Cycle-Loop Experiments | 120 |
| Instantaneous Fission-Gas-Release Experiment | 120 |
| 6. OUT-OF-PILE TESTING OF MATERIALS AND COMPONENTS | 123 |
| Compatibility Tests of Graphite, Structural Materials, and Helium | 123 |
| Evolution of Gases from Graphite | 125 |
| Transport of Gases Through Graphite | 137 |
| Permeability Studies | 137 |
| Low-Temperature Diffusion Experiments | 141 |
| Diffusion of Fission Products in Graphite | 142 |
| Chemical Analyses of Reactor Materials | 143 |
| Automatic Continuous Analysis of Helium | 143 |
| Determination of Helium in Air | 145 |
| Investigation of Adsorbers for Removing Fission-Product Gases from Helium | 147 |
| Measurement of High Temperatures | 151 |
| Drift Studies of Chromel-P-Alumel Thermocouples in Various Atmospheres | 151 |
| Tungsten-Rhenium Thermocouples | 154 |
| 7. DEVELOPMENT OF TEST LOOPS AND COMPONENTS | 155 |
| ORR Gas-Cooled In-Pile Loops | 155 |
| Loop No. 1 | 155 |
| Loop No. 2 | 155 |
| EGCR In-Pile Loops | 157 |
| Through-Tube Design | 157 |
| Component Designs | 158 |
| Demineralized-Water System | 161 |
| Cell Ventilation System | 161 |
| Hazard Studies | 162 |
| Supporting Facilities | 163 |

| | |
|--|-----|
| Hydrogen-Cooled Loop Design Study | 165 |
| Loop Component Tests | 166 |
| Heater, Evaporator, and Condenser for GC-ORR Loop No. 2 | 166 |
| Ceramic-Metal Seal for Heater Leads | 168 |
| Heater Electrical Breakdown Test | 170 |
| EGCR Loop Valves | 171 |
| Special Compressors | 172 |
| Regenerative Compressors | 172 |
| Compressors with Gas-Lubricated Bearings | 172 |
| High-Temperature Gas-Bearing-Compressor Test System | 173 |
| Compressors for GC-ORR Loop No. 2 and EGCR Loops | 173 |
| Mechanical Joint Service Testing | 173 |

SUMMARY

Part 1. Design Investigations

1. Reactor Physics

The relative merits of three proposed methods of control-rod programming for operation of the EGCR have been evaluated. The three methods are (1) uniform bank operation of all rods, (2) partial or full insertion of a few selected control rods, and (3) full insertion of selected control rods and uniform bank operation of the remaining rods. The third method incorporates the advantages of the other two and provides greatest flexibility. It is recognized, however, that the wide range of operating conditions anticipated for the EGCR will present situations that cannot be handled by this method and that special solutions must be sought by the operator. A complete study of control-rod reactivity worth and effect on the reactor will be essential during initial critical experiments and shakedown operation for accurate analyses of subsequent operation.

Calculations have been made of the amount of heat that will be deposited in the EGCR control rods. The cases considered conformed with the method of control-rod programming suggested above.

Calculations have also been made of the gamma-ray heat deposition to be expected in the EGCR moderator and other core components. These data provide information needed for determining the over-all core cooling requirements.

2. Reactor Design Studies

The hot-channel factors have been determined for the EGCR core for both the normal operating case and for a channel with an additional 10% heat input. For these calculations the uncertainty in the heat transfer coefficient, which is the largest single contribution to the hot-channel factors, was considered to be $\pm 10\%$ rather than the 30% used previously in the hazards summary report. The reduction of the uncertainty is justified by recent data on the thermal conductivity of helium.

Criteria for the failure of EGCR fuel elements have been established based on excessive temperatures and/or excessive fission-gas release. The maximum allowable temperature has been set at 1800°F. This temperature, above which any element is assumed to fail, is based on the lack of data above this temperature rather than on known properties. In the case of fission-gas release, it is assumed that the operating time of an element will be limited to the time when the internal pressure on the capsule is equal to the external pressure. These criteria apply only to normal long-time operation.

Design data based on results of irradiation experiments on UO₂ have been applied to EGCR operating conditions, and the UO₂ temperatures and the fission-gas pressure buildup have been computed. For these calculations the gas-gap resistance between the cladding and the UO₂ was taken to be equivalent to a 0.001-in. clearance. These fuel element life calculations indicate that approximately one-third of the inner surface of the UO₂ in channel position 4 operates at a temperature in excess of 1600°C. At the end of life, when the quantity of UO₂ at this temperature is a maximum, it amounts to only 2% of the total oxide volume in the capsule. The fuel exceeds 1600°C only during the last 120 days of irradiation (total exposure time is 1040 days); therefore the assumption of 100% release of the fission gases generated in this volume increases the total internal pressure only from 178 to 192 psia and the gas release only from 9.1 to 10.5%. None of the fuel assemblies have final internal pressures in excess of the coolant pressure of 300 psia, and only the assembly in position 4 significantly exceeds an internal pressure of about 100 psia during the last half of its exposure period.

A calculation of the pressure drop across the six fuel assemblies in the highest power channel has given a maximum value of 9.44 psi. This value is just below the allowable 9.5 psi.

The design of the EGCR control rods has been modified to overcome difficulties encountered in attaching the central wire rope to the inside of the rod. The current design consists of four spring-loaded 5-ft-long segments having a ball-and-socket type of joint with a

3/8-in.-diam rod attached to spiders at the top and bottom of the control rod. One centering spacer on the 3/8-in. rod is used in each segment.

The thermal characteristics of the modified rod were calculated in order to determine the effects on cooling requirements. Calculations were also made for determining the effect of the reactor radial flux gradient on the circumferential variation in rod cladding temperature and any subsequent rod bowing. The maximum average temperature drop across the rod was found to be 181°F. This temperature could cause a bow of only 0.255 in. over a 5-ft-long control-rod segment and thus should not cause any difficulty in the operation of the rods.

Experimental data have been obtained for a stress analysis of the EGCR pressure vessel. A model of the upper head and the adjacent portion of the cylindrical section that was instrumented with bonded-wire strain gages was used to obtain the data. The data are being interpreted in terms of the load-carrying capacity and structural integrity of the reactor vessel. A theoretical model has been developed for use as a guide in the analysis.

3. Experimental Investigations of Heat Transfer and Fluid Flow

The channel entrance for the apparatus used in the study of the thermal characteristics of the EGCR fuel cluster was modified in an effort to correct for a flow maldistribution observed in earlier experiments. Circumferential temperature profiles were obtained for all seven tubes at 11 axial positions with the altered inlet configuration; the average Reynolds modulus was 50 500 and the surface heat flux was maintained at 6500 Btu/hr·ft². Some anomalies exist in the data, particularly with regard to the axial distribution of the mean tube temperature; and additional studies to resolve the issue are in progress. The data indicate that a flow deficiency exists in the region surrounding the central tube. An examination of the data obtained thus far in this study (both for $\gamma = 2$ and $\gamma = 4$ tube spacings) has disclosed an appreciable sensitivity to the inlet plenum configuration. Accordingly, a new apparatus containing two clusters equipped with Title II spiders (arranged

so that one cluster is capable of rotation with respect to the other) is being fabricated.

An evaluation has been completed of preliminary mass-removal measurements obtained in the study of the role of relative cluster orientation on the heat-transfer distribution in an EGCR fuel cluster. The data can, in general, be analyzed in terms of the effect of the spiders and the mid-cluster spacer on the flow in the rod bundle. While a number of discrepancies point up the need for duplicate runs, the over-all pattern is self-consistent. The j factors for mass transfer and heat transfer were found to be in excellent agreement, with the ratio j_M/j_H just upstream of the mid-cluster spacer being 1.13. A greater deviation between j_M and j_H observed downstream of the mid-cluster spacer suggests that the mass-transfer data for this region may be in error. This is supported by the observation that the asymptotic value of the mass-transfer factor for the exit half of the cluster is 17% higher than the corresponding value for the inlet portion of the bundle.

Mapping of the isothermal velocity field in the EGCR cluster has concentrated on the effect of relative cluster orientation on the velocities 0.05 in. from the rod surface at four axial levels. The measurements have been restricted to a 120-deg sector of the channel, embracing four rods. Data taken in the vicinity of the end spiders and the mid-cluster spacer show no unexpected characteristics in the axial flow. The velocities in the region of the central rod appear to be generally greater than those observed for the peripheral rods. A regular variation in the magnitudes of the velocity maxima around the inner rod just downstream of the spacer may reflect a displacement of this rod from its central position.

Part 2. Materials Research and Testing

4. Materials Development

Work has continued in the development of a process for recovery of UO_2 by the nitrate-recycle process. Excellent powder has been produced,

but none has been identical to that produced by the fluoride-ammonium diuranate process. Specimen pellets of UO_2 of two different grain sizes have been fabricated for use in prototype irradiation experiments. Thin plates of UO_2 and ThO_2 were prepared for fission-gas-release experiments.

The release-rate parameter, D' , for the release of Xe^{133} has been determined for additional grades of UO_2 , including a specimen of fused oxide. The activation energy associated with the diffusion of this isotope was determined to be 86 kcal/mole. Previous tests had shown that D' increased rapidly when the sintering temperature of UO_2 was surpassed. In tests to determine the effect of additional sintering, pellets were resintered for 9 hr at $1900^\circ C$, and the value of D' at $1800^\circ C$ decreased by a factor of 5.

Processes are being developed for the preparation of fueled graphite bodies. Graphite fueled with UC by an admixture method and fabricated into cylindrical shapes showed laminations and surface bumps due to partial oxidation of the UC during firing. This condition could not be eliminated by purifying the furnace atmosphere.

The rate constants for the reaction of -60 +80 mesh UO_2 with graphite at reduced pressures were determined to be 0.18 at $1275^\circ C$ and 0.44 at $1375^\circ C$. Results obtained in this study have indicated that the reaction rate is sensitive to particle size below about $1325^\circ C$ and relatively insensitive above this temperature.

The elastic moduli of AGOT graphite were determined by the sonic method. On a specimen from a block prepared with needle coke, the Young's modulus was essentially constant over the temperature range from 75 to $1000^\circ F$.

In order to evaluate the effects of defects in graphite fuel element support sleeves, "brittle-ring" and flexure-test specimens were prepared from selected sleeves, along with specimens containing artificial defects. While the inclusions and laminations in these specimens did affect the tensile strength adversely, the minimum strength was still well in excess of the calculated stress of 1300 psi in service. Techniques are being developed for evaluating and inspecting coatings on graphite sleeves.

Spectrographic analyses of BeO containing about 200 ppm of lithium indicate that lithium is not evolved from BeO at 850°C. The reactivity of the BeO was measured in a critical assembly before and after heating.

Procedures are being developed for producing stainless-steel-clad, hot-swaged rods containing UO₂ for irradiation tests. Densities as high as 94% of theoretical have been achieved in the UO₂ in rods swaged at 800°C. The reduction schedule and initial wall thickness of tubing required to achieve a final wall thickness of 0.015 in. are being determined.

Additional data on the weight gain of stainless steel in helium containing CO and CO₂ impurities show that the reaction rates are approximately proportional to the square root of time and are not strongly affected by the concentration of CO₂ plus CO. The effect of the ratio of CO₂ to CO on carburization of stainless steel is being studied. Results of two tests indicate that the extent of carburization depends on this ratio.

An experimental program for investigating the creep buckling and instantaneous collapse of stainless steel tubes is being carried out to obtain the information needed for design of the ECCR experimental loops. Specimens being tested at 1200°F at pressures of 400 and 600 psi have shown no evidence of collapse. The critical pressure for instantaneous collapse at 1200°F was determined to be 800 psi.

Investigations of the effect of environment on the time to rupture of seamless type 304 stainless steel tubing have shown a definite strengthening effect in atmospheres containing CO. Mechanical property tests on specimens from a low-carbon heat of AISI-type 502 steel having five different heat treatments have shown that the creep properties of the material are not affected by the environment and that the ductility is not strongly affected by the thermal history.

Studies of the fracture characteristics of specimens of artificial weld-heat-affected zones from ASTM A212, grade B, plate have shown that exposure to thermal cycles with a maximum temperature of 2400°F using energy inputs of 150 000 and 200 000 joules/in. cause a reduction in notch toughness.

The reactions of molybdenum with CO_2 , CO , H_2 , H_2O , and CH_4 , the gases normally present as impurities in a helium-cooled reactor, were predicted from thermodynamic calculations. Refractory metals, such as molybdenum are being considered for use in high-temperature, gas-cooled reactors.

A series of welding experiments on EGCR fuel-capsule closures has shown that the tolerances for positioning of the end cap are not critical but that close contact of the end cap with the fuel column will cause restraint of the closure weld and should be avoided. In a series of brazing experiments on mid-plane spacers, the grain sizes of capsule tubing having various amounts of cold work were not significantly different after typical furnace-brazing cycles.

A commercially available welding torch was modified for use in remote welding of the through tubes for the EGCR loops. High-quality welds were made on concentric-pipe specimens.

Results of studies of the reactions of beryllium with CO_2 over the temperature range from 600 to 720°C have shown that the reaction is relatively independent of pressure. One test on the reaction of beryllium with water vapor at 700°C at a pressure of 1×10^{-3} mm Hg showed an even lower reaction rate than in CO_2 at 600°C.

In the investigation of the effect of extrusion variables on beryllium tubing, the lowest degree of preferred orientation was found in tubes extruded by the filled-billet method from hot-compacted cores. In general, tubing extruded at low temperatures and reduction ratios exhibited a low degree of preferred orientation and tubing produced from hot-compacted cores by extrusion with a mandrel had a high degree of preferred orientation.

The evaluation of beryllium tubing from various sources is being continued. Tubing machined from block or extruded rod is of high quality, except for the difficulty in maintaining tolerances on the wall thickness. Much of the warm- and hot-extruded tubing shows pitting and high-density inclusions, as well as some axial and circumferential cracking. The causes of excessive defect indications noted during eddy-current inspection are being studied.

Beryllium-clad capsules of two sizes fueled with UO_2 pellets were prepared for irradiation along with a group of foreign-made capsules. Successful, crack-free fusion welds were made on these capsules. Porosity in welds of extruded tubing continues to present a problem, but it has been relieved by increasing the flow of inert gas during welding. Shear tests on a series of end-cap fusion welds showed high joint efficiency, particularly on specimens with tight-fitting caps.

5. In-Pile Testing of Components and Materials

Irradiation in the ORR of the eight group II full-diameter prototype EGCR fuel capsules was completed. Irradiation of 14 similar capsules designed for various UO_2 burnups is continuing in the ETR.

Irradiation of eight group III capsules was started in the ORR. Six of these capsules consist of beryllium-clad solid UO_2 pellets, and the remaining two are stainless steel clad. One of the stainless-steel-clad capsules contains large-grain-size cored pellets and the other small-grain-size cored pellets. Irradiations of miniature capsules for fission-gas-release determinations have continued in the LIIR. A second fueled graphite assembly is being irradiated in the MIR.

Additional postirradiation examinations of miniature-capsule experimental assemblies have been completed. A small increase in immersion density after irradiation has been noted. Variations in grain size have been correlated with the temperature gradient during irradiation. Columnar growth and grain reorientation have been observed in capsules irradiated at central temperatures of $2700^\circ F$ or higher.

The eight group II capsules removed from the ORR have been dismantled. Dimensional measurements have shown 0- to 0.008-in. increases in the average diameters of the capsules.

A measurement of the pressure buildup in an EGCR prototype fuel capsule has supported the prediction, based on physical property data, that the pressure buildup from alkali-metal fission products that have low boiling points will not be significant.

A new sweep-gas system has been installed in the instantaneous fission-gas-release apparatus in order to assure oxygen-free gas. The new system uses argon or helium containing 3% hydrogen.

6. Out-of-Pile Testing of Materials and Components

Examinations were made of steel specimens containing various amounts of chromium after exposure at 1100°F in a helium atmosphere to which 0.18 vol % CO had been added. The weight gains of the chromium-containing steels were only slightly less than the weight gain of T-1 steel, but the oxide films were considerably more adherent. Comparison of these results with data for similar specimens tested in air at 1100°F showed the trends in oxidation rates to be similar.

Experimental studies of the degassing behavior of selected grades of graphite have been continued. Data on the rate of gas evolution at 600 and 1000°C were collected for the various specimens tested, as well as data on volume and composition of gas evolved at the temperatures of interest.

Gas permeability determinations were made on typical, uncoated, EGCR fuel element sleeve graphite specimens, with and without joints, and on plugs. The lateral flow of helium through these sleeves and the graphite columns in the EGCR will affect the fuel element surface temperatures. Tests on the plug specimens showed that permeability varied somewhat with pressure, whereas the sleeve materials followed Darcy's law. For plug specimens, large differences in permeability were found when specimen shapes and flow patterns were varied.

Data obtained in tests of the proposed joint designs for the graphite sleeves indicate that a graphite-to-graphite joint is as effective as a brass plate-to-rubber gasket closure.

Measurements of the mutual diffusion coefficients of argon and helium in AGOT graphite have been made at room temperature, 0°C, and -65°C. The data indicate that the diffusion mechanism is classical and that if mechanisms such as the surface diffusion which might result from an adsorbed (liquid) layer exist, their effects must be less than the experimental error (~8%). On the other hand, data on diffusion of fission

products in graphite indicate that surface diffusion and carbide-formation reactions may be significant.

A second process-gas chromatograph has been obtained for automatic continuous gas analyses. The new model has improved valves and means for external adjustment of carrier gas flow rates. Additional modifications have been made at the Laboratory to improve the utility of the instrument.

A procedure has been developed for the measurement of small increments in the concentration of helium in air. Increments of 8 to 400 ppm have been measured with a coefficient of variation of 2%.

Investigations of the removal of radioactive fission-product gases from coolants and other carrier gases have been continued with additional dynamic adsorption measurements on charcoal. A related study of longitudinal diffusion of krypton in adsorbers was made, and the heating effects occurring on pressurization of charcoal traps were studied.

Further studies of the large negative drifts obtained with Chromel-P-Alumel thermocouples in stagnant helium at 1000°C have indicated that the protection tubes used (quartz or alumina) have no effect on the thermocouple drift. When dull Chromel-P wires were exposed, a progressive brightening of the wire surface occurred from the hot zone toward the thermal-gradient region. Longer heating resulted in disappearance of the bright film in the hot zone. The bright film proved to be nickel. Experiments with a unilateral gradient furnace showed a gradual buildup of error voltage in the thermal-gradient region during time of exposure. Removal of the nickel film did not appreciably reduce the large error voltages in the gradient region. Titanium wire included with Chromel-P wires in the protection tube prevented most of the negative drift but did not eliminate it completely. Chromel-P wires tested in vacuum showed practically no negative drift. Geminol-P wires did not show the negative drifts in a helium atmosphere that were found for the Chromel-P wires.

Two, helical, tungsten-rhenium, stainless-steel-sheathed, exposed-junction thermocouples were tested for 675 hr at 1100°C in a helium atmosphere. The emf output indicated temperatures within 10°C of those

reported by another investigator, and the emf values did not increase in error when the thermocouples were cycled between 500 and 1100°C. Failure of the junction occurred in one thermocouple and a break in the sheath occurred in the other.

7. Development of Test Loops and Components

Installation of gas-cooled loop No. 1 in the ORR is essentially complete and shakedown tests are in progress. A revised operational and hazards report was prepared. Fabrication of the primary components of loop No. 2 is nearly complete.

Design layouts were completed for the 5 1/2-in.-o.d. through tubes for the EGCR in-pile loops. An evaluation of the axial loads indicated that there would be no problem of buckling. Work continued on the design of loop components, such as the gas filters, the gas heaters, the diversion valves, the leak detection equipment, the gas transfer equipment, and the loop coolers. The demineralized-water cooling system was modified to provide secondary containment, and a study was made of the proposed cell ventilation system. Hazards analyses were made that included studies of heat removal by natural convection, transient thermal stresses in the loop piping, and the thermal expansion differences of process piping and containment piping. The dynamic behavior of the EGCR loop is being investigated with the ORNL Reactor Controls Analog Facility.

A preliminary study of the proposed hydrogen-cooled in-pile loop has indicated the need for extensive study of potential hazards. The hazards study has indicated the desirability of lowering the loop performance specifications with respect to operating pressure and test fuel element power.

An out-of-pile test loop is being assembled for testing ORR loop No. 2 components. Preliminary tests of a ceramic-metal heater-lead seal developed for this service were terminated when a helium leakage rate of 10 cm³/min was noted at 600°F with a pressure difference across the seal of 20 psig. Chromalox tubular heating elements in hairpin form inserted through and welded into a single header plate are being investigated for gas heating.

Two regenerative compressor units have been installed in the twin-turbine vessel of the GC-ORR loop No. 1. The delivery of the Bristol Siddeley compressor with gas-lubricated bearings has been delayed because of inability to eliminate bearing metal-to-metal contact. A test system for high-temperature performance checks of such compressors has been assembled.

High-temperature thermal- and load-cycling tests of mechanical pipe joints were continued. It has been found that 10-in.- and 2 1/2-in.-IPS Conoseal joints will remain leaktight at the temperatures of interest.

Part 1. Design Investigations

1. REACTOR PHYSICS

Suggested Operating Program for EGCR Control Rods

A problem that will be encountered in operating the EGCR, as mentioned previously,¹ is that of selecting a pattern of control rod insertions which will produce the desired reactivity decrease and at the same time result in a reactor power distribution which is not excessively peaked. This problem is made especially severe by the large reactivity increase which results from high-power-density in-pile loop experiments, and by the marked effect these loop experiments have on the reactor power distribution. The effect of loop experiments on the reactor power distribution is especially adverse when only the four small loops are being used. This case has been studied in considerable detail for homogeneous graphite-U²³⁵ experiments in the central loops.¹ A carbon-to-uranium ratio of 200 (0.33 kg of U²³⁵ per foot) has been chosen as a typical loading, and it has been found to result in power-generation rates of between 0.8 and 1.1 Mw, depending on the control-rod positions.

The limitations on the reactor power distribution are most easily discussed in terms of the axial and radial peak-to-average power ratios. By axial peak-to-average ratio for a given channel is meant the ratio of the peak power per unit length in the channel to the average power per unit length. By radial peak-to-average ratio is meant the ratio of the total power generated in the highest power channel to the average power per channel in the core.

The maximum allowable radial peak-to-average power ratio will be accurately known only when the maximum capabilities of the blowers and the pressure drop across each component in the primary coolant circuit are determined. The current design basis for these quantities permits a maximum radial peak-to-average power ratio of ~1.35.

If the limitation on the radial peak-to-average power ratio is not exceeded, the flow in each channel may be matched to the power generated

¹"GCR Quar. Prog. Rep. June 30, 1960," ORNL-2964, p. 3.

in the channel by proper setting of the channel orifices. The maximum fuel element surface temperature will then be determined primarily by the axial peak-to-average power ratio and by the axial position at which the peak occurs. Most manipulations of the EGCR control rods will produce the desirable effect that an increase in the axial peak-to-average power ratio will be accompanied by a displacement of the position of peak power downward into a cooler portion of the core. Nevertheless, it appears that axial peak-to-average power ratios greater than about 2.0 must be avoided to prevent excessively high cladding temperatures.

The discussion of control rod operation is simplified by defining a reference reactivity point as the least-reactive condition of the core which still results in criticality. This condition exists when the eight through tubes are empty, the reactor is operating at full power, xenon poisoning is at its peak, and there is a maximum run-down of fuel with respect to refueling operations. The initial fuel enrichment is fixed by the requirement that the multiplication factor be exactly equal to unity for the above condition when the control rods are fully withdrawn, and departures from this reference condition will require control rod insertion in order to maintain the multiplication factor at unity.

It is convenient to differentiate between the situations for the initial core and the equilibrium core, since a larger operating margin of excess reactivity will be required in the initial core in order to yield satisfactory fuel-cycle economics for the first loading. This is also desirable, since it will defer to a conveniently advanced date the time at which refueling operations are required for criticality.

The deviations of the initial and equilibrium cores from the reference condition are listed in Table 1.1 for the case of the four central loops containing experimental assemblies with a carbon-to-uranium ratio of 200. Full-power operation with equilibrium xenon poisoning is assumed.

Based on the typical control requirements given in Table 1.1, it is possible to discuss the methods of control-rod programming that are available for operating the core. The three methods considered are

Table 1.1. Deviations of Initial and Equilibrium Cores
from Least-Reactive Reference Condition

| Type of Deviation | Reactivity (Δk) | |
|--------------------------------|---------------------------|---------------------|
| | Initial Core | Equilibrium Core |
| Operating margin | | |
| Burnup | +0.040 ^a | +0.004 ^b |
| Peak xenon - equilibrium xenon | +0.007 | +0.007 |
| Four experiments | <u>+0.042</u> | <u>+0.042</u> |
| k_{excess} (no rods) | +0.089 | +0.053 |
| Control-rod insertion | <u>-0.089</u> | <u>-0.053</u> |
| k_{excess} | 0.000 | 0.000 |

^aBased on 12 months of operation.

^bBased on 1 month of operation.

(1) uniform bank operation of all control rods, (2) partial or full insertion of a few selected control rods, and (3) full insertion of selected control rods and uniform bank operation of the remaining rods. The individual control rods are identified in Fig. 1.1.

Method 1. Operation of all control rods as a bank provides no deliberate control of the reactor power distribution. For the case considered here, the radial peak-to-average power ratio would be 1.76.¹ In the equilibrium core an insertion to a depth of 91 in. would be required, and the resulting axial peak-to-average power ratio would be 2.48. In the initial core an insertion to a depth of 110 in. would be required, and the resulting axial peak-to-average power ratio would be 2.91. Both the radial and axial peak-to-average ratios exceed the maximum allowable values.

Method 2. The situation of full insertion of selected control rods has been examined in considerable detail.¹ In order to provide the degree of radial power flattening which is required, the reactivity decrease must be accomplished with the nine central control rods, and,

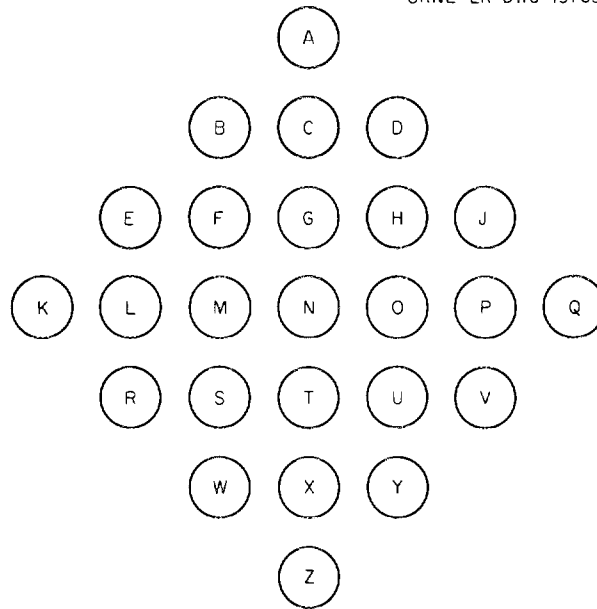


Fig. 1.1. Identification Letters Assigned to EGCR Control Rods.

in order to prevent the axial peaking factor from exceeding 2.0, no rods other than the central rod can be inserted past the core mid-plane unless it is fully inserted. In order to prevent a radial tilt of the power distribution, a symmetrical pattern of control rods, in groups of four rods, must be maintained. It can be shown that a continuous range of control cannot be provided without violating these conditions.

Method 3. Full insertion of individual control rods and uniform bank operation of the remaining rods appears to offer the greatest promise for satisfactorily fulfilling the control requirements under all anticipated operating conditions and incorporates the desirable characteristics of the two methods discussed above. These are (1) the continuous reactivity control provided by bank operation and (2) the positive control of the radial power distribution provided by the full insertion of selected rods. This possibility for controlling the reactor is suggested by observing that bank operation of the control rods produces an acceptable axial power distribution provided the reactivity decrease due to the bank is approximately 0.025 or less in Δk . If, therefore, discrete

Δk steps of this magnitude or less are available with the full insertion of selected rods (and allowed by considerations of the radial power distribution), a continuous range of control will be available. A continuous range of control is not available with the present design of the control rod bank. Such would be provided, however, if the combined worth of rods G, O, T, and M were reduced from a Δk of 0.079 to 0.040. This modification would allow a continuous range of control up to a Δk of approximately 0.15, without exceeding a bank insertion greater than a Δk of 0.020. The range up to the Δk of 0.053 anticipated for operation of the equilibrium core could be covered with, at most, a Δk of 0.015 inserted as a bank. In summary, a reduction of a Δk of 0.039 in the worth of the rod bank would allow adoption of the control-rod operating program illustrated by Table 1.2.

The feasibility of the suggested reduction in control-rod worth rests upon the demonstration that the reactor will have sufficient shutdown margin in the most reactive configuration anticipated. If the least-reactive condition, as described above, is taken as the reference point, the maximum anticipated deviations from this condition for the hot reactor are as given in Table 1.3.

For the reactor at room temperature, the maximum excess multiplication factor will be the value given in Table 1.3 plus the change in k in going from room temperature to the operating temperature and the reduced power condition covered by Table 1.3. This change will be a Δk of approximately 0.02 and will result in a maximum excess reactivity in the room-temperature reactor of

$$k_{\text{excess}} = 0.124 + 0.020 = 0.144 \quad .$$

These values for the maximum excess reactivity (0.124 in hot reactor, 0.144 in cold reactor) must be compared with the worths of the bank of control rods for these two conditions in order to determine the maximum shutdown multiplication factor for the hot and cold cores. The control rod worths and maximum shutdown multiplication factors are summarized in

Table 1.2. A Possible Control-Rod Operating Program
Based on a Reduction in the Worth of Rods
G, O, T, and M to a Δk of 0.040

| Desired Range of Control (Δk) | Fully Inserted Rods | Maximum Δk in Bank |
|---|---------------------------------------|----------------------------------|
| (0.000-0.025) ^a | (None) | (0.025) |
| 0.000-0.025 | Partial to full insertion of rod N | 0.000 |
| 0.025-0.040 | N | 0.015 |
| (0.040-0.050) | (N) | (0.025) |
| 0.040-0.050 | G, O, T, M | 0.010 |
| 0.050-0.060 | G, O, T, M | 0.020 |
| 0.060-0.070 | N, G, O, T, M | 0.010 |
| 0.070-0.090 | F, H, S, U | 0.020 |
| 0.090-0.100 | N, F, H, S, U | 0.010 |
| | . | |
| | . | |
| | . | |
| | etc. | |

^aThe generally less desirable options are enclosed in parentheses.

Table 1.3. Anticipated Maximum Deviations from
Least-Reactive Condition

| Type of Deviation | Δk |
|---|------------|
| Allowance for fuel burnup (12 months for initial core) | +0.040 |
| Complete decay of xenon | +0.028 |
| Reactivity of eight experiments | +0.050 |
| Operation at reduced power | +0.006 |
| | +0.124 |

Table 1.4 for a 21-rod bank in which rods A, Q, Z, and K are missing. This condition is considered to be the present design configuration.

Since it was assumed for the calculations summarized in Table 1.4 that all control rods were installed in the core and were operable, it is necessary to consider the condition of the reactor when (1) control rods are removed for repair, (2) control rods are removed for service machine access, and (3) control rods are stuck in the retracted position. The minimum departure from the condition of Table 1.4 that is allowable is given by assuming that one rod is out for repair and one rod sticks in the retracted position when a shutdown is attempted. In order to be conservative, it is usually assumed that the unavailable control rods are those with maximum worth, but it is important to observe that this condition cannot occur when the core has a high shutdown multiplication factor if method 3 is used for controlling the reactor. For example, with eight experimental assemblies in the core, representing the most reactive anticipated condition, the four or five most valuable rods will already be fully inserted at the time the shutdown is attempted. Of the rods remaining in the retracted position, the most valuable will be worth a Δk of 0.015. If three of these are not available for shutdown for any of the three reasons listed above, the shutdown multiplication factor will still be 0.948 in the hot core and 0.995 when the core cools to room temperature, as may be seen from Table 1.4. Situations in which the most valuable rods are in a retracted position when the shutdown

Table 1.4. Values of the EGCR Control-Rod Worths and Shutdown Multiplication Factors for Three Core Conditions

| Core Condition | Control Rod Worth (Δk) | Shutdown Multiplication Factor (k) |
|--------------------------------------|----------------------------------|--|
| Operating temperature, 8 experiments | 0.221 | 0.903 |
| Room temperature, 8 experiments | 0.194 | 0.950 |
| Room temperature, no experiments | 0.223 | 0.871 |

is attempted correspond to conditions of less inherent reactivity of the core (as with no experiments, for example), and even if these rods fail to insert the situation is improved over the case considered above.

Several additional distinct advantages may be listed for method 3 as a standard operating program for the control rods:

1. The peak in the axial power distribution occurs in the range of 65 to 80 in. from the bottom of the core. This places the positions of maximum power density well into the instrumented portions of test fuel assemblies, in contrast to the result with method 1 and 2 which would place the peak at about 50 in. or less from the bottom of the core.

2. A range of reactivity control of 0.025 in Δk may be obtained with no appreciable change in the radial power distribution. This is a highly desirable feature that is not provided by method 2 and which minimizes the required frequency of making orifice changes.

3. All anticipated reactor operating conditions produce very nearly the same power distribution in the core. This is a result of the nearly complete control over the power distribution which is provided, and it simplifies the choice of conditions for the analysis of operating or accident conditions.

4. Manipulation of the control rods during a reactor startup is greatly simplified with respect to method 2. All control rods, except those to remain fully inserted, may be withdrawn as a bank until the desired operating condition of the core is obtained.

5. Physics analysis of the core is much simpler than with method 2. This will aid in predicting the operating conditions at a given startup.

The major disadvantages which will result if the core is operated in the suggested manner are the following:

1. A decrease in a Δk of 0.039 for the shutdown worth of the control rod bank is required. This appears to present no hazard, but it may result in slight restrictions in flexibility of operation. For example, if one rod is removed for repair, another rod should not be removed for service-machine access to the core if the core is in its

condition of maximum inherent reactivity. In a condition of lower reactivity this restriction would not be present.

2. The axial peak-to-average power ratio is very nearly the same in all channels. If the axial peak-to-average power ratio is high, this is a disadvantage compared with the case with method 2, which generally results in low output power from the channels with the highest axial peak-to-average power ratios.

3. More spare control rods will be required to allow for the occurrence of an unusual operating condition in the reactor which requires full-worth rods in all positions.

The selection of any method as standard for operating the control rods must not be considered to be an exclusion of all other methods. The wide range of operating conditions anticipated for the EGCR will certainly include some which cannot be handled by the combination of fully inserted rods and bank operation suggested here, but these conditions constitute special problems for which special solutions must be sought by the reactor operator. It is important that the initial critical experiments and shakedown operation of the reactor include a complete study of control-rod reactivity worth and effect on the reactor power distribution, since this information will be essential to doing accurate core analyses during subsequent operation of the core.

Heat Deposition in the EGCR Control Rods

Calculations have been made to determine the amount of heat that will be deposited in the EGCR control rods. The cases which have been considered have been chosen largely to conform with situations which will arise with the proposed method of control-rod programming described in the preceding section. In this manner of operating the reactor, certain selected control rods near the center of the core are fully inserted, and the remaining bank of rods is inserted to a maximum depth of about 5 ft.

As illustrated in Table 1.5, the heat deposition in any control rod depends to a considerable extent on the positions of all the other control

Table 1.5. Axially Averaged Heat Deposition in Fully Inserted EGCR Control Rods

| Rods Inserted | Rod Described | \bar{Q} (Btu/hr·ft) |
|----------------------------|----------------|-----------------------|
| N | N | 7340 |
| G, O, T, M | G | 6165 |
| G, O, T, M ^a | G ^a | 3265 |
| N, G, O, T, M | N | 4465 |
| N, G, O, T, M | G | 5665 |
| N, G, O, T, M ^a | G ^a | 2965 |
| C, P, X, L | P | 4675 |

^aRods G, O, T, and M reduced in worth from 0.079 to 0.040 in hot core.

rods. If any control rods are fully inserted into the core during full power operation, they will normally be either rod N; rods G, O, T, and M; or rods N, G, O, T, and M. Although these rods may routinely be fully inserted, any control rod may at some time be fully inserted when the reactor is at full power.

On the basis of calculations such as those described in Table 1.5, the maximum anticipated heat deposition in each rod when fully inserted is as tabulated in Table 1.6, and axial variation is as shown in Fig. 1.2 for a 62-in. insertion of the remaining rods.

Table 1.6. Maximum Anticipated Axially Averaged Heat Deposition in Fully Inserted EGCR Control Rods

| Control Rod ^a | \bar{Q} (Btu/hr·ft) |
|--------------------------|-----------------------|
| N | 7500 |
| O, U, T | 6500 |
| P, V, Y, X | 5000 |
| Q, Z ^b | 3000 ^b |

^aOne quadrant of the core is shown; other quadrants are the same.

^bThese rods will not be installed in initial core.

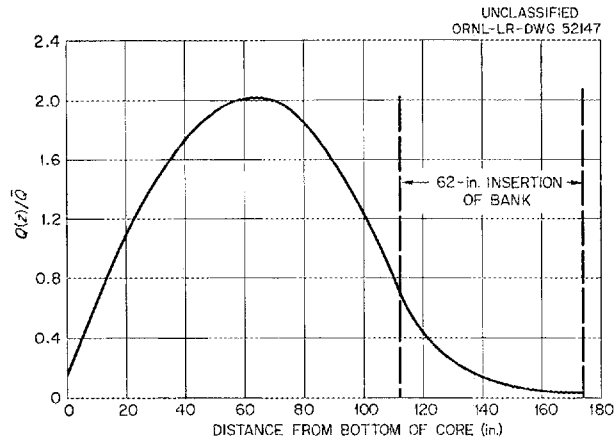


Fig. 1.2. Axial Distribution of Heat Deposition in Fully Inserted EGCR Control Rods.

When the bank of control rods is inserted 62 in. to give a Δk of 0.025, the total amount of heat deposited in the rods will be 1.8×10^5 Btu/hr. The axially averaged heat deposition rate in each rod for a representative case is given in Table 1.7, and the axial variation is as shown in Fig. 1.3. The axial variation shown in Fig. 1.3 includes the peaking factor for the tip of the rod.

Table 1.7. Axially Averaged Heat Deposition in Bank-Operated EGCR Control Rods for a 62-in. Insertion

| Control Rod ^a | \bar{q} (Btu/hr·ft) |
|--------------------------|-----------------------|
| N | (Fully inserted) |
| O, T | 2570 |
| U | 2080 |
| P, X | 1700 |
| V, Y | 1410 |

^aOne quadrant of the core is shown.

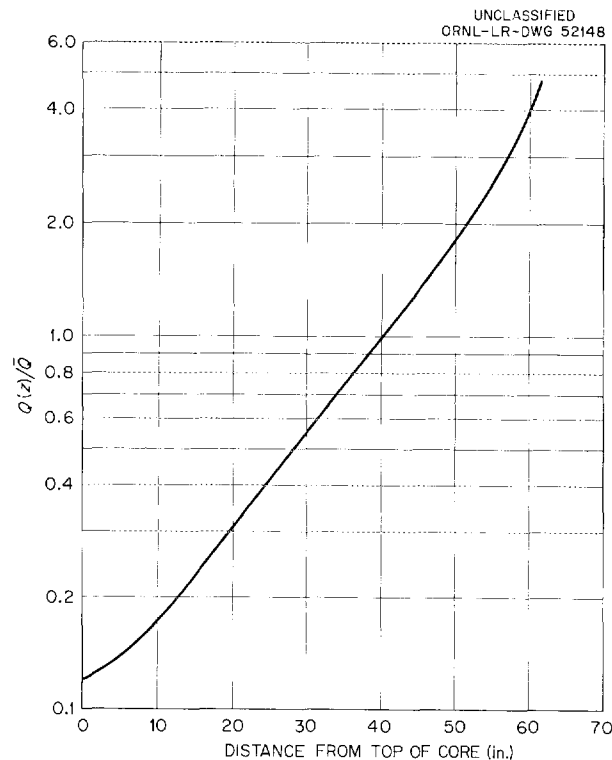


Fig. 1.3. Axial Variation of Heat Deposition in Bank-Operated Control Rods for 62-in. Insertion.

Gamma-Ray Heat Deposition in the EGCR Core

In the EGCR core a fraction of the total fission energy is not deposited near the point of fission but is transported outside the fuel elements and deposited in other parts of the reactor. The carrier mechanism for this transported energy is primarily the penetrating gamma rays and fast neutrons. In order to determine the over-all core cooling requirements, information on the heat-deposition rates in the moderator and other core component materials is required. A study has therefore been made of the gamma-ray heat deposition rates throughout the EGCR core as a function of radial and axial position. This study differed from a previous study² in that a more detailed analysis was made of the fraction of gamma-ray energy which escapes a fuel element

²"GCR Quar. Prog. Rep. March 31, 1960," ORNL-2929, pp. 3-5.

and a revised gamma-ray source spectrum was used. The total gamma-ray source was taken as 20.74 Mev/fission, with 9.25 Mev/fission escaping from the fuel rods. A breakdown of the various gamma-ray energy sources in the EGCR fuel element is given in Table 1.8. In addition, the calculations are based on a reactor power distribution corresponding to a more typical operating condition than was used in the previous study.

Because of the complex nature of the interaction of gamma rays with matter, the varying operating conditions of the EGCR core, and the complicated geometries involved, the following simplifying assumptions and initial conditions were selected:

1. The radial and axial power distribution in the core is that resulting from the operating condition in which the four central loops contain homogeneous graphite-uranium experiments ($C/U = 200$), with the central control rod fully inserted, and all other control rods in a bank inserted to 62 in.

2. The energy-distributed gamma-ray source spectrum is that calculated for the core reaction rates which prevail at 5000 Mwd/T in an equilibrium cycle to 10 000 Mwd/T. The energy-distributed spectrum is represented by six discrete energy groups.

3. The seven-rod cluster fuel elements are represented by finite long-line sources whose gamma-ray source strengths, $S(x,y,z)$, are proportional to the reactor power distribution, $P(x,y,z)$, and to the fraction

Table 1.8. Sources of Gamma-Ray Energy in the EGCR Core

| Gamma-Ray Source | Energy (Mev/fission) |
|--|-------------------------|
| Prompt fission and U^{235} , Pu^{239} , Pu^{241} capture | 9.25 |
| Fission-product decay | 7.00 |
| Stainless steel capture | 1.74 |
| U^{238} capture | 2.50 |
| U^{236} and Pu^{240} capture | <u>0.25</u> |
| Total | 20.74 |

of gamma-ray energy in the actual volume-distributed source region which succeeds in escaping from the cluster.

4. The gamma-ray heat deposition rate at a point in the reactor is the sum of the contributions of all of the filament sources to the heating at that point. The contribution of a single filament source is calculated by direct exponential attenuation modified by an energy-absorption buildup factor.

For a given gamma-ray energy group, that fraction of the total gamma-ray energy which escapes from a seven-rod cluster is taken as

$$\int_A \int_{\Omega} S(\bar{r}) e^{-\mu_T P(\bar{r}, \bar{\Omega})} B_E[\mu_T P(\bar{r}, \bar{\Omega})] \frac{d\bar{\Omega}}{4\pi} d\bar{r} ,$$

where

$S(\bar{r})$ = gamma-ray source strength as a function of position in the cluster,

\bar{r} = point of gamma-ray origin in the cluster,

$\bar{\Omega}$ = direction of gamma-ray trajectory,

$P(\bar{r}, \bar{\Omega})$ = the straight-ahead distance in UO₂ and stainless steel traversed by a gamma-ray originating at \bar{r} and leaving the cluster in direction $\bar{\Omega}$,

μ_T = total linear attenuation coefficient of the UO₂ and stainless steel medium,

$B_E[\mu_T P(\bar{r}, \bar{\Omega})]$ = energy buildup factor of the medium.

The seven-rod cluster was taken as being infinitely long, and the integral was evaluated over a 4π solid angle and the cluster cross sectional area, A. The function $P(\bar{r}, \bar{\Omega})$ was first determined for the seven-rod cluster with the use of the IBM-704 computer. The double integral given above was then evaluated by means of a fifth-order Gaussian quadrature procedure on the computer. The results of this phase of the study are given in Table 1.9.

Table 1.9. Seven-Rod Cluster^a Self-Shielding Factor

| Energy Group (Mev) | Escape Fraction | Filament Sources ^b (Mev/fission) |
|-----------------------|-----------------|--|
| 0.5 | 0.2237 | 1.156 |
| 1.0 | 0.4458 | 2.648 |
| 2.0 | 0.5698 | 3.413 |
| 4.0 | 0.5782 | 1.104 |
| 6.0 | 0.5584 | 0.365 |
| 8.0 | 0.5280 | 0.570 |

^aThe oxide rods have dimensions 0.707 in. o.d. by 0.323 in. i.d.; the steel tubes are 0.750 in. o.d. with a 0.020-in. wall; the six outer rods have their centers on a 2-in.-diam circle.

^bEnergy escaping from cluster.

Contributions of each energy group to the gamma-ray heat deposition rate at a point in graphite, for a filament source, have been evaluated on the IBM-704 in watts/cm³ according to the formula

$$H \cdot R(x, y, z) = \int_0^H \mu_E \frac{S(E, z) B_A(E) e^{-\mu R_g}}{4\pi R^2} dz ,$$

where

R_g = distance in graphite from source point to sink point, cm,

R = total distance, cm,

B_A = energy absorption buildup factor for graphite,

μ_E = energy absorption coefficient, cm⁻¹, for graphite,

$S(E, z)$ = filament gamma-ray source strength, watts/cm,

H = height of reactor, cm.

The results of integrating the computed head deposition rates over quadrants of each moderator column in the EGCR core are shown in Table 1.10. The point (0,0) corresponds to the center of the reactor. The total gamma-ray heating (kw) in graphite is given for each quadrant of the square graphite column (16 x 16 in.). This heat deposition includes

Table 1.10. Gamma-Ray Heat Deposition (kw) in Graphite Columns
of Southeast Quadrant of EGCR Core

| | | x (in.) | | | | | | | | | |
|---------|----|--------------------|-------|-------|-------|-------|-------|-------|-------|-------------------|------|
| | | (0,0) | 16 | | 32 | | 48 | | 64 | | 80 |
| y (in.) | 16 | 15.04 ^a | 16.82 | 19.24 | 20.17 | 19.19 | 17.25 | 15.05 | 12.50 | 9.14 | 2.11 |
| | | 16.82 | 6.77 | 18.66 | 19.79 | 18.67 | 16.73 | 14.46 | 11.74 | 8.31 | 1.85 |
| | 32 | 19.24 | 18.66 | 19.19 | 19.06 | 17.58 | 15.53 | 13.26 | 10.28 | 7.01 ^b | |
| | | 20.17 | 19.79 | 19.06 | 17.77 | 15.84 | 13.60 | 11.34 | 8.42 | | |
| | 48 | 19.19 | 18.67 | 17.58 | 15.84 | 13.28 | 10.46 | 8.20 | 6.04 | 2.48 | |
| | | 17.25 | 16.73 | 15.53 | 13.60 | 10.46 | 4.07 | 2.23 | 1.42 | | |
| | 64 | 15.05 | 14.46 | 13.26 | 11.34 | 8.20 | 2.23 | | | | |
| | | 12.50 | 11.74 | 10.28 | 8.42 | 6.04 | 1.42 | | | | |
| | 80 | 9.14 | 8.31 | 7.01 | | 2.48 | | | | | |
| | | 2.11 | 1.85 | | | | | | | | |

^aDeposition in one quadrant of core column.

^bTotal deposition in core column.

the heat deposited in the graphite fuel assembly sleeves, which is about 30% of the total heat in each column quadrant.

The detailed features of gamma-ray heating in a quadrant of a graphite column are shown in Table 1.11 and Fig. 1.4. These gamma-ray

Table 1.11. Gamma-Ray Heat Deposition Rates in a Symmetry Cell of a Graphite Column Quadrant Based on a Uniform Reactor Power Distribution

| Position Shown in Fig. 1.3 | Gamma Heating (w/cm^3) | Position Shown in Fig. 1.3 | Gamma Heating (w/cm^3) |
|----------------------------|----------------------------|----------------------------|----------------------------|
| A | 0.0753 | I | 0.0926 |
| B | 0.0769 | J | 0.0938 |
| C | 0.0805 | K | 0.1130 |
| D | 0.0839 | L | 0.1020 |
| E | 0.0870 | M | 0.1175 |
| F | 0.0810 | N | 0.1020 |
| G | 0.0860 | O | 0.1435 |
| H | 0.0905 | P | 0.1436 |

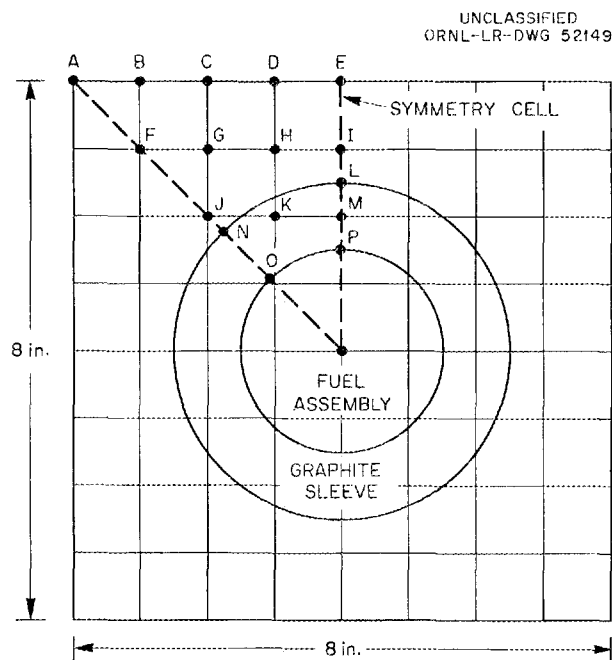


Fig. 1.4. Symmetry Cell of an EGCR Graphite Column Quadrant.

heating rates are based on the assumption of uniform power distribution throughout the volume of the EGCR core. Since nearly all the gamma-ray heat deposition at a given point is from gamma-ray sources located within a distance of about 20 in., it is felt that a reasonable estimate of gamma-ray heating for a particular power distribution can be obtained by renormalizing the results shown in Fig. 1.4.

A study has also been made of the gamma-ray heat deposition in the fuel assembly sleeves, the small and large loop tubes, the large loop-tube graphite plug, and the control rods. The additional heat deposition due to a 1-Mw seven-rod cluster experimental fuel assembly operating in either a small or large loop tube has been estimated. Concurrently, a study to determine the heat deposition rates due to fast neutrons is being conducted and is near completion.

2. REACTOR DESIGN STUDIES

EGCR Fuel Assemblies

Hot-Channel Factors

The hot-channel factors have been determined for the EGCR core for both the normal operating case and for a channel with an additional 10% heat input. In all cases the hot-channel factors have been applied to the highest power channel. In addition to using the highest power channel, the factors are applied to the case of 62 in. insertion of the control rods. Since this case represents the most severe operating condition that can be visualized and gives the maximum flux peaking, the flux uncertainty used in the calculations is small and represents only the uncertainty in the flux for the case considered. It is quite probable that the degree of accuracy with which the fluxes will be known for actual operating cases will be considerably greater, but, since the conditions analyzed are maximum operating limits, the use of the smaller uncertainty is justifiable.

The largest single contribution to the hot-channel factors is the uncertainty in the heat transfer coefficient, which, for these calculations, is considered to be $\pm 10\%$. As reported previously,¹ the experimental data fit the correlations used to calculate the nominal temperature to within $\pm 5\%$. Two recent reports^{2,3} have given values of the heat transfer coefficient of helium and a comparison with other gases. The NASA report³ compares results obtained for helium and for air and shows the helium coefficient to be a few per cent higher than that for air. The helium properties used in the NASA analyses are almost identical to those

¹"GCR Quar. Prog. Rep. June 30, 1960," ORNL-2964, pp. 23-26.

²M. E. Davenport and P. M. Magee, "Heat Transfer to a Gas at High Temperature," Technical Report No. 247-1 (May 1960), Nuclear Technology Laboratory Stanford University.

³M. F. Taylor and T. A. Kirchgessner, "Measurement of Heat Transfer and Friction Coefficients for Helium Flowing in a Tube at Surface Temperatures Up to 5900°R," NASA-PN-D-133 (October 1959).

for the EGCR helium, and therefore it is probable that the extrapolations of air data to the EGCR helium operating conditions were conservative by 4 or 5%. This conclusion is fortified by recent data on the thermal conductivity of helium which indicate that the thermal conductivity data used in the EGCR calculations were probably 5 to 10% low. Thus, the $\pm 10\%$ factor used, although much less than the 30% used in the hazards summary report,⁴ is justified by the additional experimental data for both heat transfer and thermal conductivity.

Ten items are considered in a hot-channel analysis. Each of these items is treated as a random variable whose frequency function is assumed to be rectangular. The assumption that the frequency functions are rectangular is made both for simplicity and for conservatism. When one specifies a dimension or design parameter as some value plus or minus a given uncertainty, it would be expected that the actual value would lie within the plus or minus bounds specified and would most probably peak near the specified value. Rather than attempt to anticipate the frequency function of each variable, it has been assumed that any value between the two extremes is equally likely; that is, a rectangular distribution is assumed. The factors considered, the tolerance range on each factor, and the variance are listed in Table 2.1.

Two cases were considered, normal operation and operation with an additional 10% heat input. For normal operation the weight-flow term is expressed in terms of five other variables which appear in the first column. This is due to the "feedback" from the exit gas temperature and the orifice position. In the second case it is assumed that the channels receiving the additional 10% power do not receive any additional flow. These conditions require a different analysis in that there is no longer any "feedback" from the exit gas temperature to the orifice position; thus, the precision with which the flow is known must be calculated for the normal operating case and then applied to the new conditions. The data for both cases are for the orifices set for uniform exit gas temperature from all channels.

⁴"Experimental Gas-Cooled Reactor Preliminary Hazards Summary Report," ORO-196 (May 1959).

Table 2.1. EGCR Hot-Channel Factors

Outlet gas temperature: 1075°F
 Maximum surface temperature: 1466°F
 Film temperature drop at maximum surface temperature: 621°F
 Gas temperature rise to maximum surface temperature: 335°F
 Inlet temperature: 510°F

| Hot-Channel Factors | Normal Operation | | Normal Operation Plus 10% Additional Heat Input | |
|------------------------------------|------------------|-------------------------------|---|-------------------------------|
| | Deviation | Variance (°F ²) | Deviation | Variance (°F ²) |
| 1. Inlet temperature | ±10°F | 7.458 | ±10°F | 33.3 |
| 2. Fission cross section | ±2% | 2.050 | ±2% | 147.6 |
| 3. Radial flux | ±1% | 0.513 | ±1% | 36.9 |
| 4. Axial flux | ±2% | 121.9 | ±2% | 147.6 |
| 5. Fuel volume per length | ±1 1/2% | 28.92 | ±1 1/2% | 35.03 |
| 6. Sleeve diameter | ±1/6% | 4.320 | ±1/6% | 5.23 |
| 7. Fuel rod diameter | ±4/5% | 59.23 | ±4/5% | 71.6 |
| 8. Heat transfer coefficient | ±10% | 1285 | ±10% | 1555 |
| 9. Thermocouple error | ±25°F | 452.0 | | |
| 10. Indicated thermocouple reading | ±25°F | 452.0 | | |
| 11. Coolant weight flow | | | | 1314 |
| | | $\sigma = 49.1^\circ\text{F}$ | | $\sigma = 57.8^\circ\text{F}$ |

The variance of the sum of all the factors is the sum of the individual variances, and the standard deviation of the sum of all factors is the square root of the variance. Thus the result is the standard deviation of some, as yet unknown, frequency function. As the number of factors considered increases, the frequency function of their sum must approach a normal frequency function. As shown by Abernathy,⁵ the sum of five rectangular frequency functions very closely approaches a normal distribution, so the addition of five more factors can only further decrease the difference between the actual and a normal distribution. The probability values given in Table 2.2 were therefore based on a normal distribution.

The data of Table 2.2 give the probability of the surface temperature of any one element exceeding the expected temperature by the amount

⁵F. H. Abernathy, "The Statistical Aspects of Nuclear Reactor Fuel Element Temperature," ORNL CF-60-7-31 (to be published).

Table 2.2. Probability That the Fuel Element Surface Temperature Will Exceed the Mean Surface Temperature by the Indicated Amount

| Temperature Difference (°F) | Probability | |
|--------------------------------|--|---|
| | Normal Operation $\bar{T} = 1466^{\circ}\text{F}$ $\sigma = 49.1^{\circ}\text{F}$ Max. Dev. = 190°F | Operation at 10% Above Normal $\bar{T} = 1562^{\circ}\text{F}$ $\sigma = 57.8^{\circ}\text{F}$ Max. Dev. = 284°F |
| 0 | 0.500 | 0.500 |
| 10 | 0.420 | 0.431 |
| 20 | 0.342 | 0.367 |
| 30 | 0.270 | 0.301 |
| 40 | 0.207 | 0.247 |
| 50 | 0.152 | 0.192 |
| 60 | 0.1115 | 0.150 |
| 70 | 0.0770 | 0.113 |
| 80 | 0.0520 | 0.0830 |
| 90 | 0.0335 | 0.0600 |
| 100 | 0.0209 | 0.0415 |
| 110 | 0.0125 | 0.0284 |
| 120 | 0.0074 | 0.0189 |
| 130 | 0.00405 | 0.0123 |
| 140 | 0.00219 | 0.00775 |
| 150 | 0.00111 | 0.00470 |
| 160 | 0.00056 | 0.00283 |
| 170 | 0.000275 | 0.00162 |
| 180 | 0.000124 | 0.00093 |
| 190 | 0.0000 | 0.00051 |

shown. The number of assemblies in any channel which can be subjected to these high uncertainties is two; the number of individual elements per channel is 14; and for normal operation the total number of elements in the reactor is 3248. The values in Tables 2.1 and 2.2 are based on a uniform exit gas temperature from all channels, so the lower power channels will have lower surface temperatures and also smaller hot-channel factors. Thus the effective number of elements to which the probability figures of Table 2.2 apply will be somewhat smaller than the total number of elements. The channels that may experience the temperature indicated for operation at 10% above normal will be limited

to those adjacent to an empty fuel channel, or, at most, eight channels. Thus the number of elements to consider for this case is 112.

Failure Criteria

The ultimate objective of all of these analyses is to evaluate the over-all performance of the fuel elements, which, in the reactor, will be measured by the number of failures. If it is assumed that the fuel assemblies are properly fabricated and inspected, the two factors which will lead to failure are excessive temperatures and/or excessive fission-gas release. Either of these factors or a combination of the two must be considered in estimating a failure rate for the EGCR fuel elements. The maximum allowable temperature has been set at 1800°F, and any element operating above this temperature is assumed to fail. Both physical property and compatibility data on type 304 stainless steel are now available up to 1800°F, and satisfactory operation at this temperature appears to be possible. The selection of 1800°F as the point of failure is based primarily on the lack of data above this temperature and not on any specific properties or reactions.

The second method of failure postulated for the fuel elements is rupture as a result of internal fission-gas pressure buildup. For this case it is assumed that the operating time of the element will be limited to the time when the internal pressure on the capsule is equal to the external pressure. Again, this limit is conservative because the cladding has considerable strength and any failure must result from excessive creep strain and be time dependent. It should be emphasized that this analysis is for normal long-time operation only. For short-time temperature excursions or the maximum credible accident in which the coolant system pressure is lost, the determination of failures should be based on the tube-burst data reported previously.⁶

⁶"GCR Quar. Prog. Rep. Dec. 31, 1959," ORNL-2888, p. 78.

Fission-Gas Release

In studying the fission-gas release and pressure buildup within a fuel element, a diffusion coefficient of 10^{-10} sec⁻¹ at 1400°C and an activation energy of 70 kcal/g·mole up to a temperature of 1600°C are assumed for normal operation. For long-time operation above 1600°C, it is assumed that there is 100% release of the fission gas. For short-time accident conditions and a temperature of 1600 to 1800°C, a linear release rate of 2% is assumed for the first 1 1/2 hr, and a release rate proportional to the square root of time is assumed thereafter. The additional release between 1 1/2 and 9 hr is assumed to be 8%. For short times between 1800 and 2000°C, a linear rate of release of 1%/min is assumed. For short times above 2000°C, it is assumed that there is 100% release of the fission gas.

These design data evolved from an analysis⁷ of determinations made in four types of experiments: (1) postirradiation measurements of the rate of release of Xe¹³³ or Kr⁸⁵ from neutron-activated samples of UO₂ in the temperature range 1000 to 2000°C, (2) postirradiation puncture test of miniature capsules irradiated in the LITR under EGCR conditions, (3) puncture tests of prototype EGCR fuel capsules after irradiation in the ORR and the ETR, and (4) the instantaneous fission-gas-release experiments in the C-1 lattice position of the ORR. The actual values of D' at 1400°C found from the experiments ranged from 10^{-10} to 10^{-14} ; thus the design value used is an upper limit for the release rate. These values are in agreement with those obtained in recent work at Chalk River.

These design data were applied to the EGCR operating conditions, and the UO₂ temperatures and the fission-gas pressure buildup were computed by use of a code⁸ developed for the IBM-704. In using the code

⁷J. L. Scott, "Interim Report on Release of Fission Gases from UO₂," ORNL CF-60-8-15 (to be issued).

⁸M. W. Rosenthal, "PANDORA -- A Computer Program for Estimating Fission Gas Release and Its Effect on the Mechanical Life of Clad Fuel Elements," ORNL CF-60-5-1 (to be issued).

an assumption must be made for the gas-gap, or contact resistance, between the cladding and the UO_2 . For the results reported below, the resistance was assumed to be equivalent to a 0.001-in. gas gap. The transfer of heat across the gap is by conduction and radiation, and therefore, as the fission gases dilute the helium with which the capsule is originally filled, the conductance is reduced. The variation in conductance across this resistance for the element operating under the most adverse conditions is from 2100 Btu/hr.ft².°F at initial conditions to about 580 Btu/hr.ft².°F at the end of an exposure of 9600 Mwd/MT. This is the burnup received by any assembly experiencing the largest gas release in a channel which receives an average of 9800 Mwd/MT for the entire channel of six assemblies.

In selecting the gap resistance for the elements, several factors were considered. The cold clearance between the cladding and the UO_2 pellets may vary from 0.002 to 0.006 in. on the diameter; i.e., a mean gap width of 0.001 to 0.003 in. Examination of the relative behavior of the cladding and pellet under reactor operating conditions shows that, for the peak power region that is of primary concern, the UO_2 will grow and close the cladding-to- UO_2 gap. The final hot clearance as a function of the cold clearance for 100% helium as the fill gas and for a fill gas with a conductance 0.276 times that of 100% helium is shown in Fig. 2.1. The lower conductance is that for the gas in the gap at the end of life of an element. The conditions for this curve correspond to those existing at the highest temperature region of the reactor where the fission-gas-release rate is a maximum. As the fission products are released from the UO_2 , the helium is diluted and the UO_2 temperature increases and reduces the gap as shown by the lower curve of Fig. 2.1.

In addition, the cladding will collapse onto the pellets. Tests have been completed in which the temperature gradient in the UO_2 has been simulated by a tantalum resistance heater inserted down the center of a stack of clad UO_2 pellets. The cladding, when subjected to a mean temperature of 1400°F and an external pressure of 320 psia, collapsed onto the pellets in 24 to 36 hr. No longitudinal wrinkles were formed, even though the original diametral clearance was about 0.010 in.

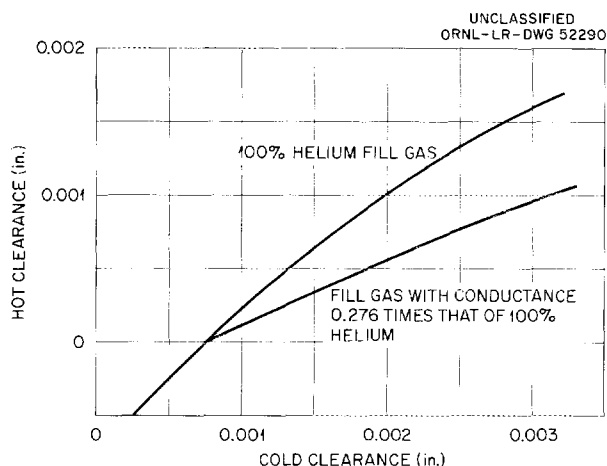


Fig. 2.1. Hot Clearance Between Cladding and UO_2 as a Function of Cold Clearance for Peak Power Region of EGCR.

No hot-channel factors have been applied to the analysis of the UO_2 temperature or to fission-gas release. The UO_2 temperature is dependent on the four factors: heat generation rate, gap resistance, quantity of gas released, and thermal conductivity. The heat generation rate has been assumed to be the maximum (62 in. insertion of control rod bank) for the entire life of a fuel channel.

The equivalent gap resistance used is the same as that assumed in the hazards summary report⁴ and is believed to be conservative. The fission-gas release is calculated from the maximum value of D' found from the experimental program. The value of thermal conductivity is based on the data of Hedge and Fieldhouse⁹ and has been found to be in good agreement with the data for irradiated UO_2 that have been obtained by both Westinghouse and Chalk River. Thus, the use of the upper expected value for three of the four factors affecting the UO_2 temperature and fission-gas release leads to calculated values which are conservative, and no additional allowances are warranted. In addition, the fuel elements will be examined at different stages of their life in the reactor to determine the actual fission-gas-release rate and, if necessary, their lifetimes will be limited to prevent hazardous operation.

The internal temperature profile, fission-gas release, and internal pressure for each fuel assembly in the maximum power channel for the inverted fuel loading program have been computed using the fuel element

⁹J. C. Hedge and I. B. Fieldhouse, "Measurement of Thermal Conductivity of Uranium Oxide," Armour Research Foundation Report G022D3 (1956).

life code. Table 2.3 gives the results of calculations for the reactor operating with the central control rod fully inserted, the balance of the control rods inserted as a bank to a depth of 62 in., and the fuel channels orificed for a uniform coolant outlet temperature of 1075°F. As discussed above, a constant cladding-to-UO₂ radial gap of 0.001 in., a noble-fission-gas effective diffusion coefficient of 10⁻¹⁰ sec⁻¹ at 1400°C, and a fission-gas-diffusion activation energy of 70 kcal/g·mole up to 1600°C were assumed in this analysis. Since these fission-gas diffusion parameters apply only for UO₂ temperatures of 1600°C (2912°F) or less, the axial temperature profile in each assembly was computed from the average cladding and UO₂ temperatures of the fission-gas-release

Table 2.3. Results of EGCR Fuel Element Life Calculations

$$D'_{1400^{\circ}\text{C}} = 10^{-10} \text{ sec}^{-1}$$

$$E_a = 70 \text{ kcal/g}\cdot\text{mole}$$

| | Fuel Assembly | | | | | |
|---|---------------|--------|--------|--------|--------|------------|
| | A | B | C | D | E | F |
| Initial assembly position within fuel channel | 1 (top) | 2 | 3 | 4 | 5 | 6 (bottom) |
| Heat generation rate, Btu/hr·ft | 800 | 4 500 | 19 000 | 32 700 | 30 800 | 14 900 |
| Average surface temperature, °F | 1 080 | 1 120 | 1 270 | 1 350 | 1 150 | 765 |
| Peak surface temperature, ^a °F | 1 185 | 1 245 | 1 475 | 1 575 | 1 535 | 1 160 |
| Internal pressure at exposure period midpoint, psia | 43 | 49 | 77 | 172 | 99 | 51 |
| Proportion of fission gas released at exposure period midpoint, % | 3.0 | 3.0 | 3.0 | 8.8 | 3.5 | 3.0 |
| Fuel exposure at exposure period midpoint, Mwd/MT of uranium | 200 | 1 300 | 5 400 | 9 400 | 8 800 | 4 300 |
| Channel position of fuel assembly during second half of exposure period | 4 | 5 | 6 | 1 | 2 | 3 |
| Internal pressure at discharge, psia | 192 | 107 | 61 | 84 | 66 | 87 |
| Proportion of fission gas released at discharge, % | 10.5 | 3.6 | 3.0 | 8.7 | 3.4 | 3.0 |
| Fuel exposure at discharge, Mwd/MT of uranium | 9 600 | 10 100 | 9 700 | 9 600 | 10 100 | 9 700 |

^aValue given is 100°F above calculated maximum surface temperature to allow for hot spots.

calculations and the detailed axial surface temperature and power distribution data. As shown in Fig. 2.2, approximately one-third of the inner surface of the UO_2 in channel position 4 operates at a temperature in

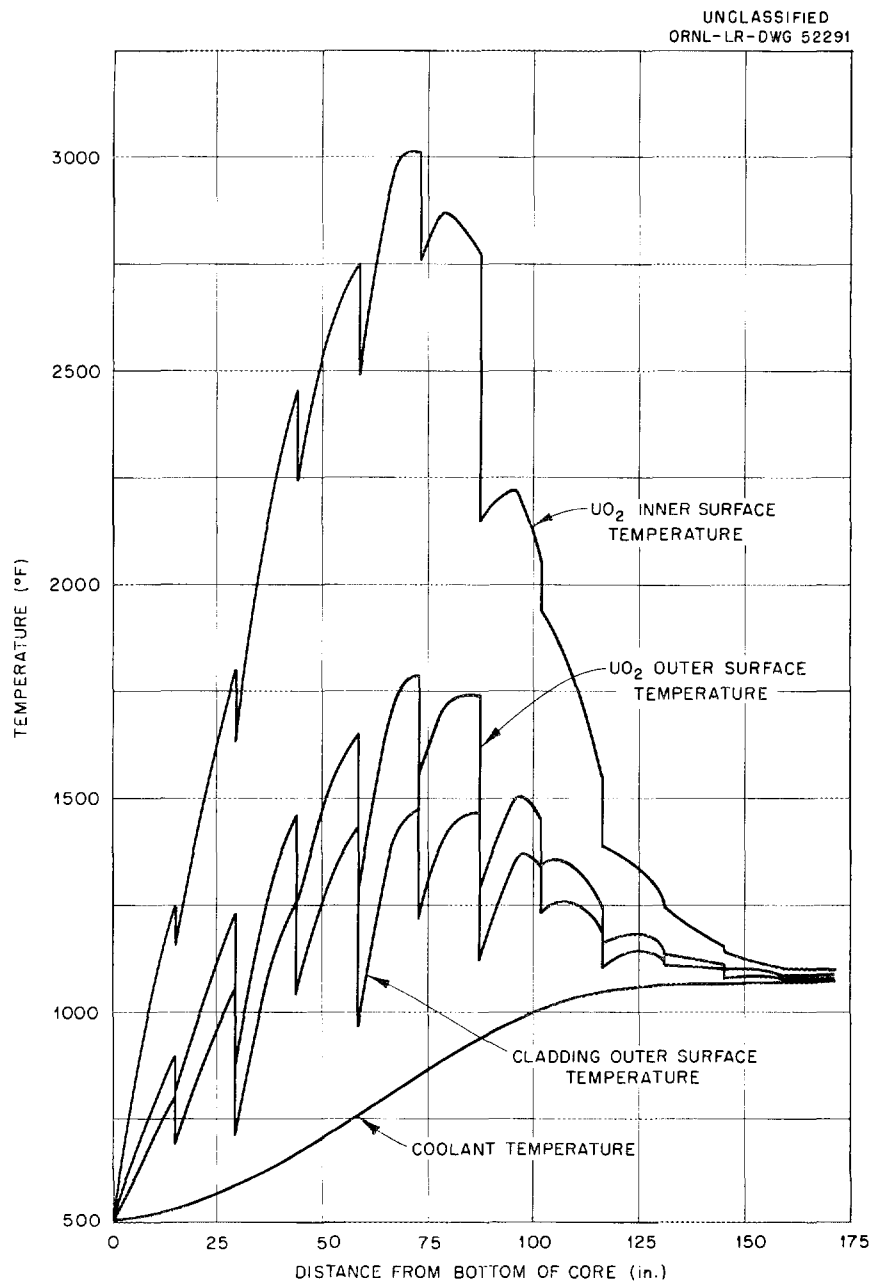


Fig. 2.2. Fuel and Coolant Axial Temperature Distributions for Channel 4-20 of EGCR.

excess of 2912°F. At the end of life, when the quantity of UO₂ at this temperature is a maximum, it amounts to only 2% of the total oxide volume in the capsule. The fuel exceeds 2912°F only during the last 120 days of irradiation (total exposure time is 1040 days); therefore the assumption of 100% release of the fission gases generated in this volume increases the total internal pressure only from 178 to 192 psia and the average gas release only from 9.1 to 10.5%. None of the fuel assemblies have final internal pressures in excess of the coolant pressure of 300 psia, and only the assembly in position 4 significantly exceeds an internal pressure of about 100 psia during the last half of its exposure period.

A second series of fuel life calculations was made with a constant 0.002-in. radial gap and all other conditions the same as in the case described above. The results of these analyses show that the fuel assembly initially loaded in channel position 4 will achieve an internal pressure slightly in excess of the coolant pressure and will accumulate a very small creep strain of the cladding very near the end of the first half of the exposure period. The internal pressure in this assembly during the second half of its exposure (in channel position 1) is well below the coolant pressure, and no further creep strain is accumulated. The assembly which is in channel position 4 during the second half of its exposure period similarly achieves an internal pressure in excess of the coolant pressure and accumulates a small creep strain. The strain reached in both these cases is well below the rupture strain. A portion of the fuel in both positions 4 and 5 will exceed a temperature of 2912°F near the end of the exposure period. The effect of the additional release due to this condition has not been factored into the internal pressure calculations, since, as shown above, the 0.002-in. radial gap condition does not truly apply in the high-power-density areas of the core.

Pressure Drop

The pressure drop across the six fuel assemblies in the highest power channel has been calculated from the air test data taken by Allis-Chalmers. An extrapolation of these data to helium operating conditions

gives a predicted pressure loss of 9.22 to 9.44 psi. The 9.22-psi value is for the case in which all six assemblies are aligned and the 9.44-psi value is for the case in which each assembly is rotated 30° with respect to those on either side. These losses include the entrance loss to the first assembly and the exit loss from the last assembly, but they do not include the losses in the dummies. The calculated losses are based on a flow of 2390 lb/hr, which is the flow in the hottest channel for the operating condition in which the orifices are set to control the maximum fuel element surface temperature. The exit gas temperature from this channel was 1052°F. If the channel is orificed to fix all exit temperatures at 1075°F, the pressure drop will be reduced by 4 or 5%. The maximum calculated loss of 9.44 psi is just within the 9.5 psi requested for the assemblies.

EGCR Control Rods

The design of the EGCR control rods has been modified to overcome difficulties encountered in attaching the central wire rope to the inside of the rod. The results of tensile tests made on stainless steel wire rope specimens indicated that, while a satisfactory attachment method could probably be developed, a portion of the rope would be in a fully annealed condition. The strength of the annealed portion of the rope would therefore be the same as an equivalent cross-sectional area of stainless steel rod. The only advantage of using a wire rope instead of a solid rod would then be that the rope would be more flexible. Since the 20-ft-long segmented rod is required to fall into a hole having a maximum bow of only 1 in., a solid 3/8-in.-diam stainless steel rod having fewer internal spacers was shown to be adequate for this design requirement.

The current design consists of four spring-loaded 5-ft-long segments having a ball-and-socket type of joint with a 3/8-in.-diam rod attached to spiders at the top and bottom of the control rod. One centering spacer on the 3/8-in. rod is used in each segment. Work has started on

assembling a mockup of this design with aluminum fillers in place of B_4C fillers.

Additional calculations on the thermal characteristics of the control rod have been made using the latest heat generation rates and axial flux distributions associated with the currently proposed operating scheme (see chap. 1). The central rod has the highest average heat generation rate, 7500 Btu/hr·ft, when fully inserted. As shown in Fig. 2.3, a coolant flow rate of 75 lb/hr down through this rod should maintain the peak cladding temperature below about 1550°F with a bottom outlet coolant gas temperature of about 1050°F. For any of the 12 outer control rods fully inserted, the heat generation rate is 5000 Btu/hr·ft. For this case, a coolant flow of 50 lb/hr is sufficient. These data are

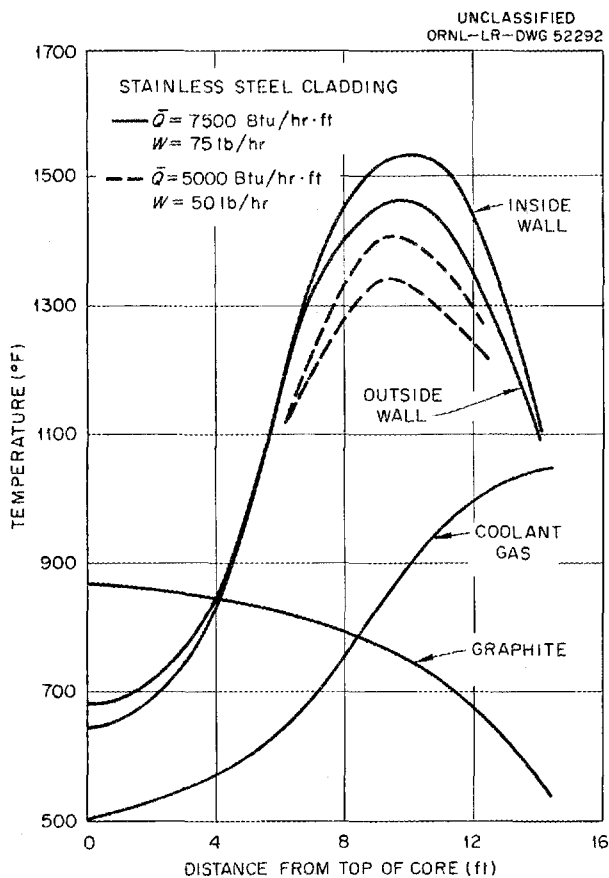


Fig. 2.3. Temperature Distribution of EGCR Control Rods.

based on calculations which include the effects of convective cooling inside the hollow rod and radiation heat transfer from the outside surface, using an emissivity of 0.6 for the stainless steel cladding (oxidized surface) and 0.8 for the graphite. As indicated in Fig. 2.3, heat is transferred from the graphite to the rod over about the top 4 ft of the rod. The graphite temperatures shown were obtained from Allis-Chalmers and were modified for the new axial flux gradient and for the reduced power generation in the surrounding graphite when the control rod is inserted.

Calculations were also made for determining the effect of the

reactor radial flux gradient on the circumferential variation in rod cladding temperature and any subsequent rod bowing. Based on the equation

$$\frac{d^2\theta}{dx^2} - m^2\theta = \frac{q'''}{k} ,$$

where

θ = temperature difference from rod to environment,

x = distance around rod,

$m^2 = hC/kA$,

q''' = volumetric heat generation rate,

h = heat transfer coefficient,

C = characteristic dimension,

k = thermal conductivity,

A = longitudinal cross-sectional area of rod,

for the case of heat conduction in a solid with simultaneous internal heat generation and heat loss to the environment, and the equation for the variation of heat generation in the rod with angle, α ,

$$\frac{q(\alpha)}{\bar{q}} = 1 - 0.1653 \cos \alpha ,$$

the following equation was derived for the EGCR control rod:

$$\theta(x) = 8.06 \bar{q}' \left(\frac{1}{6h} - \frac{0.165}{6h + 68} \cos \frac{\pi x}{0.38} \right) .$$

Using this equation, the maximum average temperature drop across the rod was found to be 181°F. This temperature drop could cause a bow of only 0.255 in. over a 5-ft-long control-rod segment and thus should not cause any difficulty in the operation of the rods.

Stress Analysis of EGCR Pressure Vessel

Experimental Results

The upper head of the pressure vessel for the EGCR has numerous nozzle penetrations. The large number of nozzles in close proximity makes an accurate theoretical analysis difficult, and the use of nozzles which are aligned vertically rather than being attached normal to the shell adds to the complexity of any analytical study. Hence, an experimental stress analysis was necessary.

A description of the nozzles in the vessel is given in Table 2.4. The control rod, special plug, and experimental loop nozzles in the upper head total 53 and form a closely spaced cluster. Since the large and small experimental loop nozzle stubs are identical to those of the

Table 2.4. Nozzles in EGCR Pressure Vessel

| Nozzle Location | Purpose | Number | Inside Diameter (in.) | Wall Thickness (in.) | Pitch (in.) | |
|-----------------|--|--------|-----------------------|----------------------|-------------|--|
| Top head | Burst-slug detection tube and thermocouple | 2 | 28 ^a | 2 | | |
| | Control rod | 25 | 11 1/8 | 1 3/16 | 24 | |
| | Experimental loop | Large | 4 | 11 1/8 | 1 3/16 | |
| | | Small | 4 | 7 3/4 | 7/8 | |
| | Special plug | 20 | 7 3/4 | 7/8 | 24 | |
| | Gas outlet | 2 | 34 | 2 1/2 | | |
| Bottom head | Experimental loop | 4 | 14 ^b | | | |
| | | 4 | 7 | 1 | 24 | |
| | Fuel charging | 12 | 16 1/2 | 1 3/4 | 32 | |
| | | 9 | 12 | 1 1/4 | 32 | |
| | Gas inlet | 2 | 22 | 2 | | |
| | Thermocouple | 2 | 11 1/2 | 1 1/4 | | |

^aThe diameter used for the scale model was 22 in.

^bOutside diameter.

control rod and special plug nozzles, respectively, only two types are represented. Each size is spaced on a 24-in. square pitch, giving an effective spacing of 12 in. and a minimum distance between nozzles of 5.47 in. All the nozzles extend through the pressure vessel to provide added reinforcement around the openings, and full penetration welds are used throughout.

A model of the upper head and the adjacent portion of the cylindrical section was fabricated from 6061 aluminum plate and instrumented with bonded-wire strain gages. The hemisphere was cold formed on a male die, and the cylindrical section was cold rolled to shape. A flange for attachment to the bottom of the cylinder was also cold rolled. The size of the male die dictated the scale factor which is $1/5.533$.

Heliarc welding techniques were used in forming the welded joints between the spherical and cylindrical sections, between the cylindrical section and the flange, and along the entire length of the cylinder. Each weld was radiographically inspected.

The shell was machined on both its inner and outer surfaces prior to installing the nozzles. Each nozzle was given a letter designation corresponding to the radius from the apex to its center. The central nozzle was designated A.

The holes for the nozzles were bored, and the two surfaces of the shell were scarfed for full-penetration welds. The Heliarc process was used in making these welds, and they were ground to provide $1/16$ -in. radius fillets between the nozzles and the sphere at both the inside and outside surfaces. Finally, all welds were inspected by radiographic techniques.

The nozzle at the apex was installed first; then holes were machined for the immediately adjacent nozzles whose centers lie on a common circle about the apex. After these nozzles were welded in place, those on the next circle were installed, and the procedure was repeated. This step-wise process was necessary in order to allow working room for finishing the fillets and to prevent excessive warpage in the head due to welding.

Since the stress distribution around any nozzle in the cluster is influenced by the neighboring nozzles, distributions similar to those in a perforated plate were expected to exist. The interaction between holes is illustrated in Fig. 2.4, where the tangential stresses around the edge of a hole in a perforated plate under biaxial tension have been plotted. From this figure it may be seen that the highest stresses exist along lines joining the centers of the holes. Therefore, the gages on the spherical shell were positioned to measure these peak stresses. In some cases, however, the locations and orientations were chosen to coincide with the circumferential and meridional directions of the shell.

All gages on the outside surfaces of the spherical head and cylindrical section were matched with corresponding gages on the inside surfaces so that both the membrane and bending stress components could be calculated from the measured strains. The locations of the gages on the outside of the shell are shown in Fig. 2.5, and those on the inside surface, including the inside of nozzle A, may be seen in Fig. 2.6.

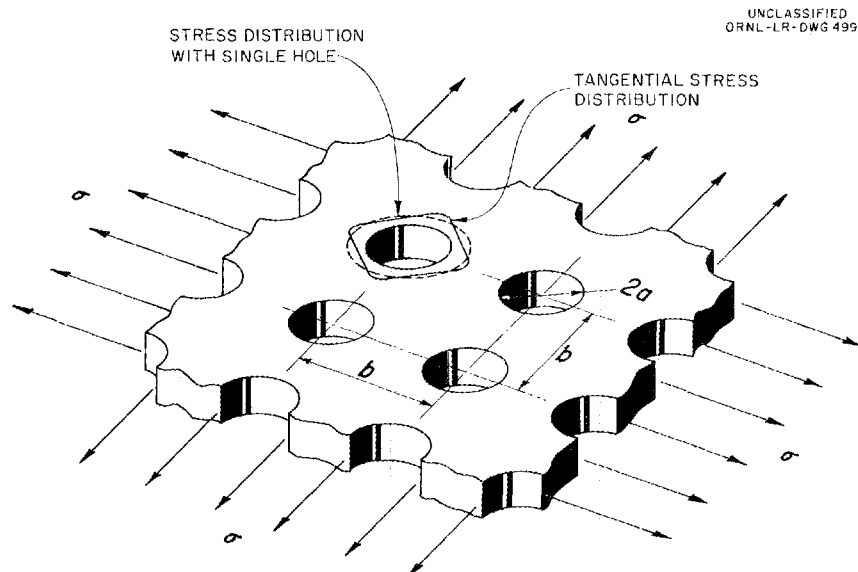


Fig. 2.4. Tangential Stress Distribution Around Hole in Perforated Plate for $a/b = 0.27$.

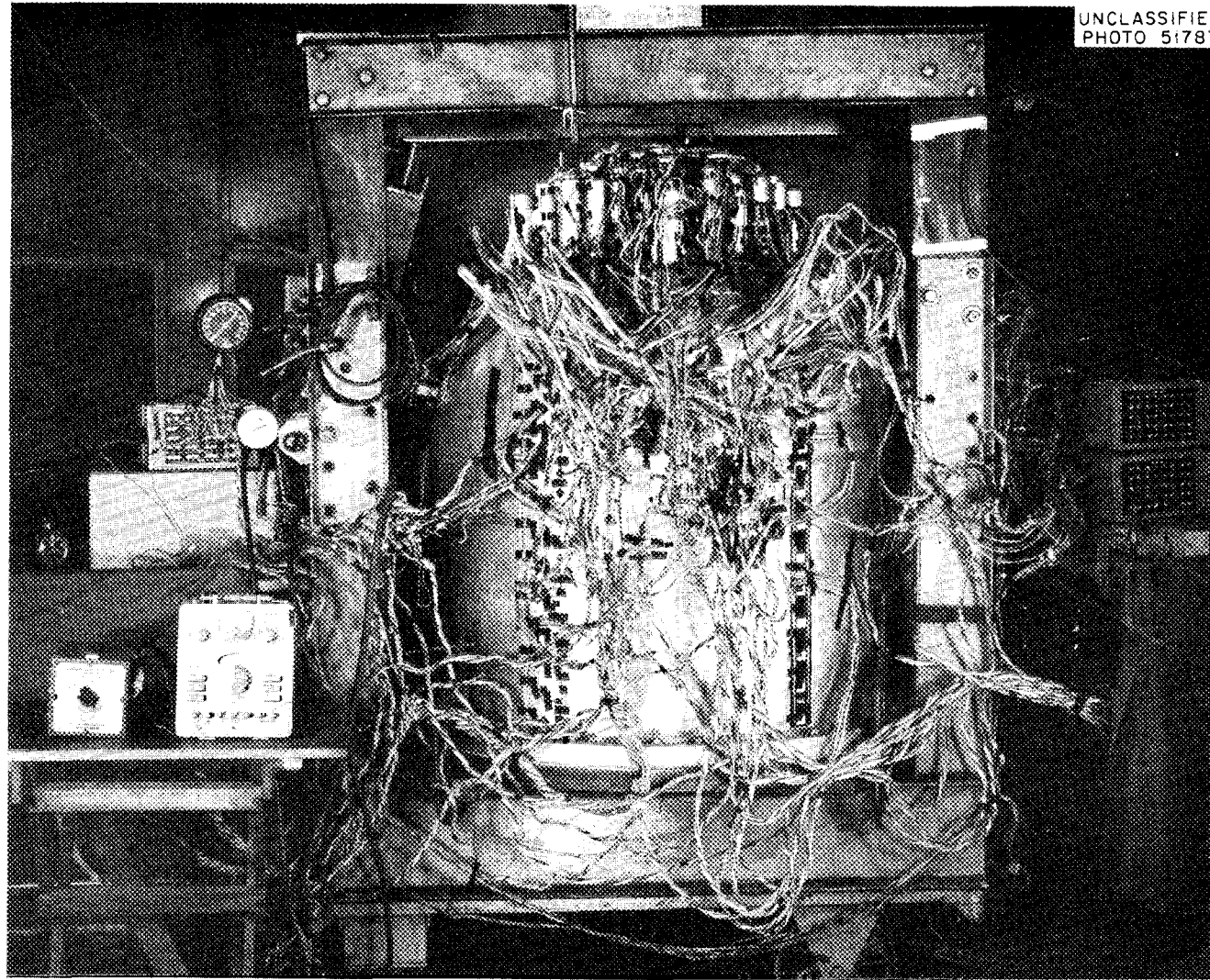


Fig. 2.5. Pressure Vessel Head Model in Loading Frame Ready for Testing.

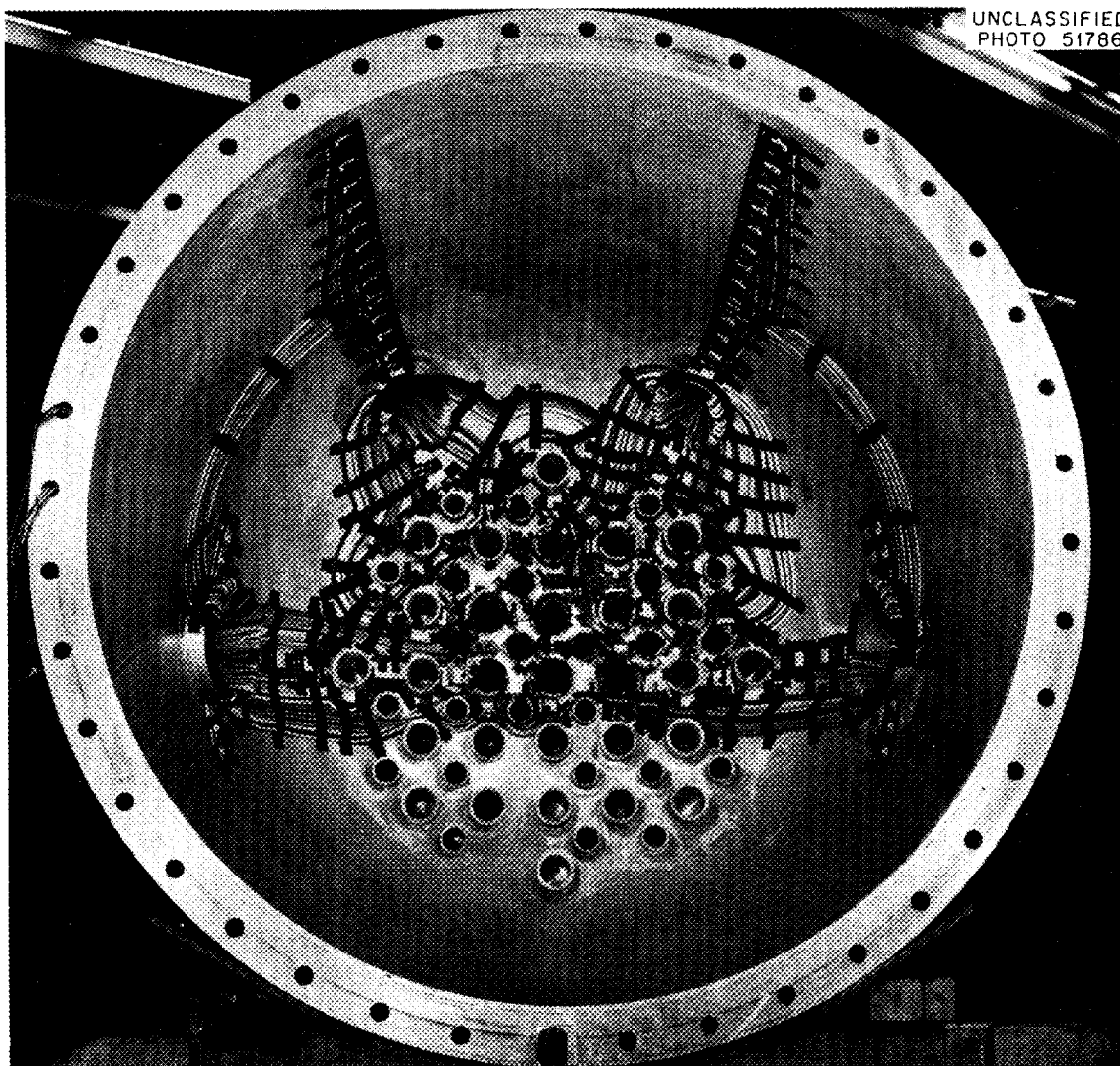


Fig. 2.6. Strain Gage Installation on Inside of Model Shown in Fig. 2.5.

Bonded wire SR-4 strain gages, type A-7, with a gage length of $1/4$ in. were used in all cases; the total number of gages was 976.

One-half the dome was instrumented, and gages were evenly spaced in two axial rows along the cylindrical section of the shell so that duplicate strain readings could be obtained for each point. These duplicate readings were used in checking the results. Two gages oriented at 90 deg to each other were mounted at each position; they were aligned

in the anticipated directions of the principal strains. The principal strain directions were later confirmed by observing the cracks in Stress-Coat lacquer that was applied to a nozzle under an axial load. After the lead wires were connected, each gage was checked for grounding and air bubbles in the cement.

The model was tested under an internal pressure of 60 psig with the nozzle loadings given in Table 2.5. Each load was applied singly so that stresses for various combined loads could be obtained by superposition. However, a separate test was conducted in which the nozzle at the apex (A) was subjected to an axial force of 2000 lb while the pressure in the vessel was 60 psig. The data derived provided a basis for checking the validity of superposition for this particular case.

The magnitudes of all the loadings were made as large as possible so that maximum strain readings could be obtained. The limiting value of the load was determined in each case by the strain value at the yield-point stress. A maximum allowable strain of approximately 400 μ in./in. was used, corresponding to a stress of 4000 psi. (The yield-point stress for annealed 6061 aluminum plate is approximately 5000 psi.)

All the normal forces, except that on A, were applied in the axial plane through nozzle A, with the load acting in the direction toward A. The normal load on A was applied in an axial plane passing through the gas outlet nozzles. The distances above the apex for points of load application correspond to the locations of the upper and lower surfaces of the biological shield in the cases of both the control rod and special plug nozzles. For the experimental loop nozzles, the distances correspond to the locations of the external piping attachment points.

In conducting all tests, gage readings were recorded at zero load, one-half load, full load, and, finally, at zero load again. Thus, the linearity and drift of the gages were checked.

The experimental results for all the tests have been reported.¹⁰ The report also gives a complete description of the model, strain-gage

¹⁰R. W. Holland and R. L. Maxwell, "Experimental Determination of Stresses In the Top Head of the EGCR Pressure Vessel," University of Tennessee Engineering Experiment Station, Department of Mechanical Engineering (August 1960).

Table 2.5. Loads Applied to Nozzles in Top Head

| Nozzle Type | Reference Circle | Reference Circle Radius (in.) | Type of Load | Magnitude of Load | Moment Arm ^a (in.) |
|-------------------------|------------------|-------------------------------|-------------------|---|-------------------------------|
| Control rod | A | 16.991 | Axial | 2 000 lb | |
| | | | Normal | 150 lb | 13 3/16 |
| | | | | 50 lb | 34 3/4 |
| | M | 72.085 | Axial | 2 000 lb | |
| | | | Normal | 150 lb | 13 3/16 |
| | | | | 50 lb | 34 3/4 |
| Special plug | J | 61.259 | Axial | 1 500 lb | |
| | | | Normal | 80 lb | 13 3/16 |
| | | | | 30 lb | 34 3/4 |
| | L | 70.052 | Axial | 1 500 lb | |
| | | | Normal | 80 lb | 13 3/16 |
| | | | | 30 lb | 34 3/4 |
| Small experimental loop | B | 16.991 | Axial | 1 500 lb (one nozzle) | |
| | | | Normal | 1 500 lb (four nozzles loaded simultaneously) | 25 1/4 |
| Large experimental loop | K | 67.960 | Axial | 2 000 lb | |
| | | | Normal | 75 lb | 24 9/16 |
| Gas outlet | | | Axial | 5 000 lb | |
| | | | Transverse moment | 19 200 in.-lb | |
| | | | Meridional moment | 19 200 in.-lb | |
| | | | Transverse normal | 2 000 lb | 8 1/2 |
| | | | Meridional normal | 2 000 lb | 8 1/2 |
| | | | Torsional moment | 32 000 in.-lb | |

^aThe moment arm is the distance above the apex, except for the gas outlet nozzle, where it is measured from the surface of the shell.

locations, and the experimental techniques employed. The experimental data are now being interpreted in terms of the load-carrying capacity and structural integrity of the reactor vessel.

Comparison of Analytical and Experimental Results

The interpretation and use of the experimental data obtained from the tests described above depends upon a detailed knowledge of the stress distributions in the region of a nozzle-to-spherical-shell junction. Therefore, a theoretical model must be used as a guide; a single nozzle attached radially to a spherical segment was chosen for this purpose. Although the influence of adjacent penetrations is not represented, the stresses in the nozzles of the vessel should be similarly distributed.

The differential equations that describe the model were obtained from thin-shell theory.¹¹ In this case, the asymptotic solutions to the two differential equations for the spherical shell,

$$\frac{d^2 Q_\phi}{d\phi^2} + \cot\phi \frac{dQ_\phi}{d\phi} - \cot^2\phi Q_\phi \pm 2ik^2 Q_\phi = 0 ,$$

were taken. The complete solution is then¹²

$$Q_\phi = \sqrt{\phi/\sin\phi} (A_1 \text{ber}' \sqrt{2} k\phi + A_2 \text{bei}' \sqrt{2} k\phi + A_3 \text{ker}' \sqrt{2} k\phi + A_4 \text{kei}' \sqrt{2} k\phi) ,$$

where Q_ϕ is the shearing force, k is a constant depending upon the shell dimensions, ϕ is the colatitude angle, and the A's are integration

¹¹S. Timoshenko and S. Woinowsky-Krieger, "Theory of Plates and Shells," pp. 468, 540, 2nd ed., McGraw-Hill, New York, 1959.

¹²F. A. Leckie, "Asymptotic Solutions for the Spherical Shell Subjected to Axially Symmetric Loading," Preprints of papers to be read at the Symposium on Nuclear Reactor Containment Buildings and Pressure Vessels to be held at The Royal College of Science and Technology, 17th to 20th May, 1960, Butterworth (1960), pp. G99-G110.

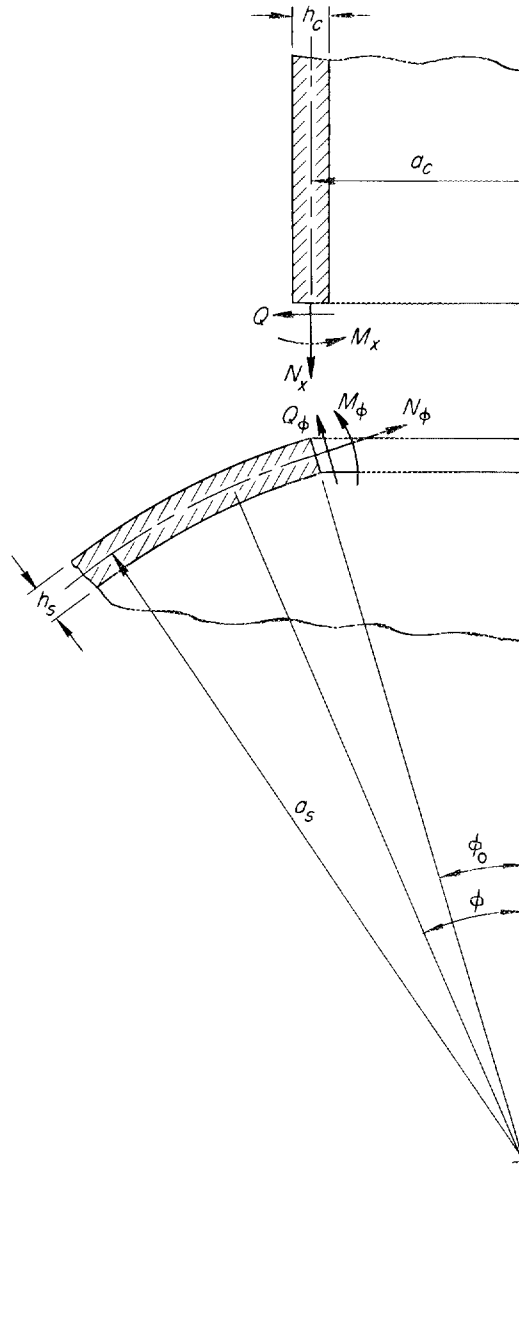


Fig. 2.8. Diagram Showing Force System at Sphere-Cylinder Junction.

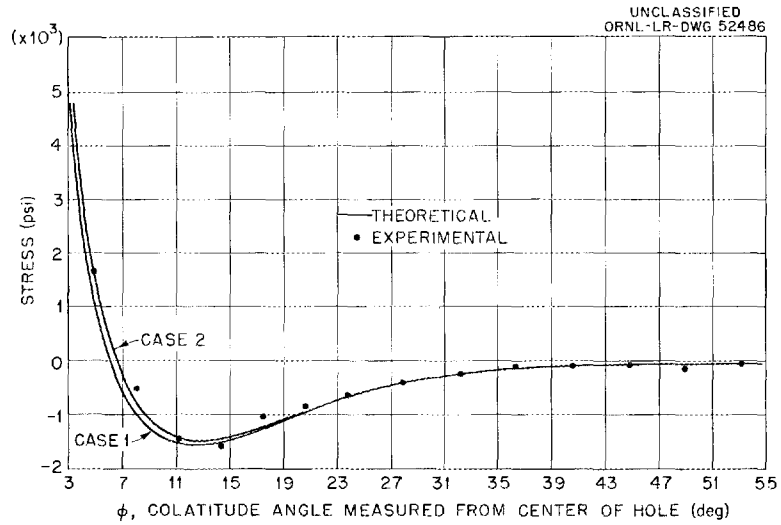


Fig. 2.9. Meridional Stresses at Inner Surface of Pressure Vessel Head Model for a Compressive Axial Force of 2000 lb.

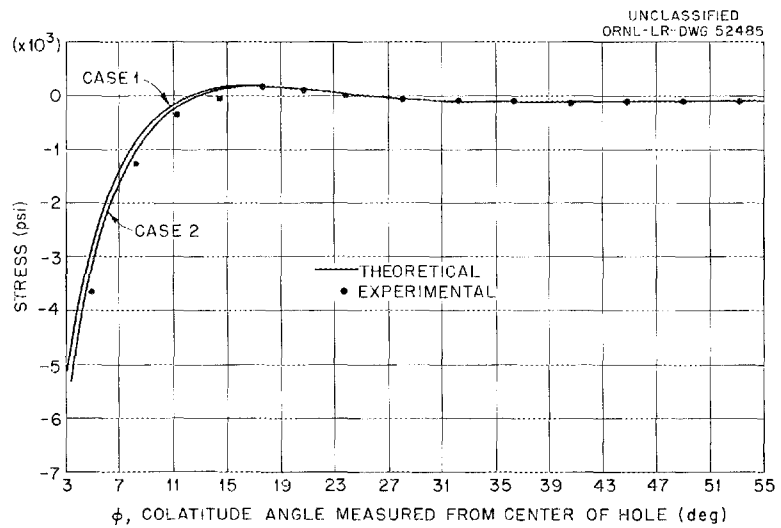


Fig. 2.10. Meridional Stress at Outer Surface of Pressure Vessel Head Model for a Compressive Axial Force of 2000 lb.

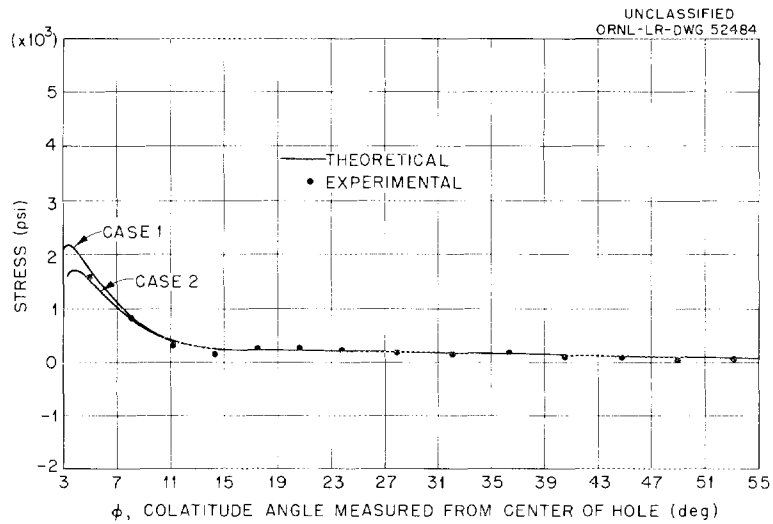


Fig. 2.11. Circumferential Stress at Inner Surface of Pressure Vessel Head Model for a Compressive Axial Force of 2000 lb.

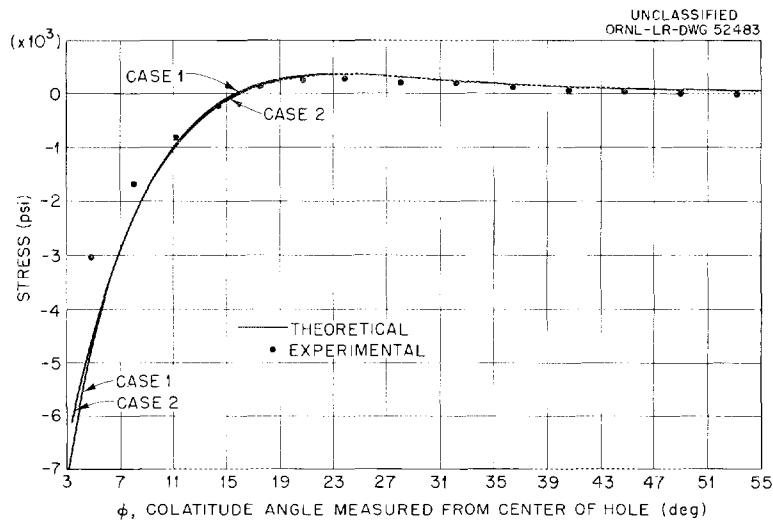


Fig. 2.12. Circumferential Stress at Outer Surface of Pressure Vessel Head Model for a Compressive Axial Force of 2000 lb.

by Leckie for the spherical shell and by Stanek¹⁴ in the case of the cylinder.

Since only tabular values of the Bessel functions were available, the exact radius and thickness of the cylinder could not be used in the theoretical analysis. Thus the two cases described in Table 2.6 were examined. The stresses are for a compressive axial force on the nozzle.

Table 2.6. Dimensions of Experimental and Analytical Models

| | Experimental Model | Case 1 | Case 2 |
|--|-----------------------|---------|---------|
| Radius to middle surface of sphere, a_s , in. | 13.4405 | 13.4405 | 13.4405 |
| Thickness of sphere, h_s , in. | 0.5070 | 0.5070 | 0.5070 |
| Radius to middle surface of cylinder, a_c , in. | 0.7500 | 0.7214 | 0.7935 |
| Thickness of cylinder, h_c , in. | 0.5000 | 0.4810 | 0.5290 |

The meridional stresses at the inner and outer surfaces are plotted in Figs. 2.9 and 2.10 while the circumferential stresses are shown in Figs. 2.11 and 2.12. The agreement is very good for both the meridional and circumferential stresses, with Case 2 more nearly duplicating the experimental results. Differences between the theoretical and experimental data, aside from those introduced through the use of approximate dimensions, can be partially attributed to the use of thin-shell theory for predicting the behavior of the cylinder. From this study it is apparent that the equations used in the analytical model adequately predict the stresses for a single nozzle-to-shell attachment.

¹⁴F. J. Stanek, "Stress Analysis of Cylindrical Shells," ORNL CF-58-9-2 (July 1959).

3. EXPERIMENTAL INVESTIGATIONS OF HEAT TRANSFER AND FLUID FLOW

Resistance-Heated-Tube Heat Transfer Experiment

A further evaluation of the data previously presented¹ for experimental series 4-A (a septafoil cluster at a 2:1 ligament-ratio spacing, $\gamma = 2$, with a modified 60-deg-pad mid-cluster spacer²) has confirmed the presence of a flow maldistribution in the channel entrance of sufficient magnitude to markedly distort the temperature patterns in the upstream half of the cluster. A number of alternate inlet-plenum arrangements³ were studied in an effort to correct this situation. In the modification examined in greatest detail, the 7/8-in. gap between the central baffle (weir) and the plenum cover plate was closed by two layers of 40 mesh (0.011-in. wire) stainless steel screen. In addition, a pair of nonmetallic screens (24 mesh with 0.0009-in.² openings) were located at the test-section inlet. These changes are indicated schematically in Fig. 3.1.

Circumferential temperature profiles were obtained for all 7 tubes at 11 axial positions with this modified inlet configuration; the data are designated series 4-B. The operational conditions were essentially identical to those for series 4-A, with the over-all mean heat flux being 6500 Btu/hr.ft² and the average Reynolds modulus, 50 500; the data were corrected⁴ to a common inlet air temperature of 97° F. Preliminary results for minimum and mean inside surface temperatures are given in Tables 3.1 and 3.2, respectively. A complete interpretation of these results will not be attempted, since a number of uncertainties exist in the data. Thus in Table 3.2, it may be seen that the mean tube temperature at the $L/d_e = 10$ position is less than that at the $L/d_e = 5$ level.

¹"GCR Quar. Prog. Rep. June 30, 1960," ORNL-2964, pp. 55-58

²"GCR Quar. Prog. Rep. Dec. 31, 1959," ORNL-2888, pp. 27-28.

³Ibid., pp. 54, 57.

⁴"GCR Quar. Prog. Rep. Sept. 30, 1959," ORNL-2835, pp. 54-59.

Table 3.1. Axial Variation in Minimum Inside Surface Temperatures for Tubes of Experiment 4-B

| Axial Position | Temperature (°F) | | | | | | |
|----------------|---------------------|-----|-----|-----|-----|-----|---------------------|
| | Peripheral Tube No. | | | | | | Central Tube, No. 7 |
| | 1 | 2 | 3 | 4 | 5 | 6 | |
| 0 | 236 | 235 | 234 | 239 | 239 | 245 | 258 |
| 5 | 379 | 355 | 340 | 366 | 346 | 359 | 582 |
| 10 | 368 | 387 | 349 | 392 | 389 | 385 | 621 |
| 15 | 383 | 407 | 383 | 411 | 414 | 415 | 520 |
| 17.9 | 391 | 411 | 398 | 422 | 414 | 421 | 481 |
| 20 | 271 | 271 | 268 | 274 | 281 | 278 | 296 |
| 22.5 | 326 | 329 | 335 | 335 | 338 | 342 | 381 |
| 25 | 367 | 366 | 373 | 372 | 379 | 380 | 437 |
| 30 | 431 | 431 | 439 | 439 | 448 | 449 | 472 |
| 35 | 466 | 470 | 479 | 473 | 484 | 480 | 489 |
| 38 | 473 | 475 | 483 | 487 | 495 | 492 | 492 |

Table 3.2. Axial Variation in Mean Inside Surface Temperatures for Tubes of Experiment 4-B

| Axial Position | Temperature (°F) | | | | | | |
|----------------|---------------------|-----|-----|-----|-----|-----|---------------------|
| | Peripheral Tube No. | | | | | | Central Tube, No. 7 |
| | 1 | 2 | 3 | 4 | 5 | 6 | |
| 0 | 245 | 245 | 243 | 247 | 246 | 249 | 262 |
| 5 | 379 | 401 | 383 | 423 | 395 | 408 | 587 |
| 10 | 393 | 408 | 381 | 418 | 409 | 412 | 633 |
| 15 | 406 | 419 | 401 | 425 | 429 | 428 | 540 |
| 17.9 | 412 | 423 | 411 | 431 | 442 | 432 | 498 |
| 20 | 280 | 278 | 279 | 281 | 288 | 287 | 305 |
| 22.5 | 340 | 341 | 346 | 346 | 352 | 355 | 388 |
| 25 | 382 | 380 | 385 | 387 | 393 | 395 | 442 |
| 30 | 444 | 441 | 446 | 448 | 457 | 461 | 476 |
| 35 | 476 | 477 | 484 | 480 | 491 | 489 | 492 |
| 38 | 480 | 480 | 489 | 491 | 500 | 496 | 495 |

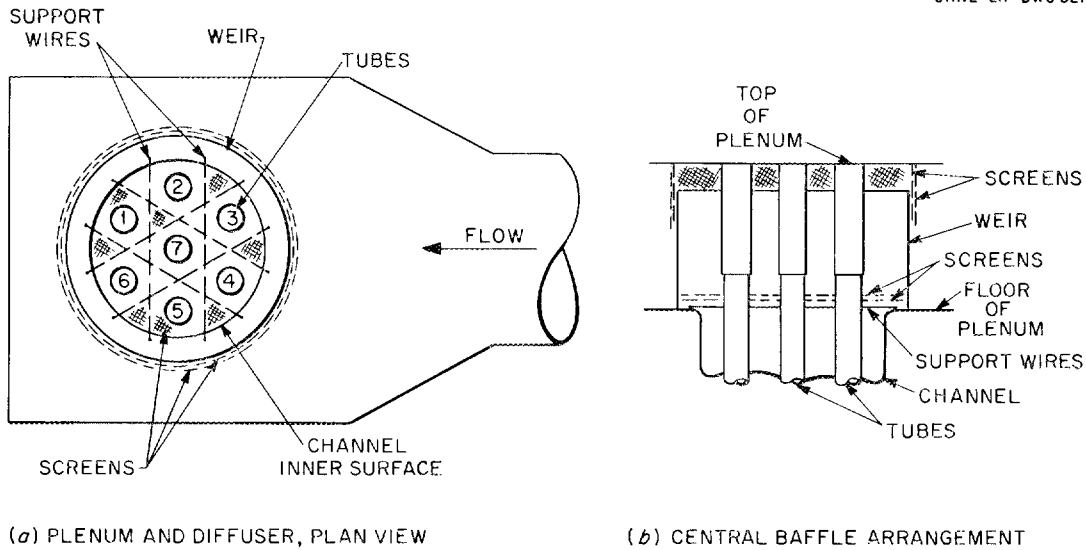


Fig. 3.1. Schematic Diagram of the Inlet Plenum Chamber of the Model-3 Heat Transfer Apparatus for the Series 4-B Experiment.

Experiments to resolve these discrepancies are in progress. Further, the mean temperatures for tubes 4, 5, and 6 are on the average higher than those for tubes 1, 2, and 3. (The relative positions of the tubes are indicated in Fig. 3.1.) While it may be speculated that these differences arise from differences in the magnitude of the flow in the two halves of the channel, the data now available are insufficient to corroborate this supposition. Alternate hypotheses are that the heat generations for the 7 tubes are not equal (a fact not borne out by the data) or that the tubes are canted within the channel (the maximum displacement possible is only 0.010 in.). This suggests that nonuniformities may exist in either or both of the sets of screens added to the inlet. Again additional experimentation is required. The central tube exhibits much higher mean temperatures than those measured for the peripheral tubes. With an average heat generation equal to that of an outer tube, it can be presumed that a flow deficiency exists in the inner region surrounding tube 7. The presence, in general, of temperature maxima on the inward facing side of the peripheral tubes (rather than on the outer side adjacent to the channel wall, as expected from the geometry)

provides some confirmation of a lower central-region flow. This aspect is examined further in the following discussion.

While an over-all understanding of the data may not be possible at this time, it is still of interest to consider some of the details. A comparison of temperature profiles for tube 4 at two axial positions, as obtained in the series 4-A and 4-B experiments, is shown in Fig. 3.2. At the $L/d_e = 5$ level, the total circumferential variation in the temperature has increased from 24°F in series 4-A to 96°F in series 4-B. In addition, the angular positions of the maximum and minimum temperatures have been reversed. This drastic shift of the temperature pattern with respect to both magnitude and location may be related to several factors inherent in the test apparatus; (1) the restriction of the flow to the central region of the cluster by the tube electrodes passing through the plenum chamber, and (2) the increased turbulence at the test-section inlet created by the screens suspended in this region. The first of these, while common to both 4-A and 4-B, may be aggravated in series

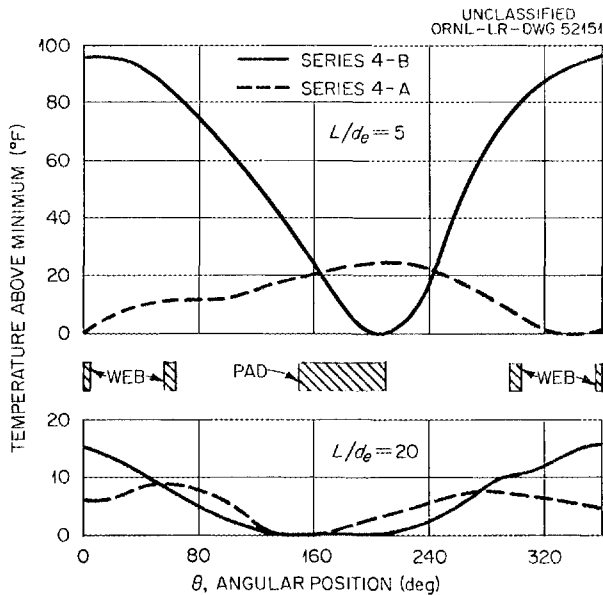


Fig. 3.2. Comparison of Series 4-A and 4-B Circumferential Temperature Profiles for Tube 4 at Two Axial Positions.

4-B by the pressure losses associated with the added screens. The result is a preponderance of the air flow in the outer regions of the channel such that the surface temperatures are lower at 180° and higher at 0° than those predicted from simple geometrical considerations. When coupled with the second factor (the turbulence level will be a function of the local velocity through the screens), there results the extreme variation indicated by the upper curve of Fig. 3.2. As expected, the magnitude of this temperature variation

for series 4-B diminishes rapidly with distance downstream, reflecting both a decrease in heat transfer as the thermal boundary layers develop and a redistribution in the gross flow between the inner and outer portions of the channel.

At $L/d_e = 20$, immediately downstream of the mid-cluster spacer (lower curves of Fig. 3.2), the circumferential distributions for 4-A and 4-B are again comparable. As discussed previously,¹ the temperature minimum in the wake of the 60-deg pad results from increased turbulence in this region. The temperature pattern for series 4-B appears more symmetrical than that observed for series 4-A; the somewhat higher maximum (16°F as against 8°F for series 4-A), occurring at the 0-deg location for series 4-B, is again indicative of the flow deficiency in the inner zone of the cluster. The effect of the webs at the 60-deg and 300-deg locations is discernable in the 4-B curve; a similar inflection expected at 0 deg is not evident.

The remaining peripheral tubes (1, 2, 3, 5, and 6) yield similar results. This is illustrated in Fig. 3.3, which compares circumferential

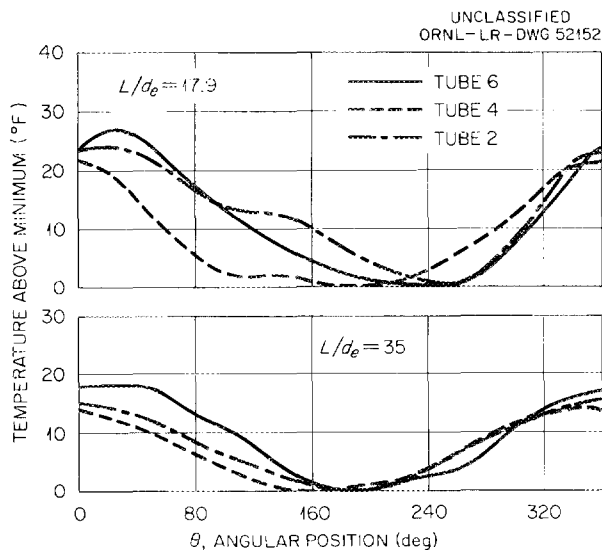


Fig. 3.3. A Comparison of Circumferential Temperature Profiles at Two Axial Positions for Tubes 2, 4, and 6 of the Series 4-B Experiment.

temperature profiles at two axial positions: the first, $L/d_e = 17.9$, being just upstream of the mid-cluster spacer, and the second, $L/d_e = 35$, being near the channel exit. The clockwise displacement of the minima for tubes 2 and 6 with respect to tube 4 is perhaps indicative of some rotational flow in the portion of the channel opposed to the plenum flow entrance (see Fig. 3.1).

The results to date with the model-3 heat-transfer apparatus at both the $\gamma = 2$ and $\gamma = 4$ tube spacings show an appreciable

sensitivity to the inlet plenum configuration. In view of the uncertainty thus created in applying these data to the prediction of surface temperatures in the EGCR, a new apparatus (model 4) is being fabricated which will incorporate two heated clusters positioned consecutively within the channel. Spacers and spiders of EGCR Title-II design² will be included. The downstream region of the two clusters will be instrumented as in the model-3 device; the upstream tube bundle will be capable of rotation to provide the complete range of reactor entrance conditions. Definitive studies with the model-3 apparatus will be continued in an effort to gain a better understanding of the effects of flow maldistributions on the heat transfer within a seven-rod cluster.

Mass-Transfer Measurements

Preliminary values have been obtained for the mass-transfer factors in the second (downstream) of two EGCR Title-II-design fuel-element clusters stacked within a Plexiglas tube.⁵ As previously indicated,⁶ traverses were made at 14 axial levels ranging from $L/d_e = 3.8$ to $L/d_e = 41.2$ (mid-cluster spacer at $L/d_e = 22.5$) for four relative displacements of the clusters with respect to each other (0, 30, 60, and 90 deg). The results are summarized in Tables 3.3 through 3.6 as the circumferential mean mass-transfer factor, j , at each axial position; the data were adjusted to a common bulk Reynolds modulus of 50 000 on the basis that $j \sim N_{Re}^{-0.2}$. Since the Reynolds modulus for these runs varied from 51 300 to 52 600, the maximum correction to j was less than 1%.

The data appear to be self-consistent (within the experimental error), with the possible exception of the runs for rod 6 at the 0-deg orientation and for rod 3 at the 30-deg orientation. In both these cases the shape of the profiles for j_l/j (where j_l is the local

⁵"GCR Quar. Prog. Rep. March 31, 1960," ORNL-2929, pp. 70-76.

⁶"GCR Quar. Prog. Rep. June 30, 1960," ORNL-2964, pp. 59-67.

Table 3.3. Mean Mass-Transfer Factors for 0-deg Cluster Orientation

| L/d _e | Mean Mass-Transfer Factor, j | | | | | | |
|----------------------|------------------------------|--------------------|--------------------|--------------------|--------------------|--------------------|--------------------|
| | Rod 1 | Rod 2 | Rod 3 | Rod 4 | Rod 5 | Rod 6 | Rod 7 |
| | × 10 ⁻³ | × 10 ⁻³ | × 10 ⁻³ | × 10 ⁻³ | × 10 ⁻³ | × 10 ⁻³ | × 10 ⁻³ |
| 3.8 | 4.42 | 4.50 | 4.66 | 4.52 | 4.66 | 4.63 | 4.33 |
| 6.1 | 3.88 | 3.98 | 4.10 | 4.01 | 4.12 | 4.13 | 3.86 |
| 9.8 | 3.63 | 3.67 | 3.81 | 3.76 | 3.63 | 3.83 | 3.50 |
| 13.6 | 3.43 | 3.42 | 3.68 | 3.60 | 3.35 | 3.52 | 3.32 |
| 17.4 | 3.34 | 3.30 | 3.59 | 3.51 | 3.26 | 3.32 | 3.21 |
| 19.6 | 3.24 | 3.27 | 3.47 | 3.31 | 3.28 | 3.25 | 3.15 |
| 21.8 | 3.25 | 3.14 | 3.36 | 3.30 | 3.14 | 3.10 | 3.00 |
| (Mid-cluster spacer) | | | | | | | |
| 23.2 | 7.71 | 7.64 | 8.12 | | | | 9.24 |
| 25.7 | 4.79 | 4.44 | 4.23 | | | | 4.53 |
| 28.1 | 4.41 | 4.06 | 4.29 | | | | 4.03 |
| 30.8 | 4.18 | 3.56 | 4.10 | | | | 3.84 |
| 35.0 | 3.97 | 3.71 | 3.92 | | | | 3.63 |
| 39.3 | 3.88 | 3.67 | 3.71 | | | | 3.56 |
| 41.2 | 3.78 | 3.65 | 3.63 | | | | 3.67 |

mass-transfer factor) as a function of angular location on the rod surface at any level differs from the profiles obtained for the other rods at the same levels. This is particularly noticeable at stations below $L/d_e = 9.8$. At the same time, it is of interest to note that, despite the abnormal variations in the local values, the mean j factors are in reasonable agreement with those for the other runs. While extreme care was exercised in handling the rods, it is possible that in these instances the coated rod could have been bent during installation in or removal from the cluster. Since this would have occurred after the initial profilometer readings had been made, a consistent bias (varying from zero at the inlet end to a maximum at the center) would have been introduced; the runs in question display this characteristic. The average mass removal during a run is of the order of 0.010 in.; thus, a small permanent displacement of the rod would be sufficient to over-shadow completely the real variations in the mass removal.

Table 3.4. Mean Mass-Transfer Factors for 30-deg Cluster Orientation

| L/d_e | Mean Mass-Transfer Factor, j | | | |
|----------------------|--------------------------------|------------------|------------------|------------------|
| | Rod 1 | Rod 2 | Rod 3 | Rod 7 |
| | $\times 10^{-3}$ | $\times 10^{-3}$ | $\times 10^{-3}$ | $\times 10^{-3}$ |
| 3.8 | 4.50 | 4.20 | 4.46 | 4.60 |
| 6.1 | 3.94 | 3.76 | 4.00 | 4.12 |
| 9.8 | 3.45 | 3.51 | 3.57 | 3.87 |
| 13.6 | 3.26 | 3.41 | 3.32 | 3.67 |
| 17.4 | 3.20 | 3.21 | 3.32 | 3.60 |
| 19.6 | 3.02 | 3.08 | 3.28 | 3.57 |
| 21.8 | 2.95 | 3.00 | 3.22 | 3.40 |
| (Mid-cluster spacer) | | | | |
| 23.2 | 7.68 | 8.26 | | 8.85 |
| 25.7 | 4.54 | 4.95 | | 4.17 |
| 28.1 | 4.11 | 4.46 | | 3.75 |
| 30.8 | 3.94 | 4.17 | | 3.47 |
| 35.0 | 3.60 | 3.93 | | 3.15 |
| 39.3 | 3.49 | 3.72 | | 3.27 |
| 41.2 | 3.41 | 3.68 | | 3.35 |

Table 3.5. Mean Mass-Transfer Factors for 60-deg Cluster Orientation

| L/d_e | Mean Mass-Transfer Factor, j | | | |
|---------|--------------------------------|------------------|------------------|------------------|
| | Rod 1 | Rod 2 | Rod 3 | Rod 7 |
| | $\times 10^{-3}$ | $\times 10^{-3}$ | $\times 10^{-3}$ | $\times 10^{-3}$ |
| 3.8 | 4.47 | 4.11 | 4.30 | 4.43 |
| 6.1 | 4.01 | 3.78 | 3.84 | 3.92 |
| 9.8 | 3.69 | 3.68 | 3.56 | 3.66 |
| 13.6 | 3.46 | 3.27 | 3.35 | 3.53 |
| 17.4 | 3.36 | 3.18 | 3.33 | 3.44 |
| 19.6 | 3.36 | 3.13 | 3.33 | 3.35 |
| 21.8 | 3.31 | 2.98 | 3.17 | 3.34 |

Table 3.6. Mean Mass-Transfer Factors for 90-deg Cluster Orientation

| L/d _e | Mean Mass-Transfer Factors, j | | | |
|------------------|-------------------------------|--------------------|--------------------|--------------------|
| | Rod 1 | Rod 2 | Rod 3 | Rod 7 |
| | × 10 ⁻³ | × 10 ⁻³ | × 10 ⁻³ | × 10 ⁻³ |
| 3.8 | 4.88 | 4.60 | 4.65 | 5.21 |
| 6.1 | 4.31 | 4.12 | 4.04 | 4.56 |
| 9.8 | 4.00 | 3.83 | 3.66 | 4.30 |
| 13.6 | 3.84 | 3.69 | 3.45 | 4.10 |
| 17.4 | 3.64 | 3.57 | 3.23 | 3.88 |
| 19.6 | 3.55 | 3.51 | 3.42 | 3.76 |
| 21.8 | 3.44 | 3.38 | 3.31 | 3.69 |

For some runs, the interpretation of the circumferential profiles was rather difficult because of a lack of precision in the data. While the cause of this decrease in precision is uncertain, factors such as occlusions in the naphthalene, variations in crystalline structure, and surface roughness are known to influence the local mass-transfer factors. The experimental portion of this study was performed over a three-week period and involved the coating, machining, and handling of 26 active rods. Under these circumstances, it is not surprising to note a precision of less than the 2% obtained in the earlier mass-transfer studies.⁷ In view of the number of individual data points involved (in excess of 13 000), no attempt was made initially to duplicate the runs. It is now planned to check those runs for which the data are questionable or obviously in error.

A set of typical circumferential traverses (as the ratio j_1/j) are given in Fig. 3.4 for peripheral rod 1 at a 0-deg relative orientation of the two clusters. The curves shown are smoothed representations of the experimental data; and, while the significance of some of the minor fluctuations shown may be questionable at this time, the gross variations should be meaningful. In interpreting the general features of the

⁷J. L. Wantland and R. L. Miller, "Heat Transfer in Septafoil Geometries by Mass-Transfer Measurements," ORNL CF-59-6-9 (June 30, 1959).

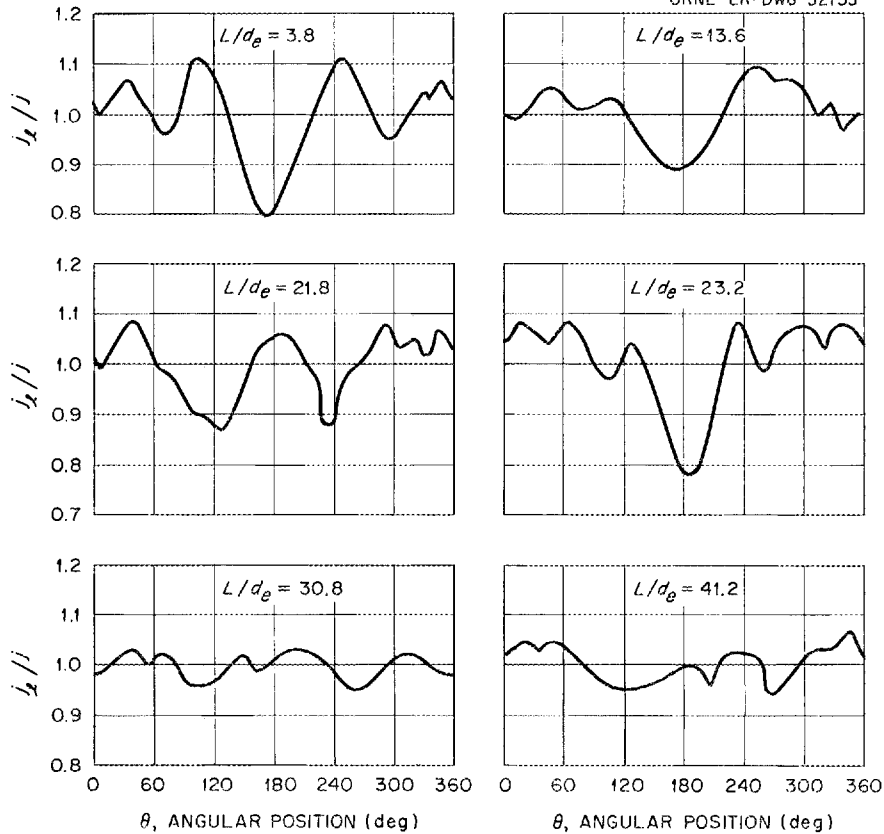


Fig. 3.4. Circumferential Variation in the Mass-Transfer Factor for Rod 1 at Six Axial Levels. Mid-cluster spacer at $L/d_e = 22.5$; $\gamma = 2$.

profiles of Fig. 3.4, reference should be made to Fig. 3.5, which indicates schematically the relative positions of the spiders and rods of the clusters for the four orientations studied (0, 30, 60, and 90 deg). The view is into the direction of flow with the solid lines being for the bottom (inlet) spider of the upper (test) cluster and the dotted lines for the top (outlet) spider of the lower (dummy) cluster. The shift in the numbered rods as the test cluster is rotated with respect to the fixed dummy-rod bundle is indicated.

The uppermost curve of Fig. 3.4 gives the j_x/j profile at the $L/d_e = 3.8$ position (2 1/3 in. from the beginning of the rods of the test bundle). The principal characteristics of this profile may be described and analyzed as follows:

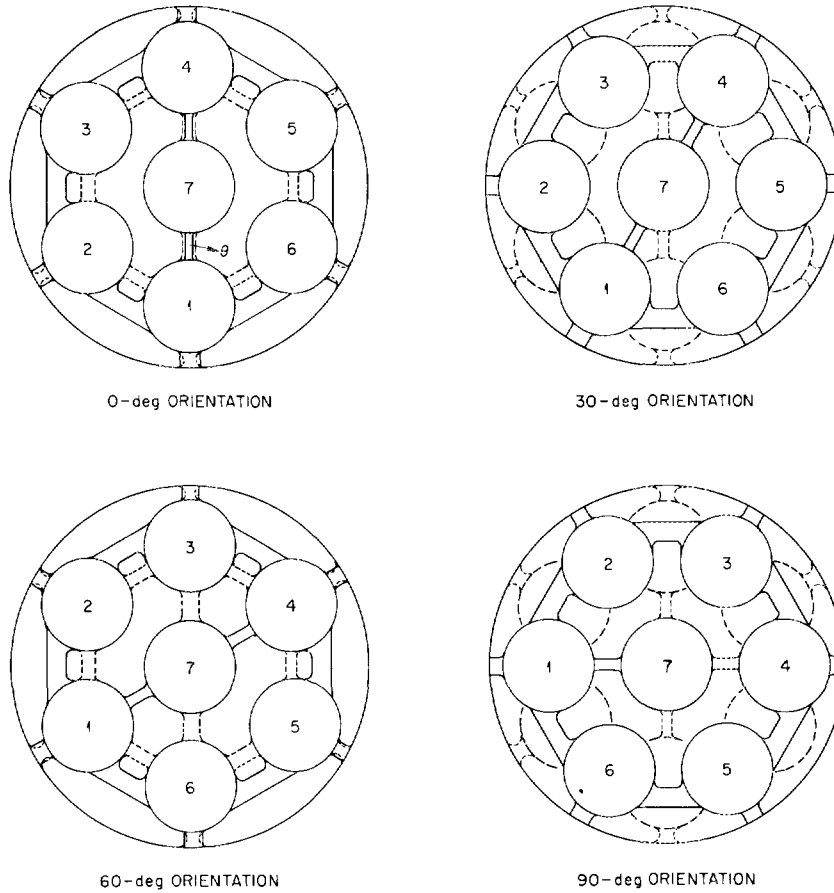


Fig. 3.5. Relative Orientations of Adjacent Title-II-Design Spiders as Examined in Mass-Transfer Studies.

1. The primary minimum appears at the 180-deg location and reflects the decreased flow in this region due to the presence of the structural elements of the spiders and to the proximity of the channel wall. Upstream of the spiders 59% of the total free flow area is in the outer region of the channel; at the spiders, this has been reduced to 48%, based on projected areas. (The outer flow region is defined as the area outside of the hexagon formed by joining the centers of the peripheral tubes.) The flow is thus forced toward the inner flow region, leaving diminished, lower-velocity flow near the channel wall. It must be remembered in viewing these curves that the mass transfer at any level

relates to the mean for the rod at that level. Thus the deeper minimum at $L/d_e = 3.8$ does not indicate less mass transfer than for the corresponding minimum at $L/d_e = 13.6$. This is shown by the curves of Fig. 3.6 in which a relative mass-transfer factor (the ratio of the circumferential mean, or minimum, to the mean at the exit) is given as a function of the axial position. In absolute magnitude, the minimum mass-transfer factor at $L/d_e = 13.6$ is 12% less than that at $L/d_e = 3.8$.

2. The primary maxima occur symmetrically at 105 and 255 deg. While these maxima might be expected at 75 and 285 deg (corresponding to the slot between the ribs in the projected view of Fig. 3.5), velocity data (see later Fig. 3.9) show that at this level sufficient redistribution of the flow has occurred for the maxima to appear at the locations anticipated in an unobstructed channel.

3. The minima at 70 and 300 deg correspond to the areas of closest approach of rod 1 to the adjacent peripheral rods. The ribs joining the outer bosses of the support spider of the dummy cluster are also located in this region.

4. The maxima at 30 and 330 deg indicate the relatively unobstructed flow occurring in the inner flow region midway between the restrictions

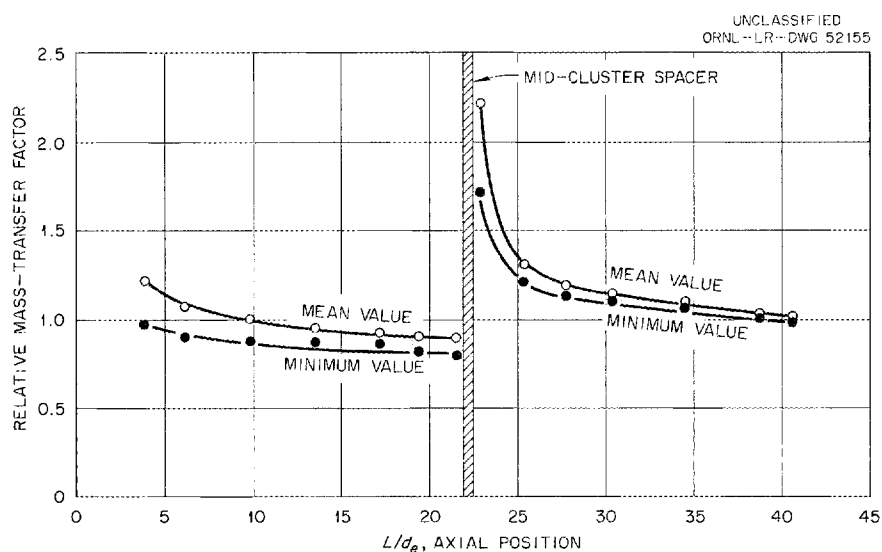


Fig. 3.6. Axial Variation of Minimum and Mean Mass-Transfer Factors for Rod 1. Relative cluster orientation: 0 deg.

of the peripheral rib and the central rib (supporting the boss for rod 7).

5. The minimum near 0 deg then signifies the presence of the central rib. The slight clockwise shift of the minimum may result from distortion of the flow by a slight misalignment of the clusters or by imperfections in the form of the spiders.

The patterns described persist, with some modification, at least as far downstream as $L/d_e = 19.6$ (12 in.). As the flow redistributes, in accord with the relative free-flow areas, the depth of the primary minimum decreases. This is illustrated at the $L/d_e = 13.6$ level as shown in Fig. 3.4. The mid-cluster spacer² is located at $L/d_e = 22.5$. The profile at $L/d_e = 21.8$ ($3/16$ in. from the upstream face of the spacer) shows a maximum in the vicinity of 180 deg which is believed to be indicative of the transverse acceleration of the fluid in the region immediately upstream of the spacer pad and perhaps some recirculation. The adjoining minima, occurring in a region of unobstructed flow, where maxima would normally be expected, may result from separation of the transverse flow.

Immediately downstream of the mid-cluster spacer ($3/16$ in.) a strong minimum occurs again near the 180 deg as the result of the flow blockage by the spacer pad. This was observed to disappear within 2 to 3 hydraulic diameters of the downstream face of the spacer. The minimum at 0 deg lies behind the central projection of the spacer and in the region of closest proximity of rod 1 to rod 7. The intervening maxima and minima (i.e., between 0 and 180 deg in both the clockwise and counterclockwise directions) appear somewhat displaced from the anticipated locations. For example, the maxima at 60 and 360 deg fall directly behind the circumferential projection of the spacer; and the minima at 40 and 320 deg fall in an unobstructed flow area. While a definitive explanation of this shift is not possible on the basis of available information, a hypothesis involving the interaction of the high-velocity streams forced inward by the spacer pads of adjacent rods (see preceding discussion) to create a region of high turbulence in the vicinity of 60 and 300 deg seems plausible.

Further downstream (see curves for $L/d_e = 30.8$ and 41.2 in Fig. 3.4), the profiles show much less circumferential variation than was observed for the inlet half of the cluster. The minima in the neighborhood of 100 and 260 deg persist throughout the remaining length of the cluster; only a vestige of the minimum at 180 deg remains.

The effect of relative orientation of the two clusters seems to be restricted to the upper half of the cluster. A comparison of circumferential profiles at the $L/d_e = 3.8$ level for the four orientations examined is given in Fig. 3.7. For the two inline arrangements, 0 deg and 60 deg (see Fig. 3.5), the patterns are similar. At the 30-deg staggered orientation, the lower mass removal in the region between 0 and 120 deg can perhaps be accounted for by the increased flow resistance engendered

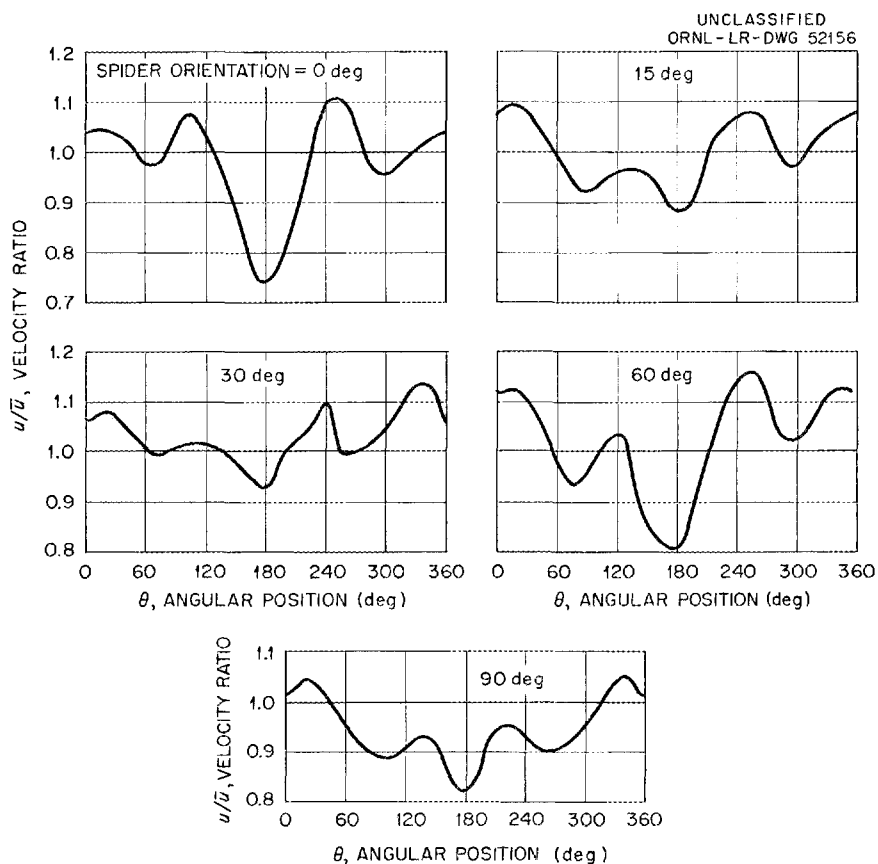


Fig. 3.7. Effect of Cluster Orientation on Mass Transfer Around Rod 1 at $L/d_e = 3.8$.

by the proximity of the central ribs. The decrease in the relative magnitude of the minimum at 180 deg (as compared with the inline arrangements) follows from the higher velocity flow reaching this area from the "open" region of the preceding cluster's outer flow channel. The maxima at 30 and 330 deg and at 130 and 230 deg are as expected. The profile for the 90-deg staggered orientation shows these same general characteristics; with the increased geometrical symmetry, the depression of a region of the profile is not observed. While significant redistribution of the flow occurs, the patterns for the staggered arrangements still differ somewhat from those for the inline situation, even at $L/d_e = 21.8$.

The axial variation of the mass-transfer factor (as indicated by the data for rod 1 at the 0-deg orientation and a rod spacing of $\gamma = 2$) is compared in Fig. 3.8 with similar results for the heat-transfer factor obtained in the series 2 experiment⁸ (tube 2, $\gamma = 4$). As expected, both curves have the same general shape; the difference in magnitude may perhaps be ascribed to the differences in the tube spacings, in the entrance geometries, and in the mid-cluster spacer designs. In view of these

⁸"GCR Quar. Prog. Rep. Dec. 31, 1959," ORNL-2888, pp. 48-51.

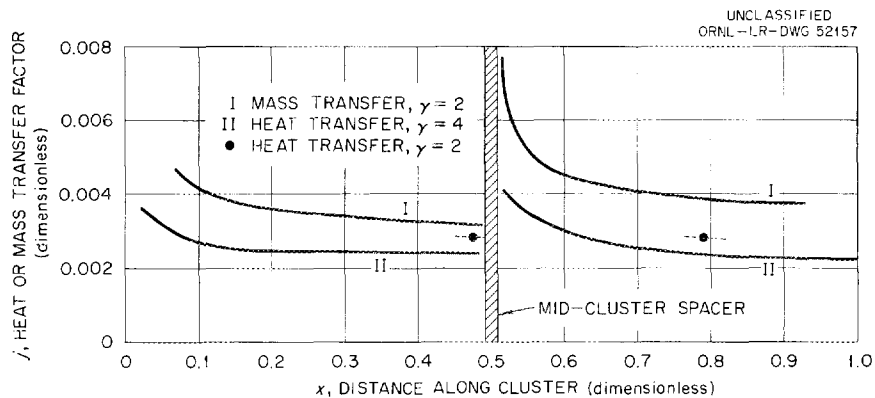


Fig. 3.8. Comparison of Mean Mass-Transfer and Heat-Transfer Factors. Relative cluster orientation: 0 deg; tube-spacing ratios: $\gamma = 2$ for mass transfer, $\gamma = 2$ and $\gamma = 4$ for heat transfer.

physical variations between the test apparatus, the 1.33 value for the ratio of the j factors (mass to heat) near the end of the inlet half of the clusters ($x = 0.49$) constitutes reasonable agreement. In contrast, the discrepancy between the two curves for the lower portion of the clusters ($j_M/j_H = 1.67$) is surprising. The upward displacement of the mass-transfer profile (asymptotes at $j \sim 0.00375$ as compared with 0.0032 for the inlet portion of the cluster) suggests that the mass-transfer data for this region of the cluster may be in error. To effect this difference would require gross changes in the cluster geometry, gas velocity, or gas temperature for run 22 (lower half) with respect to run 1 (upper half). A re-examination of the original data is in progress, and additional experiments aimed at obtaining data on the mass-removal for both portions of the rod in the course of a single run are planned. Preliminary results for series 4-B ($\gamma = 2$) heat transfer are also shown in Fig. 3.8. The agreement at $x = 0.475$ is excellent, with the ratio j_M/j_H being 1.13.

Velocity Distribution in Septafoil Channels

The mapping of the isothermal velocity field for a septafoil geometry has been continued using the experimental channel previously described.⁹ The apparatus contained two EGCR fuel cluster models (one being capable of rotation with respect to the other) with Title-II-design top and bottom spiders¹⁰ and a 60-deg-pad mid-cluster spacer.² Except in length ($L/d_e = 54$ as opposed to $L/d_e = 45$ for the EGCR), both clusters were 4/3-scale models. Therefore, in order to approximate the EGCR situation, the mid-cluster spacers were located off-center at $L/d_e = 22.5$ above the lower spider of the test cluster and $L/d_e = 22.5$ below the upper spider of the dummy cluster. While it is planned to obtain sufficient data to characterize, in detail, the flow in the EGCR cluster, initial measurements have been made primarily to determine the effect of relative cluster orientation on the velocities at $R = 0.05$ in. (measured radially outward from

⁹"GCR Quar. Prog. Rep. June 30, 1960," ORNL-2964, pp. 67-80.

¹⁰Ibid., pp. 61-62.

the tube surface) for tubes 1, 2, 3, and 7 (see Fig. 3.5) at four axial levels. The $R = 0.05$ point was chosen on the basis of previous results, which showed that measurements at this distance could be taken as representative of the flow in the immediate vicinity of the rod surfaces. It should be kept in mind that the pitot probes, as used in this apparatus, indicate only the axial component of the flow. Five rotational orientations (0, 15, 30, 60, and 90 deg) and four levels ($L/d_e = 3.8, 20.9, 26.0,$ and 52.8) were examined. The Reynolds modulus during the course of this study varied from 49 000 to 53 000, with the majority of the data being obtained at $N_{Re} = 50\ 000 \pm 500$.

Typical results are shown in Fig. 3.9, which gives the axial variation around rod 1 for a 0-deg orientation; Fig. 3.10, which gives the effect of cluster orientation on profiles near rod 1 at $L/d_e = 3.8$; and Fig. 3.11, which gives the effect of cluster orientation and axial position on profiles in the vicinity of the central rod. In each case, the ratio of the local (point) velocity to the mean (or bulk) velocity (calculated from N_{Re}) is given as a function of the angular position around the rod

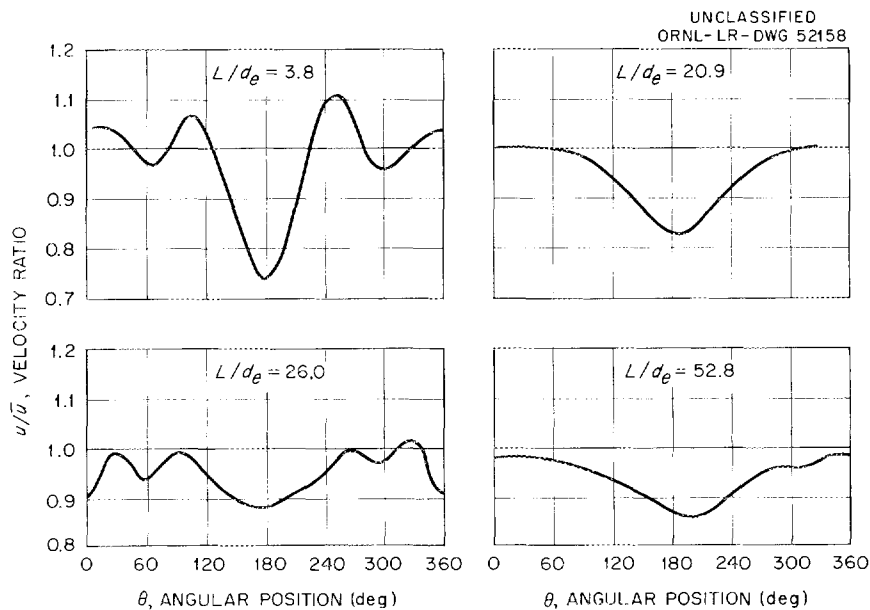


Fig. 3.9. Axial Variation in Experimental Velocity Profiles Around Peripheral Rod 1 of an EGCR Fuel Cluster with 0-deg Relative Cluster Orientation. Pitot probe 0.05 in. from tube surface; $N_{Re} \sim 50\ 000$.

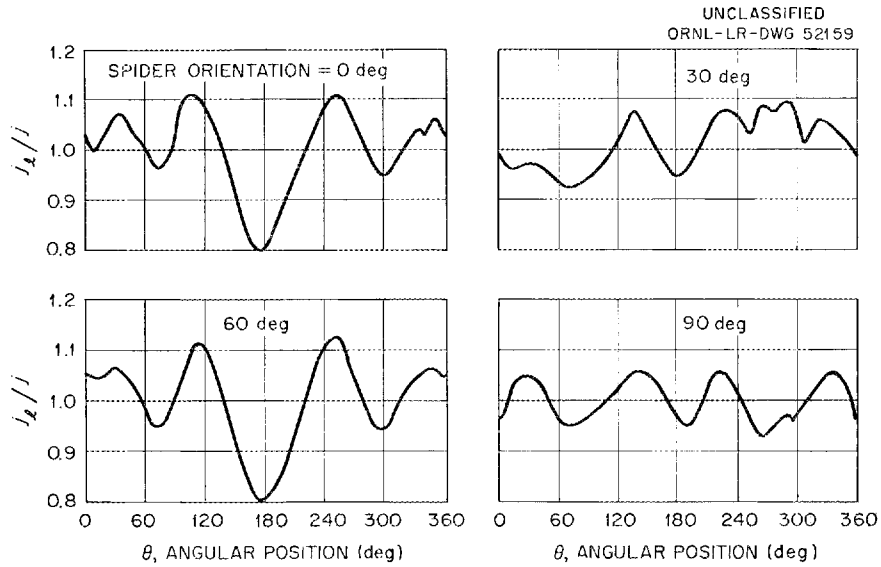


Fig. 3.10. Effect of Cluster Orientation on Velocity Profiles Around Peripheral Rod 1 Near the Entrance of an EGCR Cluster. Pitot probe 0.05 in. from tube surface; $L/d_e = 3.8$; $N_{Re} = \sim 50\ 000$.

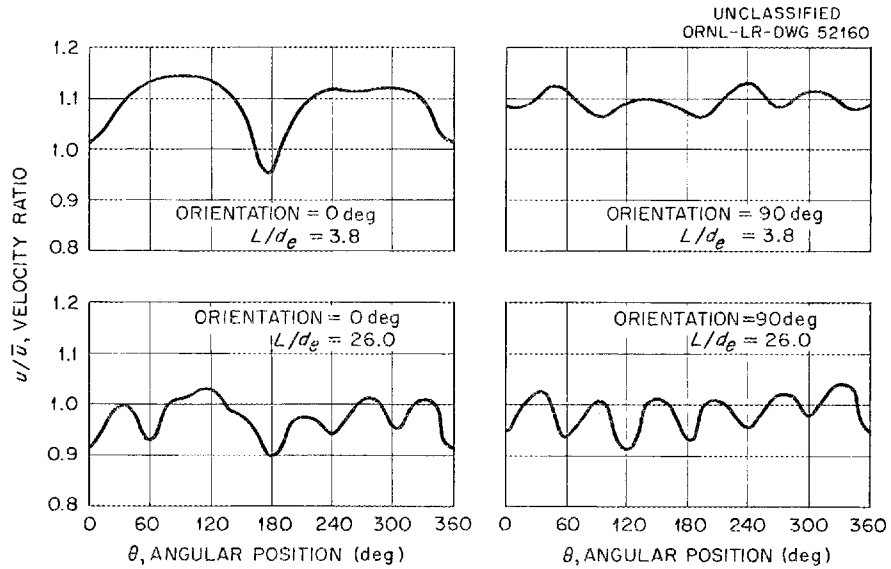


Fig. 3.11. Effect of Cluster Orientation and Axial Position on Velocity Profiles Around Central Rod of an EGCR Cluster. Pitot probe 0.05 in. from tube surface; $N_{Re} \sim 50\ 000$.

surface. (For the peripheral rods, the angular distance is measured in a clockwise direction with the 0-deg location lying on the radial line connecting the rod centers with the center of rod 7, see Fig. 3.5; for the central rod, θ runs clockwise from the line joining the centers of rods 1 and 7.)

Velocity profiles in the vicinity of rod 1 at four axial levels are given in Fig. 3.9. Since the effect on the flow of the spiders and spacers is of major interest, axial locations in the vicinity of these obstructions were selected for initial study. Thus, the uppermost profile of Fig. 3.9 was obtained at $L/d_e = 3.8$, approximately 3 in. downstream of the spider at the inlet end of the cluster. Succeeding profiles were measured 1.15 in. upstream of the mid-cluster spacer ($L/d_e = 20.9$), 2.75 in. downstream of this spacer ($L/d_e = 26.0$), and 1.0 in. upstream of the exit spider. A comparison of these profiles with the ones given in Fig. 3.4 for the mass-transfer studies shows that the primary features of the two sets of data agree quite closely. For example, at $L/d_e = 3.8$, both curves show a minimum at 180 deg, maxima at 105 and 255 deg, and minima at 70 and 300 deg. The minimum near 0 deg does not appear in these velocity data. Since this minimum (resulting from the central rib joining rods 1 and 7) is present for other orientations (see Fig. 3.10) and for rod 7 (see Fig. 3.11) at $L/d_e = 3.8$, it may be that the measurements for rod 1 in this region are in error. This will be checked experimentally at a later date. Further downstream ($L/d_e = 20.9$) the effect of the 60-deg pad in the outer flow channel on the axial velocity is apparent. The absence of other minima may indicate that the succession of peaks and valleys in the j -factor curve for mass transfer at $L/d_e = 21.8$ over the region 0 ± 80 deg arises from radial or circumferential flows. Below the mid-cluster spacer, the 180-deg minimum results from the flow blockage of the spacer pad. The secondary minima (0, 30, and 330 deg) correspond to the points of closest proximity to adjacent rods; the spacer spurs are also located at these positions. The minimum near the channel wall (180 deg) persists even at the $L/d_e = 52.8$ level; the data for rods 2 and 3 (not shown) display this same characteristic. There is some slight indication of other perturbations, as for the $L/d_e = 26.0$ profile.

The effect of cluster orientation on the velocity profiles at $L/d_e = 3.8$ is shown in Fig. 3.10. The results are again comparable to those for mass transfer, as given in Fig. 3.7, particularly at the 60- and 90-deg rotations. At the 30-deg orientation, while agreement is not unreasonable, a wider discrepancy exists. As discussed for the mass-transfer experiments, the velocities at 180 deg are in general higher in the staggered rod arrangements than in the inline configuration.

Results on the velocity distribution in the vicinity of the central rod are shown in Fig. 3.11 for two levels at two orientations. The shape of the 0-deg rotation profile at $L/d_e = 3.8$ is dominated by the central ribs, which interrupt the flow at 0 and 180 deg. The local velocities are, on the average, greater than those in the vicinity of the peripheral rods. This is in accord with the previously advanced hypothesis that the spiders force the flow into the inner flow region surrounding the central rod. At the $L/d_e = 26$ level, the mean velocity has decreased, although it still appears somewhat higher than for the outer rods. The progression of maxima and minima around the rod are as anticipated, except at 120 deg, where a minimum was expected; this value may be in error. The 90-deg orientation at $L/d_e = 3.8$ again shows a higher mean velocity than for peripheral tubes. Minima at 0, 90, 180, and 270 deg show the presence of the central ribs of the upstream pair of spiders (see Fig. 3.5). Below the mid-cluster spacer, the effect of the central projections of the peripheral rod spacers is again apparent. The regular variation in the magnitudes of the velocity maxima may arise from a displacement of rod 7 from a central position with relation to the outer rods or from an eccentricity in the spacer ring around tube 7, which serves as bearing surface for the spacer spurs.

Part 2. Materials Research and Testing

4. MATERIALS DEVELOPMENT

Fuel and Moderator Materials Development

Development of UO₂ Fabrication Processes

Studies of the conditions necessary for producing UO₂ powder by the nitrate-recycle process have continued. A variety of excellent powders has been made, but none has yet been obtained that is identical to the powder produced by the fluoride-ammonium diuranate process. The oxygen-to-uranium ratio tends to be higher, and the shrinkage characteristics are somewhat different. It has been established that process control is exceedingly critical and difficult when precipitation is carried out in straight nitrate solutions. Therefore nitrate solutions containing small amounts of fluoride are now being used.

Fabrication of UO₂ for Experimental Assemblies

Pellets of UO₂ fabricated from powder of two grain sizes were produced for in-pile tests of full-diameter prototype EGCR fuel capsules. Pellets were also produced for in-pile testing in beryllium capsules. The tests of the experimental assemblies in which these pellets are being used are described in Section 5 of this report.

Thin plates of UO₂ and ThO₂ were prepared for fission-gas-release experiments (also described in Section 5). Attempts to polish these plates to a final thickness of 0.030 in. have been only partially successful.

Development of Apparatus for Bulk-Density Measurements

A direct-reading mercury volumeter is being developed for use in making rapid, high-precision determinations of bulk density on low-porosity materials with volumes on the order of 0.01 cm³. Tests of a model based on an initial design showed that a sample immersed in the mercury was not completely contacted by the mercury after the system had been evacuated to 10⁻⁵ mm Hg. A stopcock modification which provided

for the gradual buildup of a slight partial pressure of air in the sample leg of the volumeter was then investigated, and complete contact between the mercury and sample was achieved. A design was completed of an alternate system that provides for greater accuracy in reading the mercury level.

Fission-Product-Release Studies

The release-rate parameter, D' , for Xe^{133} has been measured for various grades of UO_2 by the neutron-activation high-temperature-annealing technique described previously.¹ The results obtained during the current reporting period are presented in Table 4.1. Based on these data, the activation energy for the diffusion of Xe^{133} from the fused UO_2 obtained from the Spencer Chemical Company was calculated to be 86.2 kcal/mole. This value is to be compared with values obtained at

¹"GCR Quar. Prog. Rep. Dec. 31, 1959," ORNL-2888, p. 68.

Table 4.1. Results of Fission-Gas-Release Measurements on UO_2

| UO ₂ Pellet Manufacturer | Sample No. | Pellet Density (% of theoretical) | BEP Surface Area (cm ² /g) | Run No. | Test Tempera- ture (°C) | Total Fractional Gas Release | Release-Rate Parameter, ^a D' (sec ⁻¹) |
|---|---------------|--|--|------------|----------------------------------|---------------------------------------|--|
| Mallinckrodt | 25-8 | 94 | 2.94 | 35 | 1400 | 5.15×10^{-4} | 2.2×10^{-13} |
| GE-Valecitos | GE-6 | 95.5 | 7.7 | 36 | 1400 | 1.25×10^{-2} | 2.2×10^{-10} |
| Davison | 33-9 | 93.5 | 12.5 | 34 | 1600 | 6.67×10^{-2} | 2.0×10^{-11} |
| Davison | 33-9 | 93.5 | 12.5 | 37 | 1400 | 1.18×10^{-2} | 1.5×10^{-11} |
| Davison | 33-9 | 93.5 | 12.5 | 38 | 1600 | 2.13×10^{-4} | 1.2×10^{-11} |
| Davison | 33-9 | 93.5 | 12.5 | 39 | 1600 | 6.15×10^{-2} | 1.1×10^{-10} |
| Mallinckrodt | 25-8 | 94 | 2.94 | 40 | 1400 | 5.26×10^{-4} | 1.1×10^{-13} |
| Mallinckrodt | 25-8 | 94 | 2.94 | 41 | 1200 | 1.86×10^{-4} | 3.7×10^{-14} |
| Mallinckrodt | 25-8 | 94 | 2.94 | 42 | 1600 | 1.99×10^{-3} | 1.5×10^{-11} |
| Mallinckrodt | 25-8 | 94 | 2.94 | 43 | 1400 | 3.53×10^{-4} | 1.2×10^{-13} |
| Spencer | SFUO-2 | 100 | $\sim 0.5^b$ | 44 | 1100 | 1.87×10^{-3} | 3.5×10^{-13} |
| Spencer | SFUO-2 | 100 | $\sim 0.5^b$ | 45 | 1200 | 5.80×10^{-4} | 1.3×10^{-12} |
| Spencer | SFUO-2 | 100 | $\sim 0.5^b$ | 46 | 1300 | 3.38×10^{-3} | 8.8×10^{-12} |
| Spencer | SFUO-2 | 100 | $\sim 0.5^b$ | 47 | 1400 | 2.30×10^{-2} | 3.3×10^{-11} |

^aCalculated on the linear portion of the curve representing fractional gas release vs square root of time.

^bCalculated surface area for 100%-dense UO_2 .

Chalk River,² which indicate that the activation energy is between 70 and 80 kcal/mole.

Previous experiments³ showed that when fission gas is released from UO₂ above its sintering temperature, normally 1650°C, the amount of gas released is increased and the shape of the curve of the fraction of fission gas released versus the square root of time is changed markedly. Two tests were performed to determine whether the fractional release, the release-rate parameter D' , and the shape of the release-rate curve would be affected by additional sintering at a higher temperature. It was expected that the additional sintering at a higher temperature would cause a reduction in both the release-rate parameter and the fraction of xenon released because of an increase in the effective diffusion path length for xenon atoms as a result of an increase in the "effective uniform sphere radius."⁴ If the shape of the curve of fraction released versus the square root of time changed, it would indicate that the additional sintering had caused a structural change in the UO₂ that affected the mechanism of release of the fission gas.

The additional sintering was carried out on UO₂ pellet NUMEC 34-30, and the data are presented in Table 4.2. The shape of the release-rate

²J. A. L. Robertson, personal communication to J. L. Scott, May 25, 1960.

³"GCR Quar. Prog. Rep. June 30, 1960," ORNL-2964, p. 92.

⁴B. Lustman, "Release of Fission Gases from UO₂," WAPD-173 (March 1957).

Table 4.2. Values of the Release-Rate Parameter and Total Fraction of Xe¹³³ Released on UO₂ Pellet NUMEC 34-30

| Sintering Time at 1900°C (hr) | Test Temperature (°C) | Release-Rate Parameter, D' (sec ⁻¹) | Total Fraction Xe ¹³³ Released in 6 hr |
|-------------------------------------|-----------------------------|---|---|
| 0 | 1400 | 2.5×10^{-13} | 1.30×10^{-3} |
| 9 | 1400 | 1.6×10^{-13} | 1.70×10^{-4} |
| 0 | 1800 | 1.1×10^{-7} | 9.43×10^{-2} |
| 9 | 1800 | 2.1×10^{-8} | 1.20×10^{-2} |

curve was not changed by the additional sintering; but, as was expected, both the release-rate parameter and the fraction released were reduced. A greater reduction in D' occurred at 1800°C than at 1400°C. The small reduction at 1400°C is probably due only to an increase in the "effective sphere radius," whereas the greater reduction in D' at 1800°C may be due to grain growth, an increase in UO_2 density, or some unknown phenomenon.

Fractional release experiments have been run on more than one sample of several UO_2 pellets in order to examine the reproducibility of D' determinations. The data are shown in Table 4.3. It appears that the D' values vary about one order of magnitude.

Table 4.3. Comparison of D' Values in UO_2 Pellets

| UO_2 Pellet Manufacturer | Test No. | Sample Designation | Test Temperature (°C) | Release-Rate Parameter, D' (sec^{-1}) |
|----------------------------------|-------------|-----------------------|-----------------------------|---|
| Mallinckrodt | 1 | 25-8 | 1400 | 1.1×10^{-13} |
| | 2 | 25-8 | 1400 | 1.2×10^{-13} |
| | 3 | 25-8 | 1400 | 4.7×10^{-14} |
| Davison | 6 | 33-5 | 1400 | 6.7×10^{-12} |
| | 7 | 33-5 | 1400 | 1.5×10^{-11} |
| Davison | 8 | 33-9 | 1600 | 1.2×10^{-11} |
| | 9 | 33-9 | 1600 | 1.1×10^{-10} |

Fabrication of Fueled Graphite

Processes are being developed for the preparation of high-density, low-porosity graphite bodies uniformly fueled with UC or other uranium compounds. Two procedures are being investigated, an admixture method and an impregnation method.

Admixture Method. Specimens formed by using natural graphite, depleted UC, and two different high-carbon-forming thermosetting binders known commercially as "Furacarb P-3" and "Durite SD-5143," respectively, were observed to be badly laminated and covered with small surface bumps after firing in argon at 1000°C. These effects were observed in specimens

containing the Durite binder even after special care was taken to prevent back-diffusion of air into the furnace and to remove oxygen and water from the gas. X-ray diffraction analyses of both type of specimens revealed the presence of UO_2 as well as UC.

A systematic x-ray diffraction study of UC processed with and without binder materials has shown that a UO_2 coating is formed only on UC grains fired with binder present, presumably because of a reaction between UC and the oxidizing gases given off by the binder. It is believed, therefore, that for fuel bodies containing binder materials there are two opposing effects: (1) an increase in volume because of the formation of a UO_2 coating on the UC and (2) a decrease in volume associated with the firing of the graphite-binder matrix. Attempts to eliminate the laminations and surface roughening by firing in dry hydrogen and by reducing the binder-to-graphite weight ratio to 1:100 were unsuccessful.

Impregnation Method. AGOT-type graphite specimens were impregnated with normal, 20%-enriched, and 30%-enriched uranyl nitrate solutions. After firing the specimens in a hydrogen atmosphere, the average percentage increases in weight as a result of the presence of UO_2 in the specimens were 3.55%, 2.79%, and 3.13%, respectively. Autoradiographs of the surface and of cross-sectional areas of some of these specimens showed, however, that most of the UO_2 existed on or near the surface of the specimens.

Reactions of UO_2 with Graphite

The rate of the reaction of UO_2 with graphite that is to be expected in a fuel element consisting of UO_2 dispersed in graphite is being studied as a function of temperature, UO_2 particle size, and CO pressure by the thermogravimetric methods described previously.⁵ The apparatus has been modified so that a platinum, platinum-10% rhodium thermocouple can be used for the temperature measurements rather than an optical pyrometer.

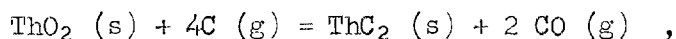
⁵"GCR Quar. Prog. Rep. March 31, 1960," ORNL-2929, pp. 98-100.

Data obtained for the reaction between -60 +80 mesh UO_2 and graphite at pressures of 1×10^{-3} to 1×10^{-4} mm Hg were fitted to the rate equation

$$x = kt^{1/2} ,$$

where x is the fraction of UO_2 converted to the carbide, k is the temperature-dependent rate constant, and t is time, in hours, at temperature. The values of k obtained were 0.18, 0.33, and 0.44 at 1275, 1325, and 1375°C, respectively. These results, when compared with results⁶ obtained for -325 mesh UO_2 , indicate that the reaction rate is sensitive to particle size below about 1325°C and relatively insensitive above this temperature.

As an extension of this work, preliminary studies of the reaction rate of ThO_2 and graphite were conducted. Free-energy calculations for the reaction,



indicate that the reaction should not occur at temperatures below about 2500°C at CO pressures greater than 1 atm and that at a CO pressure of 1×10^{-4} mm Hg it should not occur below 1225°C. The maximum temperature attainable in the present apparatus is about 1500°C at a pressure of 1×10^{-4} mm Hg; no reaction between -325 mesh ThO_2 and graphite has been observed up to this temperature.

Determination of the Elastic Constants of AGOT Graphite

Elastic constant determinations were made by the sonic method on specimens taken from two different blocks of AGOT graphite. The Magnaflux Elastomat was used for these tests. Both the shear modulus and Young's modulus were determined from the three fundamental modes of vibration

⁶"GCR Quar. Prog. Rep. June 30, 1960," ORNL-2964, p. 98.

of each specimen. The test pieces were nominally 6 in. long and 1/2 in. in diameter.

The results obtained at room temperature are presented in Table 4.4. It is felt that the discrepancies between the results obtained from different specimens from the same block may be attributed to variations of the size and the density of voids in the specimens.

Table 4.4. Elastic Constants of AGOT Graphite at Room Temperature

| Specimen No. | Apparent Density (g/cm ³) | AGOT Graphite Block No. | Orientation of Specimen to Extrusion Axis | Mode of Vibration | Elastic Modulus (psi) |
|--------------|---------------------------------------|-------------------------|---|-------------------|-----------------------|
| | | | | | × 10 ⁶ |
| 1 | 1.72 | 1 | Parallel | Transverse | 2.08 |
| | | | | Longitudinal | 2.18 |
| | | | | Torsional | 1.11 |
| 2 | 1.73 | 1 | Parallel | Transverse | 2.07 |
| | | | | Longitudinal | 2.27 |
| 3 | 1.67 | 2 | Parallel | Transverse | 1.57 |
| | | | | Longitudinal | 1.66 |
| | | | | Torsional | 0.88 |
| 4 | 1.65 | 2 | Parallel | Transverse | 1.56 |
| | | | | Longitudinal | 1.62 |
| | | | | Torsional | 0.85 |
| 5 | 1.69 | 2 | Normal | Transverse | 1.50 |
| | | | | Longitudinal | 1.62 |
| | | | | Torsional | 0.75 |
| 6 | 1.68 | 2 | Normal | Longitudinal | 1.59 |
| | | | | Torsional | 0.82 |

The variation of the modulus of elasticity of AGOT graphite with temperature was determined from the change of the transverse resonance frequency of specimen 4 in the temperature range 75 to 1000°F. Specimen 4 was from a large block prepared with needle coke. The results of this test are presented below:

| Temperature (°F) | Young's Modulus (psi) |
|---------------------|--------------------------|
| | × 10 ⁶ |
| 75 | 1.540 |
| 100 | 1.536 |
| 200 | 1.524 |
| 300 | 1.516 |
| 400 | 1.513 |
| 500 | 1.513 |
| 600 | 1.513 |
| 700 | 1.515 |
| 800 | 1.520 |
| 900 | 1.526 |
| 1000 | 1.533 |

The constancy of these values indicates that the modulus of graphite is not affected by temperature up to 1000°F.

Mechanical Property Tests on EGCR Graphite Sleeves

Eddy-current inspections of graphite sleeves supplied by three vendors resulted, as reported previously,⁷ in the rejection of 34, 88, and 92%, respectively, of the three lots. The sleeves contained defects in the form of cracks and low-density inclusions. Since stresses in the range 1200 to 1300 psi may develop in the graphite sleeves during service in the EGCR because of fast-neutron-induced differential shrinkage,⁸ the effects of such defective areas on rupture strength have been studied.

Defects were marked in three sleeves containing low-density areas and cracks, and test specimens were machined to include the defect areas. Defect-free specimens and specimens containing artificial defects were also prepared. The artificial defects were V-grooves, 1/8 in. × 1/8 in., and slots 0.01 in. wide by 0.10 in. deep. Two types of test specimens were made: (1) a ring cut perpendicular to the axis of the sleeve with the defect area on the inside diameter and (2) a bar specimen for a flexure test.

⁷"GCR Quar. Prog. Rep. June 30, 1960," ORNL-2964, pp. 121-2.

⁸Ibid., pp. 41-43.

The ring specimens were used in a "brittle ring" test of the type developed by the Armour Research Foundation.⁹ In these tests, which allowed the determination of the rupture strength of the graphite at the defect area, the specimens were stressed to rupture by compression loading on the outer surface to produce tensile stresses on the inner surface directly under the points of load application. The flexure specimens were broken in a three-point-loading flexure test, with the defect areas in the tension zone. The fracture surfaces of the samples were examined visually in order to estimate the approximate sizes of the defects. The results of the rupture tests and the defect size examinations are presented in Table 4.5.

There were only two flexure specimens that contained observable defects. The other specimens were machined from areas containing defects, but the defects were apparently removed during the machining operation. While it is obvious that the defects do lower the strength to some extent, the strengths of all but two ring specimens containing defects fell in the range of strengths (1710-2780 psi) of defect-free specimens from the three sleeves. The two flexure specimens containing defects had strengths in the range of the defect-free flexure specimens, that is, 2360 to 5620 psi. The effect of the size of the defect is illustrated by comparing results of tests on specimens 31 and 32. These rings were adjacent in the sleeve and had the same type of defects. The results of this study indicate that defects of the type observed in these tests would not lower the strength of the graphite to values below the calculated maximum tensile stress of 1300 psi.

Evaluation of Graphite Coatings

Several samples of SiC-coated graphite were obtained for use in developing techniques for inspecting coatings on graphite. The first method studied was an electrode-potential test, which is based upon the action of an electrolyte that creates a galvanic cell when both the

⁹S. W. Bradstreet, "Investigation of Graphite Bodies," WADC-TR-59-760 (October 1959).

Table 4.5. Evaluation of Rupture Tests of EGCR Graphite Sleeve Specimens Containing Defects

| Sleeve No. | Specimen No. | Approximate Dimensions of Defect (in.)* | Specimen Rupture Strength (psi) | Rupture Strength of Defect-Free Specimens from Same Sleeve (psi) | |
|--------------|--------------------------|---|---------------------------------|--|-----------|
| | | | | Average | Range |
| Flexure Test | | | | | |
| 126 | 4 | None observed | 3760 | 4230 | 3280-5140 |
| | 5 | 1/2 x 1/4 | 3170 | | |
| | 6 | None observed | 4640 | | |
| 138 | 33 | 3/8 x 1/8 | 2780 | 5190 | 4660-5620 |
| | 34 | None observed | 5960 | | |
| 19 | 63 | None observed | 2930 | 3270 | 2360-4700 |
| | 64 | None observed | 2450 | | |
| Ring Test | | | | | |
| 126 | 1 | 1/2 x 1/4 x 1/4 | 1930 | 2450 | 2170-2780 |
| | 2 | 3/4 x 3/8 x 1/4 | 2090 | | |
| | 3 | 1/2 x 1/4 x 1/8 | 2360 | | |
| | | V groove, 1/8 x 1/8 | 1630 (2)** | | |
| | | Slot, 1.00 x 0.01 x 0.10 | 1730 (2)** | | |
| 138 | 29 | 3/4 x 1/4 x 3/16 | 1670 | 1960 | 1710-2190 |
| | 30 | 1 x 3/8 | 1800 | | |
| | 31 | 1 x 1/4 x 3/8 | 1640 | | |
| | 32 | 1/4 x 1/4 x 1/4 | 2250 | | |
| | | V groove, 1/8 x 1/8 | 1500 (2)** | | |
| | Slot, 1.00 x 0.01 x 0.10 | 1690 (5)** | | | |
| 19 | 60 | Crack on angle | 1910 | 1870 | 1820-1910 |
| | | Slot, 1.00 x 0.01 x 0.10 | 1630 (2)** | | |

*Two dimensions indicate length and depth, respectively, and three dimensions indicate length, thickness, and depth, respectively.

**Number in parentheses indicates number of specimens tested; the rupture strength reported is an average value.

coating and the graphite are exposed. This method is so sensitive to pinholes in the coating that it can be used only to determine whether the graphite is 100% coated. As a result, this method has been discarded, and an eddy-current technique is being investigated.

Evolution of Lithium from BeO

Beryllium oxide test blocks containing approximately 200 ppm of lithium were subjected to a 14-week heat treatment in a dynamic atmosphere of CO₂ at 850°C. In order to determine whether lithium was evolved during the treatment, the reactivity of the beryllium oxide was measured in a critical assembly before and after heating. A decrease in measured reactivity values indicated that the samples had become contaminated during the test. Subsequent spectrographic analyses of several test pieces showed that the lithium content remained essentially unchanged at about 200 ppm; however, the boron content had increased from 2 to 100 ppm. Based on these spectrographic-analysis results, it appears that lithium was not removed during the heat treatment.

Fabrication of Swaged-Rod Irradiation Capsules

Procedures are being developed for producing stainless-steel-clad, hot-swaged rods containing UO₂ for irradiation tests in the ORR Poolside Facility. The capsules will be 0.500 in. in diameter clad with 0.015 in. of type 304 stainless steel.

Tests have been made to determine the initial tubing size that will yield a 0.500-in.-i.d., 0.015-in.-wall rod without internal cladding defects when filled with UO₂ and swaged at 800°C. Composite rods have been processed from tubing initially 3/4 in. in outside diameter and 0.010 in. and 0.020 in. in wall thickness. The 0.010-in.-wall tubing failed when swaged at 800°C to 0.530 in. in outside diameter because of severe folding and wrinkling, in addition to longitudinal cracking completely through the tube wall. On the other hand, the composite rods formed with tubing with an initial wall thickness of 0.020 in. exhibited good surface finishes that were free from visible folds or defects after hot swaging. Ultrasonic inspection of three of these rods failed to reveal any discontinuities, indicating that the cladding was free of internal defects. Difficulty is being experienced, however, in swaging to the reference dimensions. Although the rods were swaged through a 0.530-in.-diam die on the final pass, the final rod diameter

was approximately 0.540 in. because of die and machine wear. The wall thicknesses were found to vary from 0.022 to 0.026 in. Typical dimensions and UO₂ densities of the swaged rods are given below:

| | Rods Prepared with Fused-and- Ground UO ₂ | Rods Prepared with High-Fired UO ₂ |
|---|--|---|
| Outside diameter of rod, in. | 0.541 | 0.540 |
| Wall thickness of cladding, in. | 0.022 | 0.026 |
| Density of UO ₂ , % of theoretical | 94.9 | 82.4 |

Four capsules packed with loose UO₂ powder by tamping were prepared and are being tested at an external pressure of 300 psi and a cladding temperature of 1300°F in order to determine whether the over-all structural rigidity of tamp-packed rods is sufficient to prevent collapse from external pressure.

Structural Materials Evaluation

Reactions of Type 304 Stainless Steel with CO-CO₂ Mixtures

A 703-hr test of type 304 stainless steel exposed to 0.4 vol % CO + CO₂ in helium at a CO₂-to-CO ratio of 0.46 showed that the reaction rate at 982°C (1800°F) follows the equation

$$\Delta w = 0.066 t^{0.481} ,$$

where Δw is the weight gain in mg/cm² and t is the reaction time in hours. In a previous test at a CO + CO₂ concentration of 2.6 vol % (CO₂/CO = 0.07) the equation

$$\Delta w = 0.086 t^{0.502}$$

described the reaction rate. Calculations based on these data indicate that a factor of 5 increase in the CO₂ + CO concentration (0.4-2.6 vol %)

resulted in a 25% increase in the reaction rate. Analyses of all the rate data obtained at 760 and 982°C for gas compositions ranging from 3 to 100% CO₂ and 0 to 97% CO show that the reaction rates are approximately proportional to the square root of time.

The variations observed in the extent of carburization of type 304 stainless steel have been postulated to depend on the CO₂-to-CO ratio, and the current test data appear to confirm this hypothesis, inasmuch as the carbon content for low CO₂-to-CO ratios is higher than for higher CO₂-to-CO ratios. For example, at 982°C and with a CO₂-to-CO ratio of 0.07, the final carbon content of the metal was 0.49%, whereas, with a CO₂-to-CO ratio of 0.46, the carbon content was 0.099%. The extent of oxidation and carburization becomes insignificant below temperatures of 700 to 775°C.

Creep Buckling and Collapse of Stainless Steel Tubes

During their expected three-year lifetime, the EGCR loop through tubes will be periodically exposed to an external pressure loading which could lead to collapse by creep buckling. Since the phenomenon of creep buckling is not well understood experimentally or theoretically, tests are under way to obtain the data needed to establish a failure criterion for tubes with external pressure loading. All tests are being run at 1200°F on type 304 stainless steel seamless tubing specimens 12 in. long that have been annealed at 1900°F for 1 hr in hydrogen. This material is identical to that expected to be used in the EGCR through tubes.

Four specimens (0.750 in. o.d., 0.025 in. wall) are being tested for creep buckling with an external pressure of 400 psi. The specimens have been examined periodically, i.e., at 508, 1252, and 2225 hr, and no evidence of collapse has been found. The test is continuing. Four identical specimens are being tested with an external pressure of 600 psi. The specimens were examined at 475 hr, and no evidence of collapse was found.

*6000 psi
uniform*

*9000 psi
uniform*

One specimen (0.750 in. o.d., 0.025 in. wall) has been tested at 1200°F to determine the critical pressure for instantaneous collapse.

The critical pressure measured in this test was 800 psi. In further tests the effects of ovality and wall thickness on the critical pressure will be determined. The results of these tests will be used as base-line data for sizing of the EGCR through tubes.

Tube-Burst Tests of Stainless Steel

It has been shown that tubing from two different sources fabricated to the same specification may exhibit considerably different times to rupture during tube-burst testing^{10,11} and that there may be some effect of specimen length. A series of tests is therefore being run on tubes 2.5 and 6 in. long fabricated from heat No. 23999X of the Superior Tube Company.

Investigations of the effect of environment on the time to rupture of seamless type 304 stainless steel tubing have continued, and the results indicate a definite strengthening effect in atmospheres containing CO. This strengthening effect of CO has also been reported in the case of uniaxial creep.¹²

Mechanical Properties of AISI-Type 502 Steel for EGCR Top Grid Structure

An investigation of the mechanical properties of AISI-type 502 steel has been initiated. Since the use of this material in the top grid structure of the EGCR core requires that it be welded both to itself and to austenitic stainless steels, a series of typical welds were made and examined metallographically. The phases present were determined, and representative hardness measurements were made. Heat treatments of the base material that would yield structures similar to those observed in the welded specimens were selected, and specimens were prepared for mechanical property tests. The specimens include (1) as-received material, (2) material annealed for 1 hr at 1900°F, cooled to room temperature, and tempered for 1 hr at 1350°F, (3) material

¹⁰"GCR Quar. Prog. Rep. March 31, 1960," ORNL-2929, pp. 115-16.

¹¹"GCR Quar. Prog. Rep. June 30, 1960," ORNL-2964, pp. 106-7.

¹²"GCR Quar. Prog. Rep. March 31, 1960," ORNL-2929, pp. 102-12.

treated as in item 2, except that it was annealed at 1700°F, (4) material annealed for 1 hr at 1700°F and cooled to room temperature, and (5) material annealed 1 hr at 1700°F, held at 1350°F for 2 hr, and cooled to room temperature.

The design service temperature for this alloy is 1200°F, and hence the initial test temperatures have been room temperature and 1200°F. The results of tests to date on a heat of material containing 4.76% Cr, 0.55% Mo, 0.53% Mn, and 0.068% C may be summarized as follows:

1. All heat treatments yielded specimens which could be bent through 90 deg at room temperature.
2. Specimens given the fourth heat treatment had superior room-temperature tensile and bend properties.
3. At 1200°F the variation of tensile properties of specimens given any one of the first four heat treatments was slight. However, the fifth heat treatment yielded material having approximately one-half the strength of the specimens given the other treatments.
4. The room temperature and 1200°F tensile properties of this alloy show good correlation with hardness measurements made at the same temperatures.
5. Creep tests run at 1200°F and a stress of 6500 psi in air, in argon, and in argon containing 5% CO and 5% CO₂ did not reveal any consistent effect of environment on the mechanical properties of the alloy.
6. The material given the second heat treatment had superior creep properties, and the as-received material had the least creep resistance.

Although these results indicate that there will be no problems associated with welding this material, even if postwelding heat treatments are not carried out, it should be realized that this material contains less than one-half the 0.15 wt % maximum carbon content specified for this steel. Several specimens were carburized in CO at 1700°F, homogeneized at 1900°F, and tested in bending at room temperature to evaluate the effect of carbon content on the toughness of the material. The results of the tests are summarized in Table 4.6. As may be seen, increasing the carbon content to approximately 0.15 wt % decreased its

Table 4.6. Room-Temperature Effect of Carbon on Bend Properties of AISI-Type 502 Steel

| Heat Treatment | Carbon Content (wt %) | Hardness, R _c | Maximum Deflection (in.) | Stress at Proportional Limit (psi) |
|--|-----------------------|--------------------------|--------------------------|------------------------------------|
| Annealed 1 hr at 1900°F in Ar | 0.068 | 35 | 0.25 | 157 000 |
| Carburized by heating 1 hr at 1700°F in CO and annealed 1 hr at 1900°F in Ar | 0.12 ^a | 41 | b | 164 400 |
| Carburized by heating 2 hr at 1700°F in CO and annealed 1 hr at 1900°F in Ar | 0.16 ^a | 46 | b | 172 200 |
| Carburized by heating 3.4 hr at 1700°F in CO and annealed 1 hr at 1900°F in Ar | 0.28 ^a | 53 | 0.060 | 393 400 |
| Carburized by heating 19 hr at 1700°F in CO and annealed 1 hr at 1900°F in Ar | 0.86 ^a | 67 | 0.014 | 164 600 ^c |
| Carburized by heating 26 hr at 1700°F in CO and annealed 1 hr at 1900°F in Ar | 1.1 ^a | 66 | 0.013 | 155 900 ^c |

^aDetermined from analysis of starting material and weight change of sample during carburization treatment.

^bExact deflection at which cracks formed not detectable, but cracks were present after 0.25-in. deflection.

^cBrittle failure.

ductility; hence, the weldability of material of this carbon level should be investigated before a welding procedure is specified.

Studies of Pressure Vessel Steels

Investigations are continuing in an effort to obtain a better understanding of the brittle-fracture characteristics of the weld-heat-affected zones in ASTM A-212, grade B, pressure vessel steel. Some

data recently obtained from the work being carried out at Rensselaer Polytechnic Institute indicate that exposure to thermal cycles with a maximum temperature of 2400°F at energy inputs of 150 000 or 200 000 joules/in. causes a reduction in notch toughness similar to that found as a result of thermal cycling to 2400°F using an energy input of 100 000 joules/in.¹³ A stress-relief heat treatment at 1150°F for 4 hr after any of these cycles did not appreciably change the notch toughness, presumably because the structure was essentially an aggregate of ferrite and pearlite.

Part of a series of experiments to simultaneously evaluate the notch toughness of ASTM A-212, grade B plate, the heat-affected zone, and the filler metal as found in a weldment has been completed. Filler metal E7018 was welded into U-shaped grooves (0.300 in. across and 0.200 in. deep) using different energy inputs. Charpy V-notch specimens were then machined in such a way that the metal below the notch consisted of equal areas of weld metal and base metal. The base-metal portion of the sample also contained the heat-affected zone.

The mid-energy-range and 50%-shear transition temperatures for these Charpy V-notch specimens for various welding conditions are shown in Table 4.7. The data show that double-pass welds have better notch toughness than single-pass welds, as indicated by the lower transition temperatures. Also, in the energy range studied, the single-pass welds made at a lower energy input appear to be slightly tougher than counterpart high-energy-input welds. Preheating the base plate to 200°F appeared to lower the transition temperature for the double-pass welds but did not significantly change the notch toughness of single-pass welds.

Compatibility of Molybdenum with Coolant Impurities

Refractory metals, such as molybdenum, are being considered for use in high-temperature gas-cooled reactors, and little is known about

¹³"GCR Quar. Prog. Rep. March 31, 1960," ORNL-2929, pp. 118-22.

Table 4.7. Effect of Various Welding Conditions on Charpy V-Notch Specimens of ASTM A-212, Grade B, 4-in.-Thick Plate^a

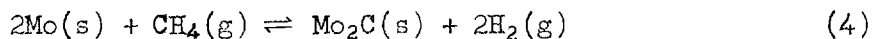
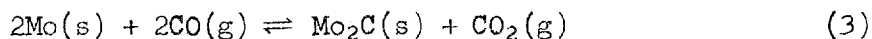
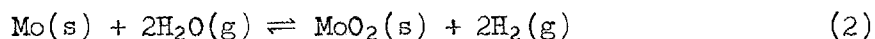
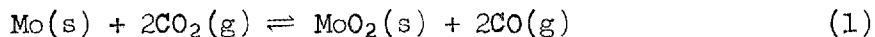
| Sample No. | Pass No. | Plate Temperature (°F) | Welding Current | | Welding Speed (in./min) | E7018 Electrode Diameter (in.) | Energy Input (joules/in.) | 50%-Shear Transition Temperature (°F) | Mid-Energy-Range Transition Temperature ^b (°F) |
|------------|----------|------------------------|-----------------|---------|-------------------------|--------------------------------|---------------------------|---------------------------------------|---|
| | | | Amperage | Voltage | | | | | |
| 1 | 1 | 80 | 160 | 21 | 8.75 | 5/32 | 23 100 | 45 | 30 |
| | 2 | 80 | 205 | 22 | 6.70 | 3/16 | 42 225 | | |
| 2 | 3 | 80 | 200 | 23 | 3.75 | 5/32 | 73 600 | 45 | 30 |
| | 4 | 80 | 235 | 23 | 4.16 | 3/16 | 78 000 | | |
| 3 | 5 | 80 | 250 | 24 | 3.97 | 3/16 | 90 700 | 65 | 55 |
| 4 | 6 | 80 | 200 | 21 | 3.60 | 3/16 | 70 000 | 55 | 40 |
| 5 | 7 | 200 | 160 | 21 | 9.00 | 5/32 | 22 400 | 25 | 25 |
| | 8 | 200 | 205 | 23 | 7.20 | 3/16 | 39 300 | | |
| 6 | 9 | 200 | 200 | 23 | 5.43 | 5/32 | 50 800 | 25 | 25 |
| | 10 | 200 | 235 | 23 | 3.10 | 3/16 | 105 000 | | |
| 7 | 11 | 200 | 250 | 24 | 4.4 | 3/16 | 81 900 | 60 | 60 |
| 8 | 12 | 200 | 200 | 21 | 4.0 | 3/16 | 62 600 | 50 | 50 |

^aAll welds were given a stress-relief anneal at 1150°F for 4 hr.

^bMid-energy-range transition temperature for the as-received material is approximately 50°F.

their compatibility with gases that might be present as impurities in the coolant stream. Studies are therefore being made of the thermodynamic equilibria for the systems involved.

Studies of the following reactions have been made based on available information:¹⁴⁻¹⁷



The calculated effects of the oxidizing or carburizing gas mixtures $\text{CO}_2 + \text{CO}$, $\text{H}_2\text{O} + \text{H}_2$, and $\text{CH}_4 + \text{H}_2$ on molybdenum are shown in Fig. 4.1 as a function of temperature. The combinations of temperature and gas ratios which lie to the left and below the curve for the MoO_2 - Mo - CO - CO_2 equilibria are reducing to MoO_2 and those to the right and above are oxidizing to molybdenum; the curve gives the specific temperatures and the ratios of the partial pressures at which Mo - MoO_2 - CO - CO_2 are in equilibrium.

In section A of Fig. 4.1, the $\text{H}_2\text{O} + \text{H}_2$ mixtures are reducing to molybdenum, the $\text{CO}_2 + \text{CO}$ mixtures are both reducing and carburizing, and the $\text{CH}_4 + \text{H}_2$ mixtures are decarburizing. In section B the $\text{H}_2\text{O} + \text{H}_2$ mixtures are reducing, the $\text{CO}_2 + \text{CO}$ mixtures are both reducing and carburizing, and the $\text{CH}_4 + \text{H}_2$ mixtures are carburizing. In section C

¹⁴K. Tonasaki, Bull. Inst. Phy. Chem. Research, Tokyo, 19, 126 (1940).

¹⁵M. deKay Thompson, "The Total and Free Energy of Formation of the Oxides of Thirty-Two Metals," pp. 21-22, The Electrochem. Soc., Inc., New York, 1942.

¹⁶K. K. Kelly, Bur. Mines Bull. 407 (1937).

¹⁷K. K. Kelly, Bur. Mines Bull. 476 (1949).

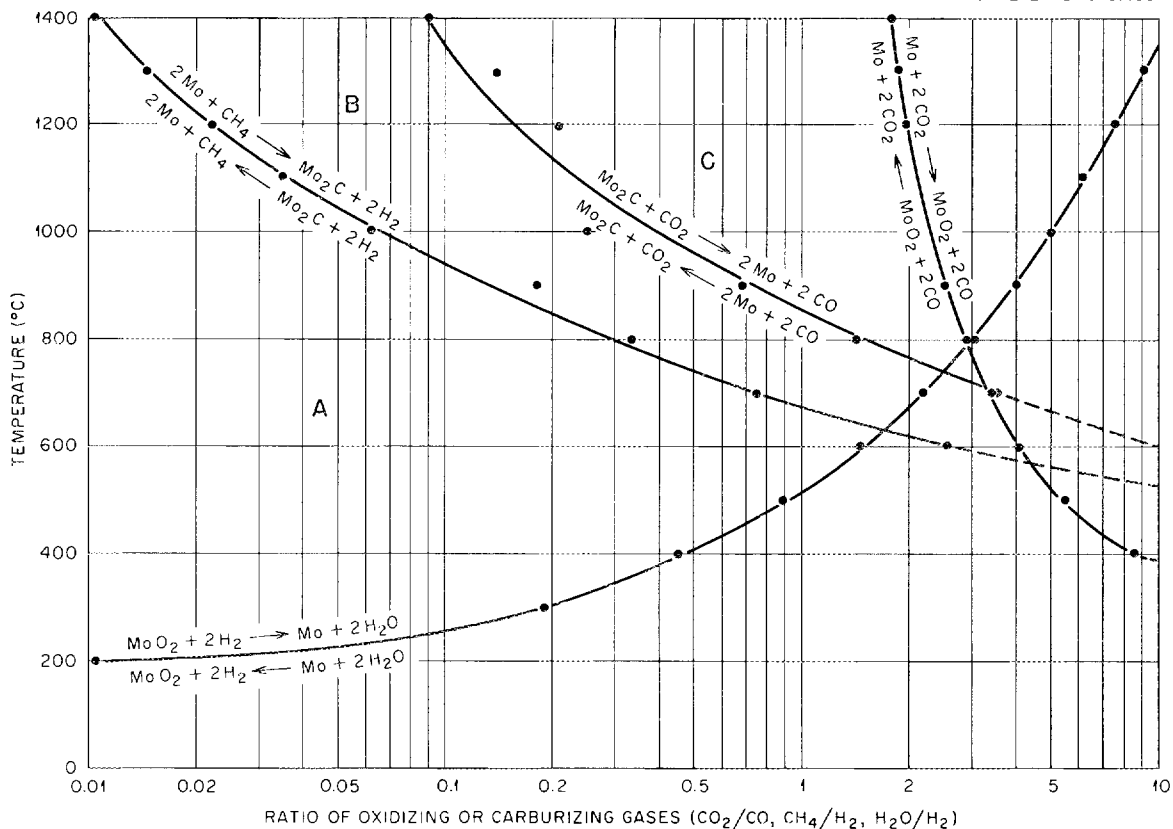


Fig. 4.1. Effect of Oxidizing and Carburizing Mixtures of $\text{CO}_2 + \text{CO}$, $\text{CH}_4 + \text{H}_2$, and $\text{H}_2\text{O} + \text{H}_2$ on Molybdenum.

the $\text{H}_2\text{O} + \text{H}_2$ mixtures are reducing, the $\text{CO}_2 + \text{CO}$ mixtures are both reducing and decarburizing, and the $\text{CH}_4 + \text{H}_2$ mixtures are carburizing. In sections C and A there are competing reactions for carburization and decarburization. There is, of course, some question in each case as to which reaction is the rate controlling one; however, free-energy calculations indicate that in section A the decarburizing reaction should take place and in section C the carburizing reaction should occur.

If the assumption is made that the amounts and species of impurities that will be present in the coolant of a gas-cooled reactor will be determined by the outgassing of the graphite moderator, then, the main impurities in the coolant will be hydrogen and carbon monoxide, with a moderate amount of carbon dioxide and very little methane, based

on the results of the graphite outgassing experiments.^{18,19} In an atmosphere such as this, the equilibrium curves predict that molybdenum will remain bright up to approximately 1000°C.

An important point that should be noted here is that the equilibrium curves show that relatively wet hydrogen will reduce MoO₂; that is, molybdenum will remain "bright" in relatively wet hydrogen. The significance of this is that if a steam leak should occur in the heat exchanger, a large amount of water would have to be present for MoO₂ to be formed and a still larger amount for MoO₃ to be formed, since the equilibrium curve for the reaction $\text{MoO}_3 + \text{H}_2 \rightleftharpoons \text{MoO}_2 + \text{H}_2\text{O}$ will lie below and to the right of the MoO₂-Mo-H₂-H₂O equilibrium curve.

At the present time these curves are tentative. Further calculations based on the work of other investigators will be made to check the validity of these curves and to determine the equilibria for other reactions.

Manufacturing and Inspection Methods Development

Fuel Element Fabrication

A series of fuel element end cap welds were made to determine the tolerance limits for protrusion of the end cap from or into the fuel element tube. It was found that no significant difference in welding characteristics could be noted with the end cap protruding from or into the tube as much as 0.010 in. The specimens were found to be leaktight by use of a helium mass spectrometer, and no indication of defects could be detected by radiography. Metallographic examination showed the configuration and penetration of the weld bead to be satisfactory.

Two specimens were also welded with the end cap flush against the fuel, since this condition might be encountered at times in the fabrication of a large number of elements. It would be expected that welding under these conditions might cause a strain on the weld because of

¹⁸"GCR Quar. Prog. Rep. Dec. 31, 1959," ORNL-2888, pp. 153-8.

¹⁹"GCR Quar. Prog. Rep. March 31, 1960," ORNL-2929, pp. 196-201.

shrinkage during cooling. When examined by fluorescent penetrant techniques, one weld of this type was found to have cracklike indications around the periphery. It is recommended that the tolerances be specified so that welds of this type will be avoided.

After brazing the mid-plane spacers to the fuel element capsule tubing with GE No. 81 brazing alloy (flow point of 2150°F), nonuniform grain growth in the tubing was observed, probably as a result of intermittent cold work introduced into the tubing from the mill-straightening operation. Such differences in grain size give variable mechanical properties to the tube wall and make predictions of the fuel element behavior difficult. Consequently, samples of 1/4-hard and 1/8-hard tubing were obtained to determine the metallurgical benefits that might be obtained with precold-worked tubing. Mid-plane spacers were brazed in place utilizing representative brazing thermal cycles of 10 min and 30 min at 2150°F, and the grain size of the tubing was compared with that obtained with annealed and straightened tubing. No significant difference in grain size was observed when the 2150°F brazing temperature was used, and thus cold-worked tubing can not be expected to materially improve the condition. Studies are now under way to determine the grain size of these tubes after brazing at the lower temperatures which would be associated with the substitution of other brazing materials, such as copper (flow temperature of 2020°F).

High-Temperature Thermocouple Development

Junction failures have been encountered frequently in the operational testing of stainless steel-sheathed tungsten-rhenium thermocouples. In order to provide a more reliable welded junction, a fabrication procedure was developed that incorporates a modified junction design. Instead of making a direct junction between the 0.025-in.-diam tungsten and rhenium wires, a spring-like length of 0.010-in.-diam rhenium is placed between the tungsten and rhenium primary wires, as shown in Fig. 4.2. This small-diameter length of rhenium serves as a flexible member and minimizes strains in the welded joints. Sample thermocouples that are

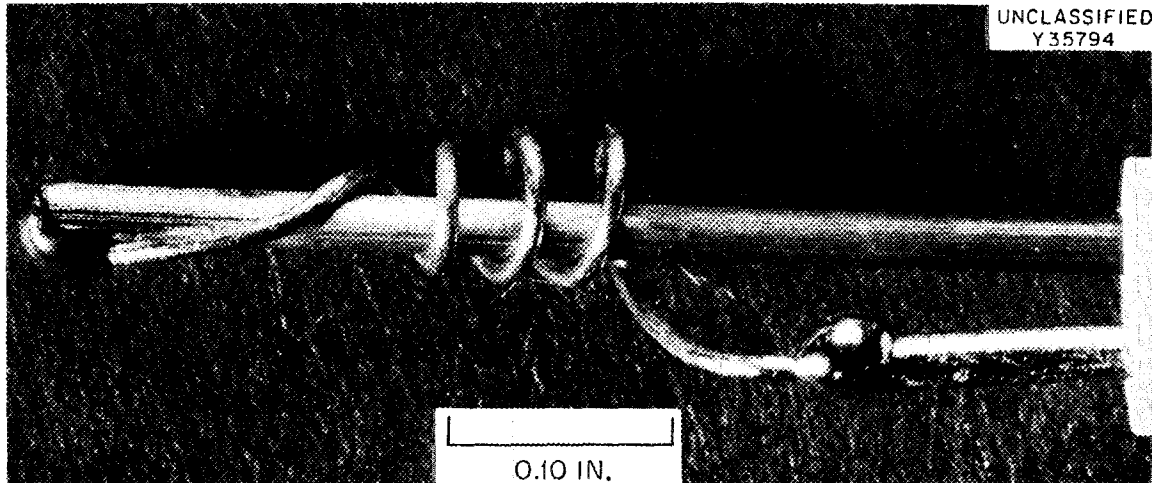


Fig. 4.2. Tungsten-Rhenium Thermocouple Weld with 0.010-in.-diam Rhenium Wire as a Flexible Member Between the Two 0.025-in.-diam Primary Wires.

being tested and calibrated have been operating continuously for over 1,000 hr.

Graphite Sleeve Inspection

Additional graphite-sleeve samples were requested for evaluation because of the discovery, as reported previously,²⁰ of cracks and low-density areas in the graphite sleeves supplied by three vendors. The additional samples received from two of the three vendors have been evaluated by the eddy-current test.

The six samples submitted by the National Carbon Company included three types of graphite: (1) small-grain AGOT, (2) large-grain AGOT, and (3) a special fine-grained graphite. Several areas that produced signals as large as, or larger than, those produced by the standard defect were found in all the AGOT samples.

Five specimens of type 9015 graphite rod, 5 in. in diameter and 11 in. long, were submitted by the Speer Carbon Company. The eddy-current inspection revealed no discontinuities, and there were no background "noise" signals, as found in previous specimens. These samples

²⁰"GCR Quar. Prog. Rep. June 30, 1960," ORNL-2964, p. 121.

appear to have uniform physical characteristics and are the best specimens examined to date.

Welding of EGCR Loop Through Tubes

Tests are continuing in an effort to develop suitable procedures for attaching the EGCR loop through tubes to the loop assembly. Linear plate welding by the inert-gas-shielded, consumable-electrode process on joint configurations similar to those anticipated in the EGCR was described previously.²¹

Since the feasibility of this welding process was demonstrated, a recently developed commercially available air-cooled torch was modified and used in producing concentric-tube seal welds for this application. Specimens for welding were machined from concentric tubes of 1/4-in.-wall type 347 stainless steel pipe. A rotary welding positioner was modified to hold and rotate the torch in relation to a stationary specimen. The specimen and torch mounted on the positioner may be seen in Fig. 4.3. As far as possible, conventional welding equipment was used; however, to supplement the existing equipment, an independent power supply for the wire feed was provided. In addition, an adjustable alignment apparatus was constructed to provide suitable rigidity to the torch, since

²¹"GCR Quar. Prog. Rep. June 30, 1960," ORNL-2964, pp. 122-6.

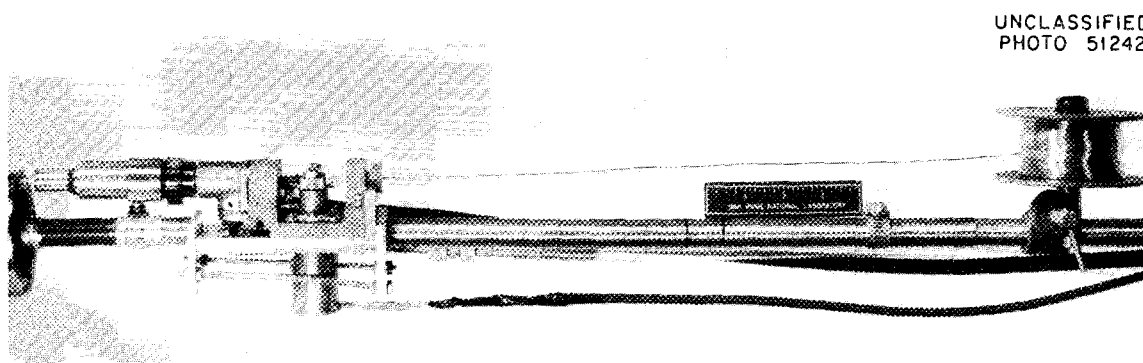


Fig. 4.3. Equipment Setup Used for Welding Concentric-Pipe Specimens.

preliminary experiments indicated that good alignment of the torch in relation to the joint was necessary. Slight modifications in the torch were also required to prevent electrical short circuits in the wire-feed mechanism.

With the use of this equipment, high-quality spray-transfer welds were made on concentric pipes that were comparable with those obtained on linear plate. The good bead contour of a typical weld may be seen in Fig. 4.4.

Welding of Dissimilar Metals

The following Welding Procedures and Operator's Qualification Test Specifications have been completed: (1) "ORNL Procedure Specification



Fig. 4.4. Typical Weld Made on Concentric Type 347 Stainless Steel Pipe.

P.S.-31 for Metal Arc Welding of ASTM A-387 Chromium-Molybdenum, Grade-D, Steel Plate to Types 304, 304L, 308, 316, 316L, and 347 Stainless Steel Plate," and "ORNL Operator's Qualification Test Specification QTS-31" for these materials combinations; and (2) "ORNL Procedure Specification P.S.-32 for Metal Arc Welding of Carbon Steel Plate ASME -- P No. 1 to Types 304, 308, 316, and 347 Stainless Steel Plate," and "ORNL Operator's Qualification Test Specification QTS-32" for these materials combinations.

Beryllium Investigations

Compatibility of Beryllium with Coolant Impurities

Reaction with CO₂. The investigation of the compatibility of beryllium with CO₂ was extended to include the determination of the effect of pressure on the reaction rates. Tests of -200 mesh beryllium powder were conducted in CO₂ at pressures of 1×10^{-3} mm Hg and 760 mm Hg. The CO₂ for the low-pressure tests was obtained by decomposing CaCO₃; purified bottle gas was used for the atmospheric pressure tests. Tests were run at 720, 650, and 600°C in atmospheric and low-pressure CO₂.

In plotting the data from the tests it was noted that the rate of weight change continuously decreased with time, as would be expected for the formation of a protective oxide film when the oxidation rate is parabolic. The equation for this type of reaction is

$$\Delta w = Kt^{1/n} ,$$

where Δw is weight gain in $\mu\text{g}/\text{cm}^2$, t is time in hours, and K and n are constants.

When the natural log is taken of both sides of this equation, the following linear relationship is obtained:

$$\ln \Delta w = \ln K + \frac{1}{n} \ln t .$$

The experimental data are being fitted to this equation by the method of least squares. Table 4.8 gives the values of $\ln K$ and $1/n$ obtained

Table 4.8. Values of $\ln K$ and $1/n$ at 99% Confidence Level for Reaction of Beryllium with CO_2

| Test Temperature ($^{\circ}\text{C}$) | Duration of Test (hr) | $\ln K$ | $1/n$ | CO_2 Pressure (mm Hg) |
|---|-----------------------|--------------------|---------------------|--------------------------------|
| 850 | 1000 | -5.869 ± 0.453 | 0.3414 ± 0.0823 | 1×10^{-3} |
| 846 | 350 | -5.778 ± 0.528 | 0.3427 ± 0.1123 | 1×10^{-3} |
| 838 | 350 | -4.963 ± 0.516 | 0.3838 ± 0.1118 | 1×10^{-3} |
| 720 | 1000 | -5.461 ± 0.477 | 0.3224 ± 0.0803 | 1×10^{-3} |
| 720 | 225 | -6.824 ± 0.715 | 0.6862 ± 0.1706 | 1×10^{-3} |
| 720 | 400 | -5.167 ± 0.667 | 0.4347 ± 0.1331 | 760 |
| 600 | 350 | -7.354 ± 0.665 | 0.6132 ± 0.1175 | 1×10^{-3} |

in this manner. In all cases the phases present after testing were beryllium and beryllium oxide.

The rate curves obtained by plotting weight change versus time are presented in Figs. 4.5, 4.6, and 4.7. The CO_2 pressures for the two experiments at one specific temperature differ by a factor of 0.76×10^6 ; however, the rate curves at a given temperature are only slightly

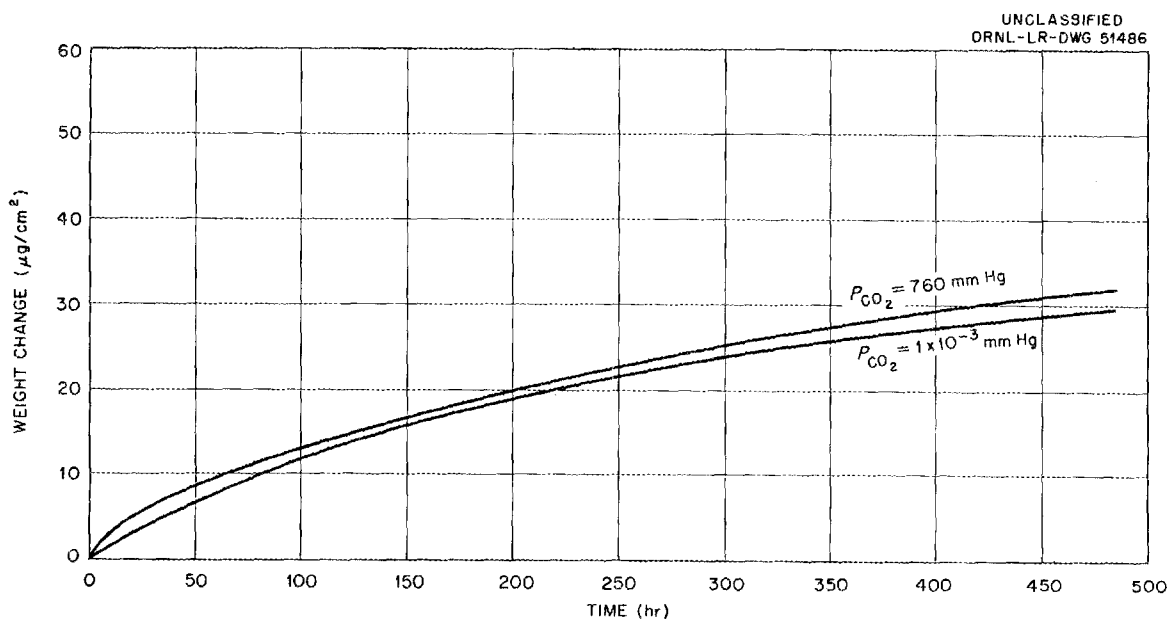


Fig. 4.5. Rate Curves for the Oxidation of -200 Mesh Beryllium Powder at 600°C by Atmospheric and Low-Pressure CO_2 .

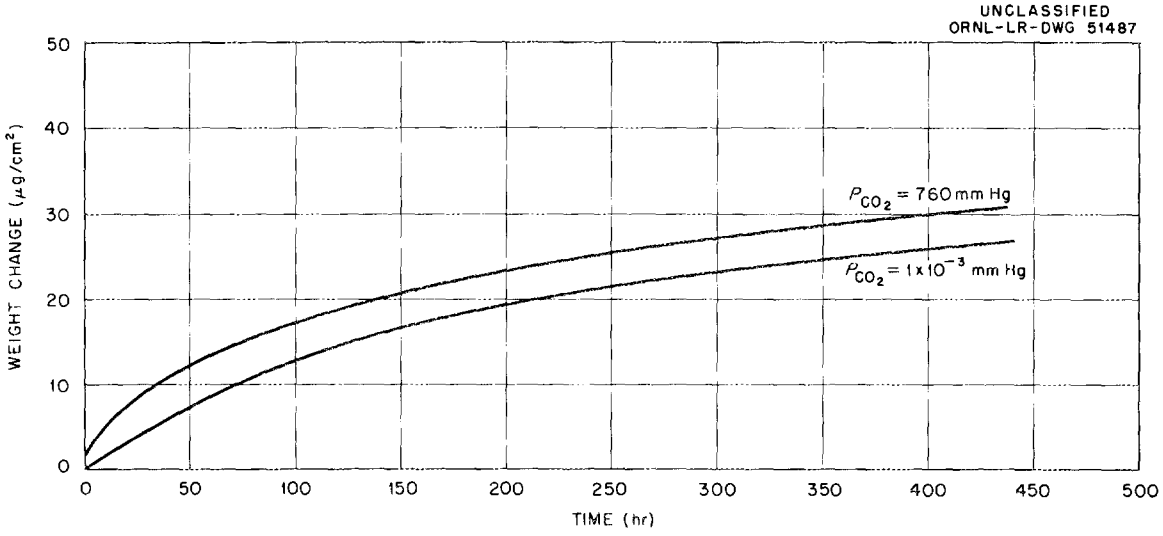


Fig. 4.6. Rate Curves for the Oxidation of -200 Mesh Beryllium Powder at 650°C by Atmospheric and Low-Pressure CO₂.

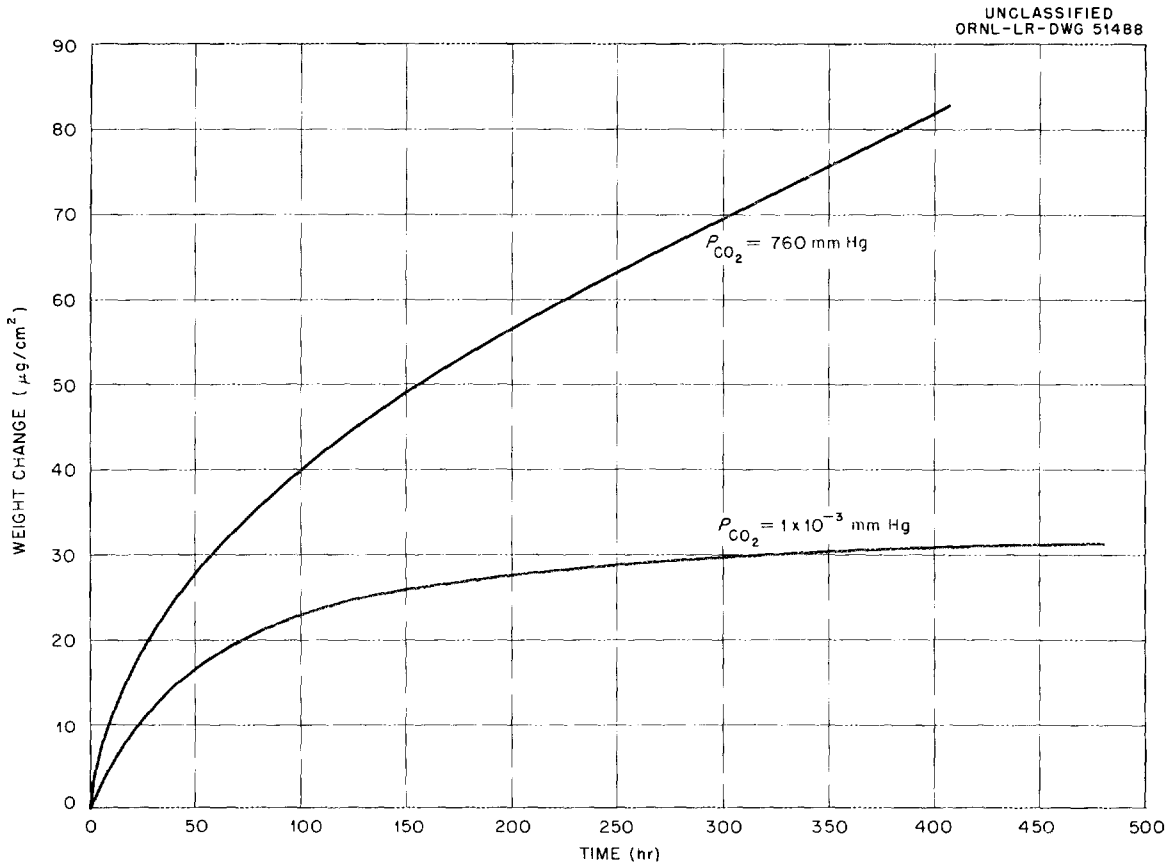


Fig. 4.7. Rate Curves for the Oxidation of -200 Mesh Beryllium Powder at 720°C by Atmospheric and Low-Pressure CO₂.

different. This strongly indicates that the reaction of beryllium with CO_2 is independent of pressure and that the rate-controlling phenomenon in the oxidation process is the diffusion of the oxidizing species through the protective oxide film.

Reaction with Water Vapor. An investigation of the compatibility of beryllium with water vapor at reduced pressures has been started. The tests are being conducted on -200 mesh powder in a system similar to that used for the Be- CO_2 compatibility studies. Water vapor for the tests is obtained by the decomposition of $\text{Ca}(\text{OH})_2$.

One test has been completed. The test temperature, which was initially 700°C , was raised to 750°C after 424 hr and allowed to remain there for the duration of the test. The weight-gain data from this test are plotted in Fig. 4.8. It should be noted that the oxidation rate is very slight (even less than the rate for beryllium with low-pressure CO_2 at 600°C) and that the rate of weight gain continuously decreases with increasing temperature. It thus appears that a protective film is being formed.

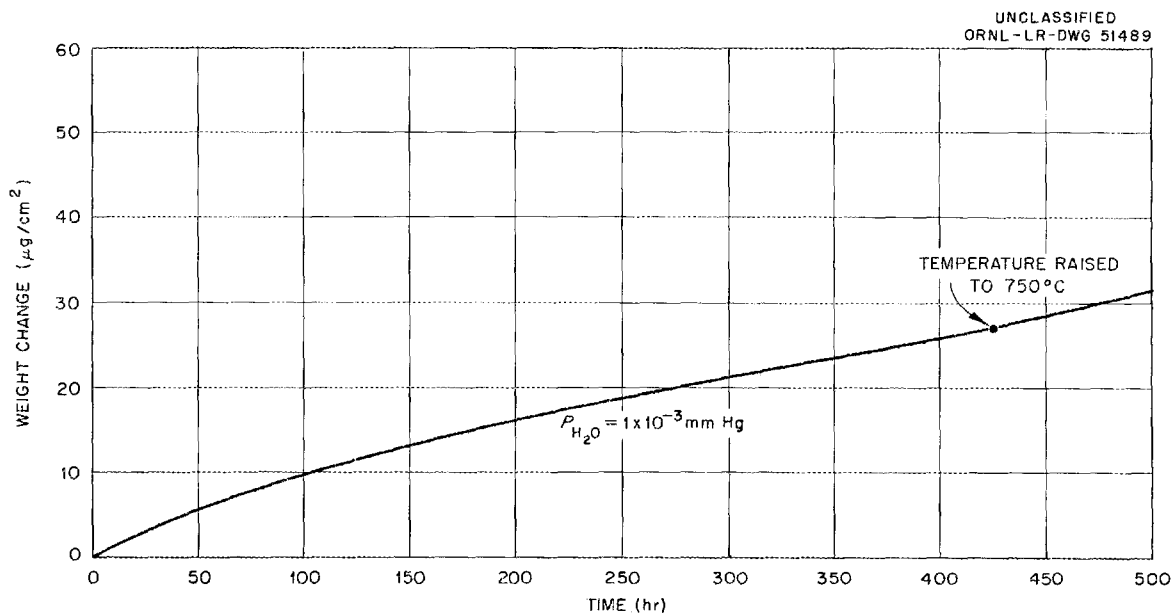


Fig. 4.8. Rate Curve for the Oxidation of -200 Mesh Beryllium Powder at 700°C by Low-Pressure Water Vapor.

Procurement of Beryllium Tubing

Additional quantities of beryllium tubing were received on the purchase orders described previously.²² The three sources are Pechiney of France, the Chesterfield Tube Company of England, and the Brush Beryllium Corporation. The Chesterfield Tube Company has been optimizing their fabrication procedures and are continually producing better quality tubing to closer tolerances. At the present time they can meet a ± 0.0025 -in. specification on the inside diameter. It is expected that the balance of the tubing on the Chesterfield Tube Company purchase order, which has been shipped, will be of higher quality as a result of the fabrication procedure improvements.

Fabrication of Tubing

A final report has been received from Nuclear Metals, Inc.,²³ describing the work completed on a subcontract for investigating the effect of extrusion variables on the quality and properties of beryllium tubing. Nuclear Metals has worked on the development of extrusion techniques for the production of beryllium tubing in the size range 0.400 to 0.750 in. in outside diameter with 0.030- to 0.100-in. walls. Three specific sizes were extruded by two different techniques during the development work: (1) 0.400 in. o.d. with a 0.030-in. wall, (2) 0.750 in. o.d. with a 0.030-in. wall, and (3) 0.750 in. o.d. with a 0.100-in. wall. In one method, the filled-billet method, a hollow beryllium core in an extrusion billet was filled with a steel filler that was removed after extrusion. In the other method a hardened-steel mandrel was used to form and control the inside diameter of the tube. Both of these methods were used to produce the 0.400-in.-o.d. tubing.

The lowest degree of preferred orientation was found in tubes extruded by the filled-billet method from hot-compacted cores contained

²²"GCR Quar. Prog. Rep. June 30, 1960," ORNL-2964, p. 135.

²³R. N. Randall and F. M. Yans, "Development of Techniques for the Extrusion of Beryllium Tubing," NMI-2602 (June 30, 1960).

within a thick-walled can. A low degree of preferred orientation was also found in tubing extruded at lower temperatures and lower reduction ratios. Tubes produced from hot-compacted cores by extrusion with a mandrel had a high degree of preferred orientation but also had the highest room-temperature burst strengths. Sections of these tubes have been received at the Laboratory for evaluation.

The 0.750-in.-o.d., 0.030-in.-wall tubing was produced by extrusion of hot-compacted billets over a mandrel. Because of equipment limitations it was necessary to extrude at reduction ratios varying from 15:1 to 25:1. Tubes extruded at the lower reductions cracked more severely than those extruded at high reductions, presumably because the heavy steel sheath held the beryllium in tension during cooling.

Beryllium Tubing Evaluation

The evaluation of beryllium tubing has been continued with tests on tubing from American, British, and French sources.²⁴ Although a considerable amount of additional tubing has been investigated, the percentage of tubing containing discontinuities is about the same. The following is a brief summary of all inspection results to date using penetrant, radiographic, ultrasonic, and eddy-current techniques.

Tubing from Brush Beryllium Company. Evaluation has been completed on 121 pieces of tubing machined from hot-pressed block, 98 from hot-extruded rod, and 62 from warm-extruded rod. In addition 38 pieces of warm-extruded tubing have been examined. All the tubing contains a few shallow pinholes. Approximately one-third of the machined tubing has been rejected because of failure to comply with the wall-thickness tolerance. Less than one-fifth of the warm-extruded tubing has been rejected for this reason. A large number of defect indications have been noted during the eddy-current examinations. Of the machined tubing, 84% from the hot-pressed block, 38% from the hot-extruded rod, and 88% from the warm-extruded rod have contained defect indications in excess

²⁴"GCR Quar. Prog. Rep. June 30, 1960," ORNL-2964, pp. 136-8.

of that from a 0.006-in.-deep reference notch. Further study of these defect indications is being conducted.

Tubing from Pechiney. A total of 179 pieces of 0.300-in.-i.d. tubing has been examined. Penetrant examination has shown small pits and pinholes in all the tubing and circumferential and longitudinal cracks in 15% of the tubes. Radiographic examination has shown some high-density material in most of the tubing and circumferential pitting in approximately one-half the tubing. Only 5% of the tubing failed to meet the wall-thickness tolerance. Slightly over one-half of the tubing presented excessive defect indications during eddy-current inspection.

Tubing from Chesterfield Tube Company. High-density material continues to prevent valid radiographic inspection. The rough outer surface is still causing difficulty during penetrant and ultrasonic examination, but 20 pieces have been evaluated by both resonance and pulse-echo ultrasonics. No rejections were made. Further evaluations are being conducted.

Beryllium Joining

The utilization of beryllium as a cladding material for advanced gas-cooled reactor fuel elements requires that suitable joining techniques for this material be developed. Investigations are therefore being conducted to evaluate various procedures for sealing tubular fuel elements and to determine suitability for extended elevated-temperature service. The procedures include fusion welding, high-temperature brazing, and diffusion bonding. In addition to these developmental efforts, beryllium-clad fuel capsules were fabricated for irradiation studies in the ORR.

In-Pile Test Capsule Fabrication. Several beryllium-clad capsules containing UO_2 fuel were received from the United Kingdom Atomic Energy Authority and the Commissariat a l'Energie Atomique of France for irradiation in the ORR poolside facility. The UKAEA and CEA capsules were nominally 0.380 in. o.d. and 0.600 in. o.d., respectively, with 0.040-in. walls, and were 6.484 in. long.

Two counterparts of each type of foreign-made capsule (one spare of each type) were fabricated for irradiation under similar conditions.

These counterpart capsules were fabricated from tubing from the Brush Beryllium Company (0.38 in. in diameter) and from Pechiney (0.60 in. in diameter). End caps were machined from Brush S200A extruded rod. The capsules were sealed with edge-fusion welds by the techniques discussed in the following section. Measurements made during assembly showed axial clearances within the capsule ranging from 0.058 to 0.064 in. and diametral clearances varying from 0.0013 to 0.0032 in.

Visual, dye-penetrant, helium leak testing, and radiographic inspection indicated that these capsules were sound. As shown in Fig. 4.9, no porosity was detected in the welds of the smaller diameter capsule;

UNCLASSIFIED
Y36208

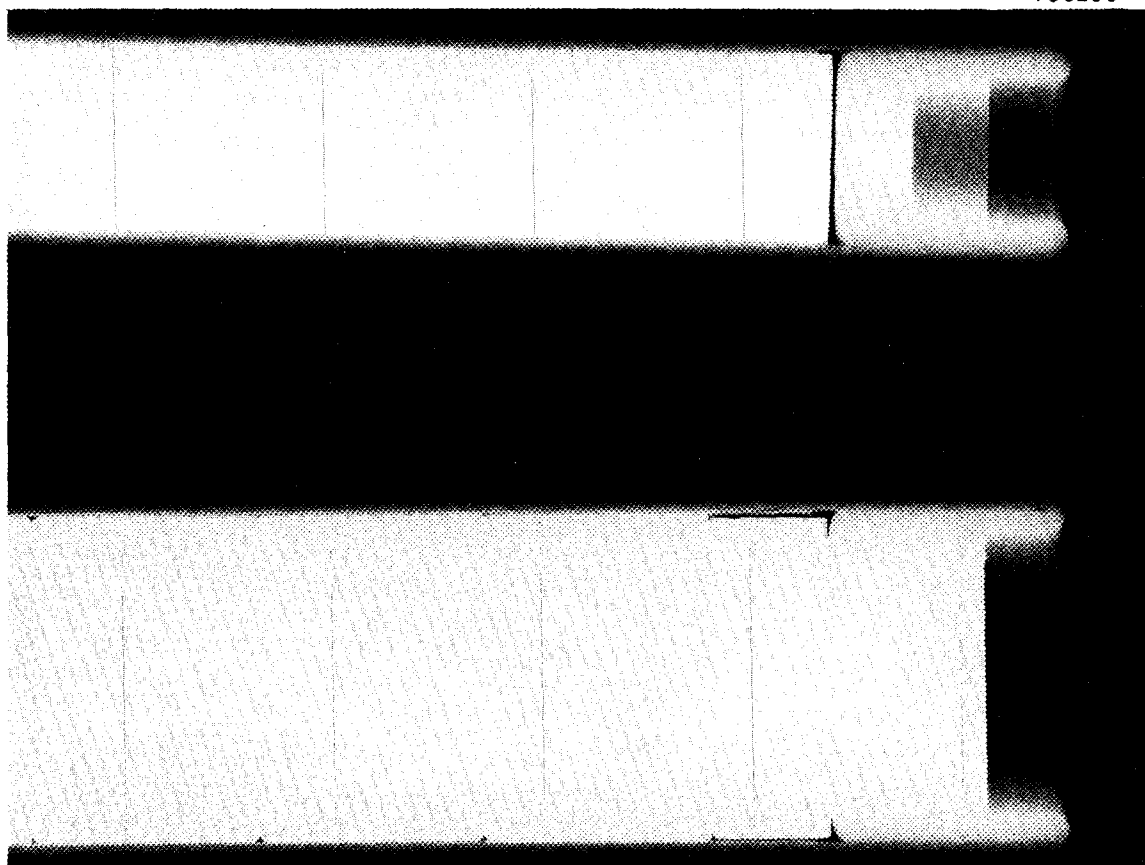


Fig. 4.9. Radiographs of the Fusion Welds on ORNL Beryllium-Clad Capsules.

however, very fine-line porosity was observed in the radiograph of the larger diameter capsule.

The foreign-made capsules were inspected by identical procedures before assembly into the test apparatus. In general, much more porosity was detected in the closure welds, but the capsules were leaktight and acceptable.

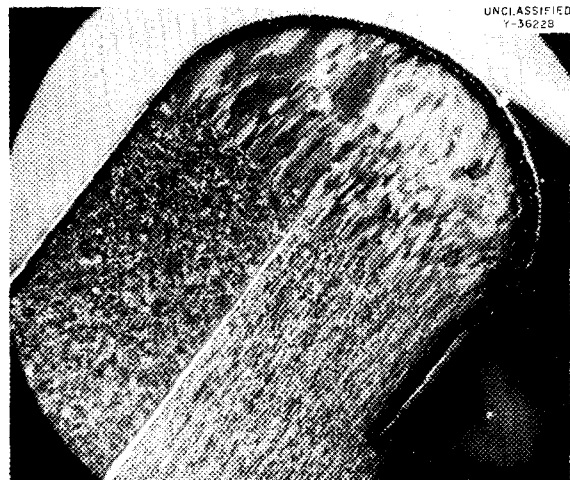
Fusion Welding. The study of fusion welding of beryllium is continuing in an effort to establish consistently reproducible techniques for fabricating end closures on beryllium tubular fuel elements. The investigation is also concerned with the evaluation of the weldability of tubing made by various fabrication processes.

Successful welds have been made on end-closure joints by using the inert-arc process. Figure 4.10 illustrates the excellent metallographic appearance of the fusion-welded beryllium joints presently being produced. These edge-welded end closures were leaktight in a mass-spectrometer test.

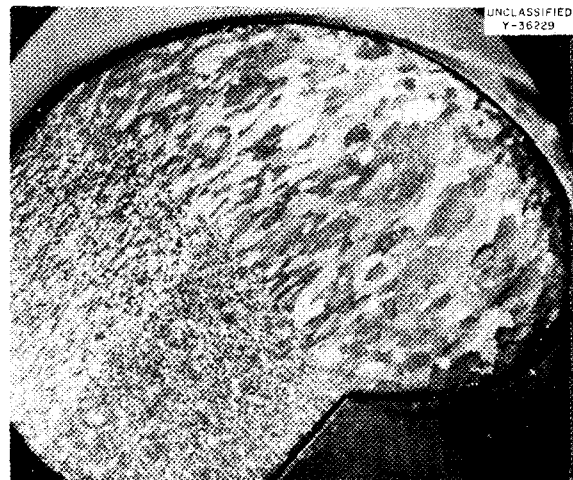
It is interesting to note that the joints shown in Fig. 4.10 are crack-free, in comparison with the joints shown in the previous report²⁵ that contained extensive root cracking. The crack-free joints were obtained by utilizing press-fitted end caps machined from high-purity material. The tight-fitting joint resulted from machining the end cap to a 1-mil interference fit with the tube and freezing the cap in liquid nitrogen prior to joint assembly. This procedure is admittedly difficult and inconvenient, and other means are being investigated. One possible solution now under study incorporates a slightly tapered end plug which would give the desired tight-fitting joint and also minimize the assembly difficulties. Closure welds of this design are being tested.

While the joints shown in Fig. 4.10 are crack-free, only welds made on Brush Beryllium Company hot-pressed tubing (Fig. 4.10a) consistently contain no porosity. The porosity generally occurring in the extruded tubing of Figs. 4.10b, c, d, and e constitutes a problem that is receiving considerable study. It has been found that an increase in inert

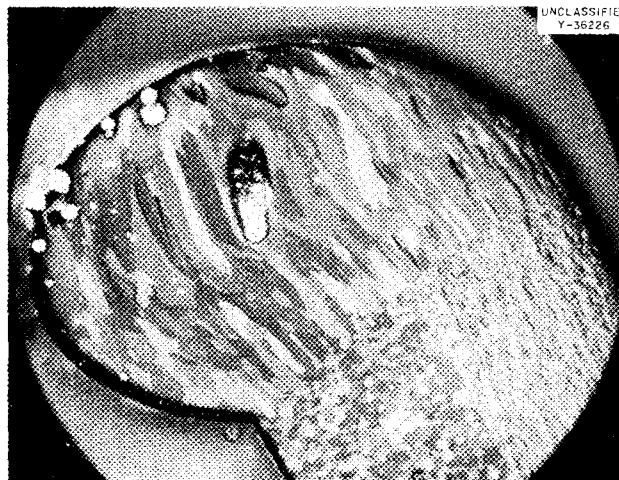
²⁵"GCR Quar. Prog. Rep. June 30, 1960," ORNL-2964, p. 144.



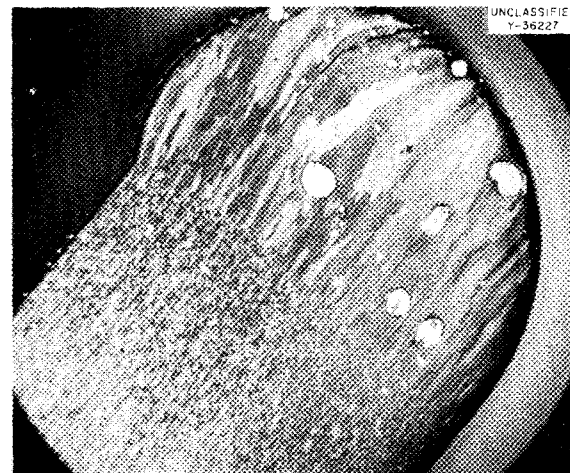
(a) BRUSH BERYLLIUM - HOT PRESSED



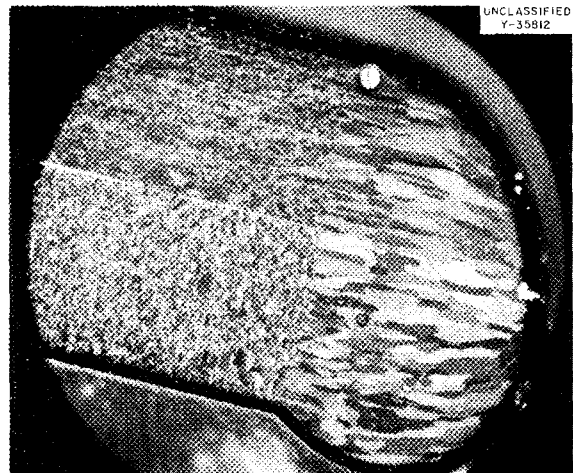
(b) BRUSH BERYLLIUM - HOT EXTRUDED



(c) BRUSH BERYLLIUM - WARM EXTRUDED



(d) PECHINEY TUBE - HOT EXTRUDED



(e) CHESTERFIELD TUBING - HOT EXTRUDED

Fig. 4.10. Beryllium Fusion Welds Made with Edge-Welded End Closures on Tubing Made by Various Fabrication Techniques. 50X Unetched.

gas flow around the electrode during welding provides improved bead coverage, with a resultant decrease in the amount of porosity occurring in weldments. The determination of the extent to which such an improvement affects the mechanical properties is being evaluated.

Shear tests have been performed on tube-to-end plug beryllium welds in an effort to determine the mechanical strength of beryllium edge welds. The joints were hydraulically stressed to failure at room temperature. The results of these tests are presented in Table 4.9. It should be noted that all end-plug joints were loose fitting, except those of the oval-shaped Chesterfield tubes. These joints, welds 69 and 70, were the only group in which all failures occurred in the tube rather than the weld bead. The probable explanation for this occurrence is that areas of very tight fit existed in these oval tubes. It has been found that severe root cracking of welds is associated with loose-fitting end caps. This might explain the low joint efficiencies observed in the other samples tested. The joint efficiency is defined as the ratio of the weld-failure stress to the tube-failure stress, expressed in percent.

Table 4.9. Evaluation of Beryllium End-Cap Welds by Shear Testing at Room Temperature

| | Fabrication Method* | Fracture Pressure (psi) | Fracture Stress (psi) | Location of Failure | Joint Efficiency (%) |
|-------------|---------------------|-------------------------|------------------------------|---------------------|----------------------|
| Tube | BA-H | 12 700 (av) | 47 000 (av) | Tube | |
| Weld No. 57 | BA-H | 7 080 | 26 500 | Weld | 56.4 |
| 58 | BA-H | 10 600 | 40 000 | Weld | 85.2 |
| Tube | BC-WE | 14 200 (av) | 53 000 (av) | Tube | |
| Weld No. 63 | BC-WE | 11 300 | 42 500 | Tube | 100 |
| 64 | BC-WE | 10 600 | 40 000 | Weld | 75.5 |
| Tube | CT-HE | 10 000 (av) | 40 000 (av) | Tube | 100 |
| Weld No. 69 | CT-HE | 10 600 | 40 000 | Tube | 100 |
| 70 | CT-HE | 5 660 | 21 200 | Tube | 100 |
| Tube | PT-HE | 15 000 (av) | 54 000 (av) | Tube | |
| Weld No. 71 | PT-HE | 11 300 | 42 400 | Weld | 78.5 |
| 72 | PT-HE | | Tube cracked during handling | | |

*BA-H: Brush tubing machined from hot-pressed rod.
 BC-WE: Brush tubing machined from warm-extruded rod.
 CT-HE: Chesterfield tubing, hot extruded.
 PT-HE: Pechiney tubing, hot extruded.

5. IN-PILE TESTING OF COMPONENTS AND MATERIALS

Fuel Element Irradiation Program

Full-Diameter Prototype EGCR Fuel Capsules

Irradiation in the ORR of the eight group II experimental capsules described previously^{1,2} was completed on June 11. Following withdrawal, the units were moved to the west pool of the reactor facility and readied for transfer into the ORR south hot cell. The operating data for this experiment are summarized in Table 5.1. Irradiation of 14 capsules designed for various UO₂ fuel burnups is continuing in the ETR.

Beryllium Cladding and UO₂ Grain-Size Studies

The eight group III experimental capsule assemblies³ that were designed for irradiation at a reactor power of 30 Mw were completed and inserted in the reactor at the beginning of cycle 28; irradiation started August 14, 1960. These eight capsules are described below:

| <u>Capsule No.</u> | <u>Capsule Description</u> |
|--------------------|---|
| 01-3 | Stainless-steel-clad, cored, large-grain-size UO ₂ pellets, 0.323 in. in inside diameter; cladding 0.75 in. in outside diameter; central thermocouple installed; ORNL fabricated |
| 02-3 | Beryllium-clad, solid UO ₂ pellets, 0.59 in. in outside diameter; ORNL-fabricated counterpart of capsules 03-3 and 04-3 |
| 03-3 | Same as 02-3; CEA France fabricated |
| 04-3 | Same as 03-3 |
| 05-3 | Beryllium-clad, solid UO ₂ pellets, 0.38 in. in outside diameter; UKAEA fabricated |
| 06-3 | Same as 05-3 |
| 07-3 | Same as 05-3; ORNL fabricated |
| 08-3 | Same as 01-3, except that capsule contains small-grain-size UO ₂ pellets |

¹"GCR Quar. Prog. Rep. Dec. 31, 1959," ORNL-2888, p. 99.

²"GCR Quar. Prog. Rep. March 31, 1960," ORNL-2929, p. 148.

³"GCR Quar. Prog. Rep. June 30, 1960," ORNL-2964, p. 149.

Table 5.1. Summary of Operating Data for Group II Full-Diameter Prototype EGCR Fuel Capsule Irradiations in the ORR

Irradiation starting date: December 3, 1959
 Irradiation ending date: June 11, 1960
 Irradiation time normalized to operation at 20 Mw: 144.9 days
 Reactor power generation during irradiation: ~69 530 Mwhr

| | Capsule Number | | | | | | | |
|--|-------------------------|-------------------------|------------------------|------------------------|-------------------------|-------------------------|-------------------------|-------------------------|
| | 01-2 | 02-2 | 03-2 | 04-2 | 05-2 | 06-2 | 07-2 | 08-2 |
| Reactor position | P-8, P-9 | P-8 | P-7, P-8 | P-7 | P-3 | P-2, P-3 | P-2 | P-1, P-2 |
| Perturbed thermal flux, neutrons/cm ² ·sec | 6.04 × 10 ¹² | 6.18 × 10 ¹² | 8.2 × 10 ¹² | 8.2 × 10 ¹² | 9.12 × 10 ¹² | 6.55 × 10 ¹² | 3.63 × 10 ¹² | 4.27 × 10 ¹² |
| Number of pellets | 12 | 12 | 12 | 12 | 12 | 12 | 11 | 11 |
| Pellet density, % of theoretical | | | | | | | | |
| Bulk, average | 95.62 | 95.81 | 94.26 | 94.35 | 94.80 | 94.26 | 95.26 | 95.44 |
| Immersion, average | 97.90 | 97.72 | 97.63 | 97.72 | 97.27 | 98.18 | 97.08 | 98.18 |
| Pellet enrichment, % U ²³⁵ | 6.49 | 6.49 | 5.03 | 5.03 | 4.60 | 6.10 | 7.49 | 6.83 |
| Oxygen-to-uranium ratio | 2.0105 | 2.0105 | 2.0044 | 2.0030 | 2.0020 | 2.0022 | 2.0026 | 2.0025 |
| Pellet diameters (cold), in. | | | | | | | | |
| Inside, average | 0.3231 | 0.3229 | 0.3233 | 0.3233 | 0.3246 | 0.3250 | 0 | 0 |
| Outside, average | 0.7057 | 0.7055 | 0.7060 | 0.7060 | 0.7061 | 0.7062 | 0.7062 | 0.7061 |
| Radial clearance between UO ₂ and cladding, in. | | | | | | | | |
| Maximum | 0.0033 | 0.0029 | 0.0031 | 0.0031 | 0.0031 | 0.0027 | 0.0028 | 0.0029 |
| Minimum | 0.0024 | 0.0024 | 0.0024 | 0.0024 | 0.0022 | 0.0020 | 0.0024 | 0.0024 |
| Total power, Btu/hr·ft | 27 870 | 28 530 | 28 820 | 28 850 | 29 530 | 28 000 | 24 640 | 26 460 |
| Total heat flux, Btu/hr·ft ² | 150 800 | 154 300 | 155 900 | 156 100 | 159 800 | 151 500 | 133 300 | 143 100 |
| Burnup, calculated | | | | | | | | |
| Total, Mwd/MT of UO ₂ | 2061 | 2109 | 2167 | 2167 | 2209 | 2103 | 1430 | 1535 |
| Rate, Mw/MT of UO ₂ (per day at full power) | 14.23 | 14.56 | 14.96 | 14.96 | 15.25 | 14.52 | 9.87 | 10.60 |
| Typical irradiation conditions ^a | | | | | | | | |
| Temperature at outer surface of cladding, °F | | | | | | | | |
| Design | 1300 ^b | 1600 ^c | 1300 ^b | 1300 ^b | 1600 ^c | 1600 ^c | 1300 ^b | 1600 ^c |
| Highest | 1375 | 1595 | 1370 | 1380 | 1595 | 1580 | 1420 | 1590 |
| Lowest | 998 | 1225 | 942 | 990 | 1370 | 1412 | 1215 | 1380 |
| Average | 1310 | 1462 | 1315 | 1320 | 1476 | 1493 | 1288 | 1485 |
| Pressure on outer surface of cladding, psig | 286 | 285 | 285 | 283 | 290 | 282 | 283 | 292 |
| Controlled thermal cycles ^d | | | | | | | | |
| First week | 0 | 0 | 20 | 20 | 20 | 20 | 20 | 20 |
| Last week | 0 | 0 | 24 | 24 | 14 | 14 | 14 | 14 |

^aAs of 9 a.m. on March 16, 1960.

^bAverage temperature to be indicated by the six thermocouples.

^cHighest temperature to be indicated by the thermocouples.

^dControlled thermal cycling conducted only during first and last week of irradiation period.

Pertinent design data and planned operating conditions for this experiment are summarized in Table 5.2.

The design was based on thermal-neutron flux values obtained from measurements taken November 30, 1959. After the group II capsules were removed, a more complete set of flux measurements was made, and lower values were obtained. These data were used for calculation of design revisions after assembly work was well under way, and adjustments were made where feasible to reposition the capsules closer to the reactor core. Unfortunately, it was not possible to attain the flux originally specified.

The 0.39- and 0.59-in.-o.d. beryllium-clad elements of group III are mounted in pressurized NaK-containing capsules with thermal-barrier gas temperature control similar to that used for the group I and II irradiations. The specimen cans are located by molybdenum spacers within slotted 3/4-in.-o.d. stainless steel tubes which are mounted as for previous experiments. The components of a mockup assembly are shown in Fig. 5.1. The gang-type cadmium shutters used for applying thermal cycles to group I and II experiments have been replaced with chimney-type units located on each individual capsule. Each shutter is operated by a cable driven by a pneumatic cylinder attached to the upper end of the experiment lead tube.

The EGCR-prototype full-diameter capsules 01-3 and 08-3 contain large and small grain-size UO_2 pellets, respectively, and tungsten-rhenium thermocouples for measurement of central temperatures. Unfortunately the rhenium wire of the thermocouple in capsule 08-3 separated within its stainless steel sheath during brazing to the capsule bulkhead and repair was not possible. At the beginning of irradiation, the central thermocouple of capsule 01-3 produced a thermoelectric signal, but again difficulties probably resulting from assembly problems were apparent. After a brief operating period and while the reactor was returning to power following refueling, the thermocouple emf drifted erratically to a low value, where it has remained. The difficulties encountered are not thought to be fundamental to the thermocouple

Table 5.2. Summary of Design Data and Planned Operating Conditions for Group III Capsules

| | Capsule Number | | | | | | | |
|--|-----------------------|--|--|--|-----------------------|-----------------------|-----------------------|-----------------------|
| | 01-3 | 02-3 | 03-3 | 04-3 | 05-3 | 06-3 | 07-3 | 08-3 |
| Experiment code number | OR-2G | OR-2B | FR-1BN | FR-2BN | BR-1B | BR-2B | OR-1B | OR-1G |
| Origin of specimen | ORNL | ORNL | CEA, France | CEA, France | United Kingdom, AEA | United Kingdom, AEA | ORNL | ORNL |
| Specimen identification | Tube 4-E | ORNL-2B-1 | 03 | 08 | 3009B | 2932 | ORNL-1B-2 | Tube F-18 |
| Thermal flux, neutrons/cm ² ·sec | | | | | | | | |
| Design (based on 11/30/59 measurements), perturbed | 1.66×10^{13} | 2.89×10^{13} | 7.62×10^{13} | 7.86×10^{13} | 2.24×10^{13} | 2.24×10^{13} | 2.39×10^{13} | 1.66×10^{13} |
| Revised estimated (based on 6/30/60 measurements) | | | | | | | | |
| Unperturbed | 2.65×10^{13} | 4.15×10^{13} | 9.20×10^{13} | 8.30×10^{13} | 3.25×10^{13} | 2.90×10^{13} | 2.80×10^{13} | 1.70×10^{13} |
| Perturbed | 1.33×10^{13} | 2.14×10^{13} | 5.00×10^{13} | 4.83×10^{13} | 1.95×10^{13} | 1.53×10^{13} | 1.52×10^{13} | 0.82×10^{13} |
| Enrichment, % U ²³⁵ | 2.30 | 1.95 | 0.71 | 0.71 | 2.45 | 2.45 | 2.30 | 2.30 |
| Heat rate, Btu/hr·ft | | | | | | | | |
| Design | 30 000 | 30 000 | 30 000 | 30 000 | 9 600 | 9 600 | 9 600 | 30 000 |
| Revised estimate | 24 000 | 22 200 | 19 100 | 18 500 | 8 400 | 6 600 | 6 100 | 14 900 |
| Specific power, watts/g of UO ₂ | | | | | | | | |
| Design | 13.9 | 20.5 | 20.3 | 20.3 | 20.0 | 20.0 | 20.0 | 13.9 |
| Revised estimate | 11.1 | 15.2 | 12.9 | 12.5 | 17.4 | 13.7 | 12.7 | 6.9 |
| Cladding temperature, °F | 1600 | 1112 | 1112 | 1112 | 1112 | 1112 | 1112 | 1600 |
| Cladding pressure, psig | 300 | 150, 1 month 225, 1 month 300, balance | 150, 2 months 225, 2 months 300, balance | 150, 1 month 225, 1 month 300, balance | 300 | 300 | 300 | 300 |
| Shutter thermal cycles | None | 20 at end of each month | 20 at end of each month | 20 at end of each month | 1 per day | 1 per day | 1 per day | None |
| Thermal barrier gas gap, in. | | | | | | | | |
| Hot | 0.012 | 0.006 | 0.006 | 0.006 | 0.023 | 0.023 | 0.023 | 0.012 |
| Cold | 0.0195 | 0.011 | 0.011 | 0.011 | 0.028 | 0.028 | 0.028 | 0.0195 |

UNCLASSIFIED
PHOTO 35565

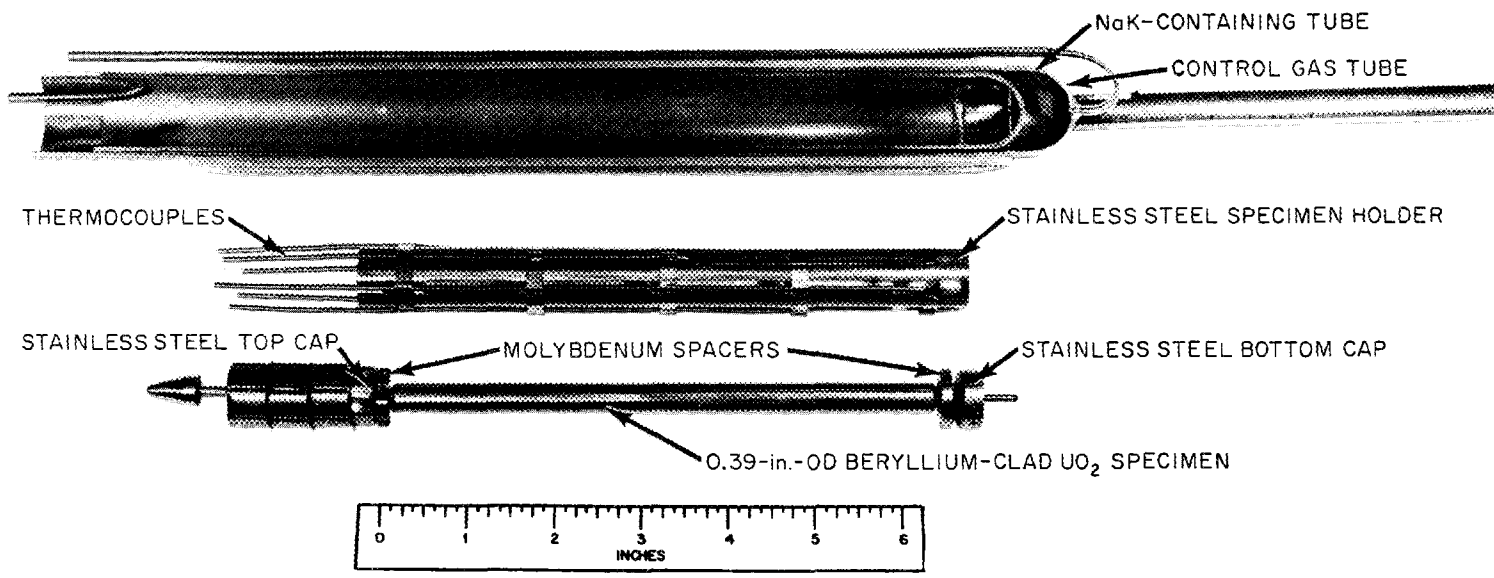


Fig. 5.1. Component Parts of 0.39-in.-o.d. Beryllium-Clad Capsule in Mockup Assembly.

installation design, but, rather, they reflect assembly problems with unfamiliar and brittle materials.

Miniature Capsule Fission-Gas-Release Experiments

Irradiations of capsules L-23ab, L-24ab, and L-27ab have been completed, and the capsules have been removed from the reactor core. The irradiation conditions for these and other capsules which remain in the reactor core are presented in Table 5.3.

Table 5.3. Operating Data for Miniature Capsule Fission-Gas-Release Experiments

UO₂ pellet density: 95% of theoretical

| Experimental Assembly No. | UO ₂ Enrichment (% U ²³⁵) | Central UO ₂ Temperature (°F) | | Date Installed | Date Removed |
|---------------------------|--|--|-----------|----------------|------------------------|
| | | Capsule a | Capsule b | | |
| L-22ab | 10 | 1380 | 1600 | 11-10-59 | Irradiation continuing |
| L-23ab | 15 | 2800 | 2800 | 12-8-59 | 6-28-60 |
| L-24ab | 20 | 2600 | 3100 | 12-16-59 | 8-23-60 |
| L-27ab | 15 | 2000 | 2600 | 3-15-60 | 8-23-60 |
| L-28ab | 30 | 2200 | 3800 | 4-5-60 | Irradiation continuing |
| L-32ab | 30 | a | 3300 | 6-1-60 | Irradiation continuing |

^aThermocouple inoperative.

The offgas system for the irradiation facility being used in the LITR for these experiments has been modified to include carbon traps in addition to absolute filters for efficient cleanup in the event of cladding failures. The modified system is capable of containing coolant air at the full supply pressure of 96 psig in the event of a line plug or inadvertant closure of offgas line valves.

Advanced Fuel Element Testing

A second fueled-graphite assembly, designated ORNL-MTR-48-2, is being irradiated in the MTR, and the activity of the sweep gas is being monitored, as described previously.⁴ The increase in the activity of the sweep gas during the first three reactor cycles is shown in Fig. 5.2. The three sets of data presented in Fig. 5.2 may not be compared directly because there has been a gradual increase in the purge gas flow rate to 60% above the design value. The flow control device has been thrown off

⁴"GCR Quar. Prog. Rep. June 30, 1960," ORNL-2964, p. 154.

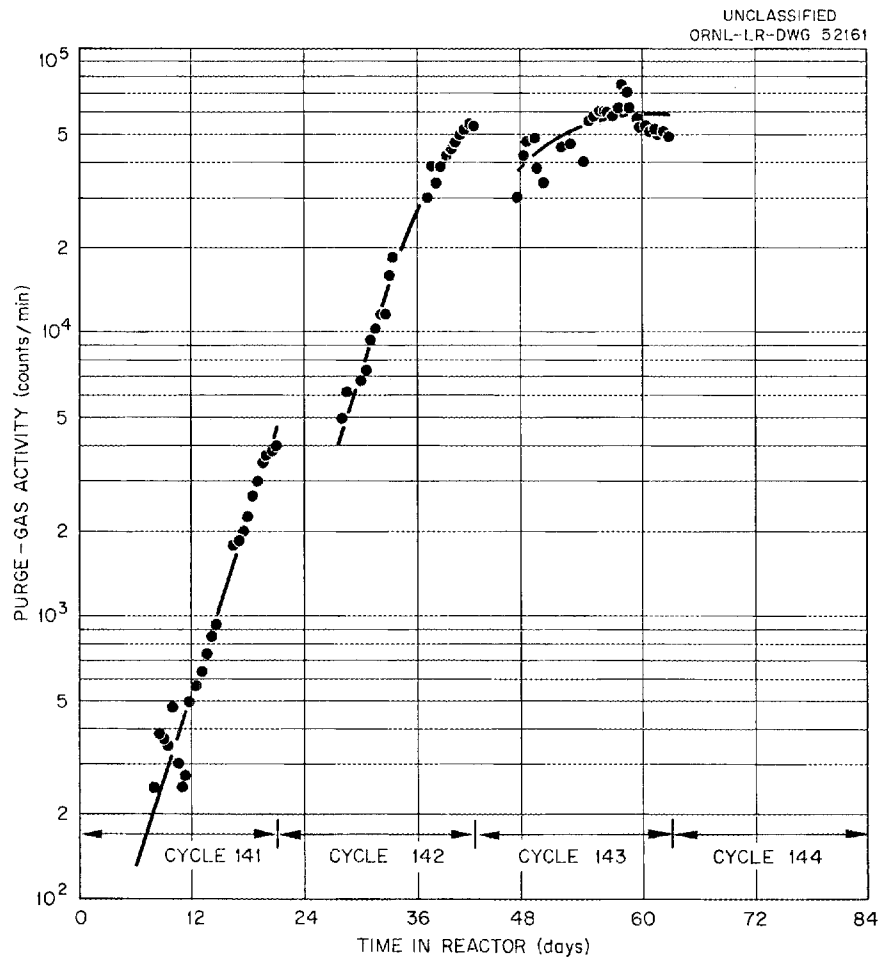


Fig. 5.2. Radioactivity in Purge Gas from Experimental Assembly ORNL-MTR-48-2 Which Contains Fueled Graphite Cylinders in a Graphite Capsule.

calibration by a slowly developing flow restriction in the experimental assembly that has caused an increase in the purge-gas pressure. Only $\text{Kr}^{85\text{m}}$, Kr^{88} , and Xe^{135} have been detected so far in gas samples analyzed with the MTR gamma-ray spectrometer.

Examination of Irradiated Capsules

LITR-Irradiated Miniature Capsules

Additional postirradiation examinations of miniature-capsule experimental assemblies have been completed, and an interim report⁵ has been issued summarizing all the fission-gas-release data obtained from irradiation experiments in the LITR and the ORR. The densities of the UO_2 pellets used in the capsules examined recently are given in Table 5.4 before and after irradiation. A small increase in immersion density after irradiation is indicated.

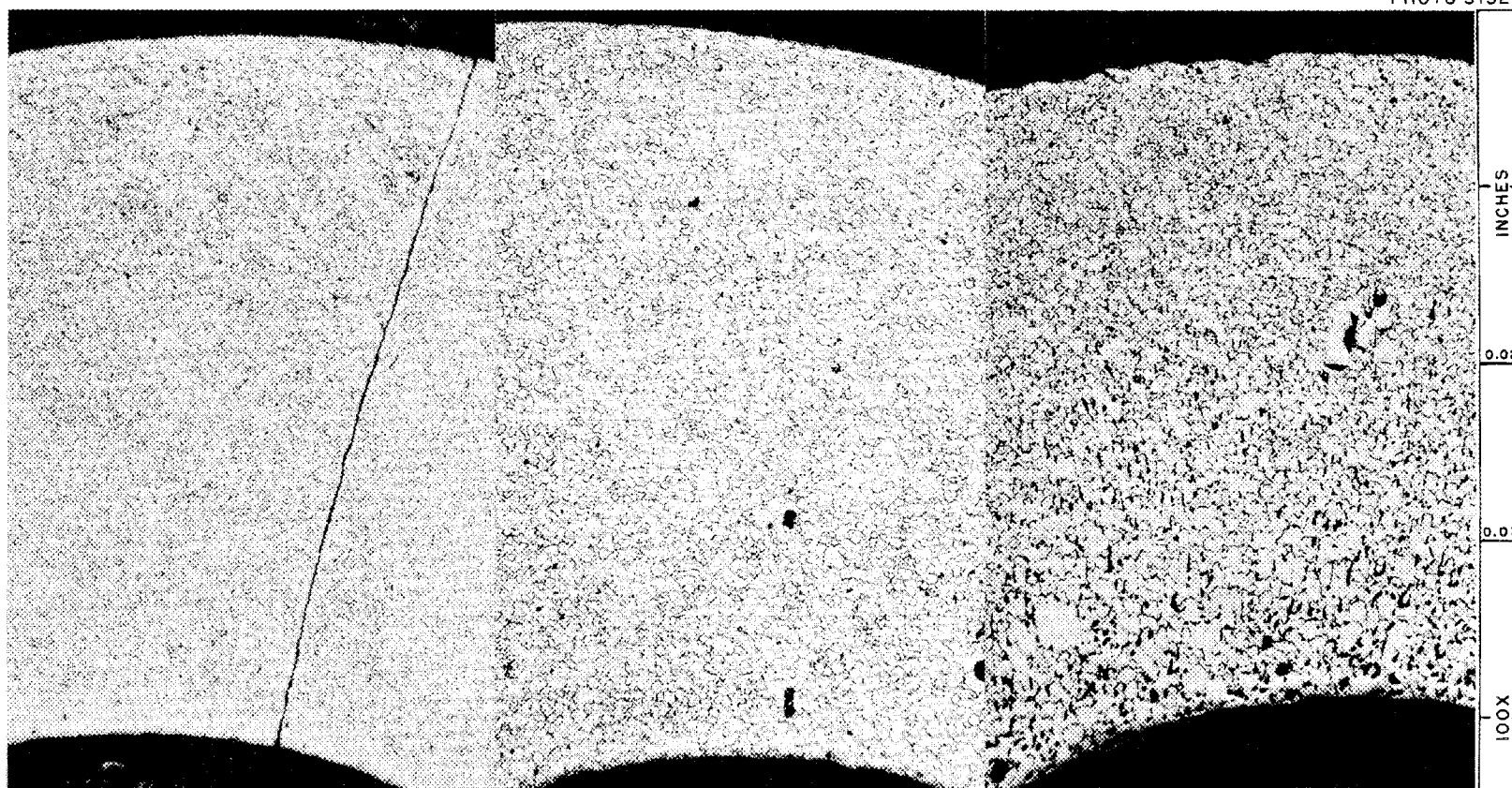
The effect of irradiation on UO_2 grain size is shown in Fig. 5.3, in which the microstructures of an unirradiated specimen, a specimen irradiated at 1900°F (capsule L-16a), and a specimen irradiated at 2700°F are shown. The variation in grain size is due to the temperature gradient.

⁵J. G. Morgan, M. T. Morgan, and M. F. Osborne, "Fission-Gas-Release from UO_2 Interim Report Number 1," ORNL CF-60-7-11 (July 29, 1960).

Table 5.4. Data Showing Effect of Irradiation on UO_2 Density

| Capsule No. | Burnup, from Co^{60} (Mwd/MT) | Effective UO_2 Central Temperature (°F) | Pellet Density Before Irradiation | | | Pellet Immersion Density After Irradiation (g/cm^3) |
|-------------|--|--|-----------------------------------|---|--|---|
| | | | Bulk Density (% of theoretical) | Bulk Density (g/cm^3) | Immersion Density (g/cm^3) | |
| L-16a | 2900 | 1900 | 94.35 | 10.35 | 10.48 | 10.66 |
| L-16b | 2900 | 2050 | 94.38 | 10.35 | 10.47 | 10.58 |
| L-16xa | 3200 | 2700 | 93.98 | 10.31 | 10.46 | 10.59 |
| L-16xb | 3200 | 3000 | 94.35 | 10.35 | 10.48 | 10.62 |
| L-17xa | 3100 | 2800 | 94.62 | 10.38 | 10.48 | 10.57 |
| L-17xb | 3100 | 3100 | 94.83 | 10.40 | 10.45 | 10.54 |
| L-18xa | 8400 | 2200 | 84.69 | 9.29 | 10.39 | 10.62 |
| L-18xb | 8400 | 2500 | 84.58 | 9.28 | 10.37 | 10.52 |

UNCLASSIFIED
PHOTO 51526



UNIRRADIATED

IRRADIATED AT 1900°F

IRRADIATED AT 2700°F

Fig. 5.3. Microstructure of UO_2 Showing Effect of Irradiation at Central Temperatures of 1900°F and at 2700°F.

Columnar growth and grain reorientation are also indicated. These effects have been observed only in capsules irradiated at central temperatures of 2700°F or higher.

Experimental assemblies L-23, L-24, and L-25 were removed from the reactor during the quarter. Fission-gas release from capsules L-25a and b (Table 5.5) was comparable with the gas release from capsules irradiated previously under similar conditions, except that the Xe¹³⁵ release was unaccountably high.

Four LITR-irradiated assemblies (L-7x, L-11, L-23, and L-25) and five ORR-irradiated group I capsules (O-1, O-2, O-3, O-5, and O-6) are being examined. Results of fission-gas analyses, gamma-ray scans, and dimensional measurements of the ORR capsules were reported previously.^{6,7}

⁶"GCR Quar. Prog. Rep. March 31, 1960," ORNL-2929, pp. 157-9.

⁷"GCR Quar. Prog. Rep. June 30, 1960," ORNL-2964, p. 157.

Table 5.5. Fission-Gas Release from LITR-Irradiated Capsules L-25a and b

| | Capsule L-25a | Capsule L-25b |
|---|------------------|------------------|
| UO ₂ density, % of theoretical | 95.17 | 94.90 |
| Maximum central UO ₂ temperature, °F | 2150 | 2500 |
| Burnup, Mwd/MT | 5100 | 5100 |
| Fission-gas evolution, % of gas formed | | |
| Kr ⁸⁵ | 0.15 | 0.15 |
| I ¹³¹ | trace | 0.09 |
| Xe ¹³³ | 0.039 | 0.22 |
| Xe ¹³⁵ | 0.019 | 2.0 |
| Oxygen-to-uranium ratio | 2.02 | 2.02 |
| Carbon content, ppm | 2.00 | 2.00 |

ORR-Irradiated Prototype Capsules

The eight group II ORR-irradiated assemblies have been dismantled in the ORR south hot cell. The fuel capsules and flux monitors were recovered, and the NaK, thermocouples, and facility tubes were discarded. The outside diameters of several NaK containers were measured and are compared with preirradiation diameters in Table 5.6. The data indicate that the 15-psi pressure differential between the NaK gas blanket and the control gas (300 psi vs 285 psi) was sufficient to cause increases in the average diameters that ranged from 0 to 0.008 in. The eight capsules may be seen in Fig. 5.4 as they appeared after they were removed from the NaK containers and cleaned.

Table 5.6. Average Diameters of ORR Group II NaK Containers

| Experimental Assembly No. | Diameter of Container ^a (in.) | | | | | |
|---------------------------------|--|----------------------|--|----------------------|--|----------------------|
| | Measured 1 in. Below Top of Capsule | | Measured 4 in. Below Top of Capsule | | Measured 6 in. Below Top of Capsule | |
| | Before Irradiation | After Irradiation | Before Irradiation | After Irradiation | Before Irradiation | After Irradiation |
| 01-2 | 0.9800 | 0.9808 | 0.9796 | 0.9802 | 0.9794 | 0.9802 |
| 05-2 | 0.9788 | 0.9809 | 0.9788 | 0.9813 | 0.9787 | 0.9787 |
| 06-2 | 0.9795 | 0.9804 | 0.9799 | 0.9833 | 0.9793 | 0.9807 |
| 08-2 | 0.9792 | 0.9801 | 0.9792 | 0.9874 | 0.9787 | 0.9806 |

^aAverage of three measurements taken 60 deg apart.

Measurement of Fission-Gas Pressure in Prototype Capsule at EGCR Operating Temperature

The possible pressure buildup in EGCR fuel elements from alkali-metal fission products that have low boiling points suggested the measurement of the pressure buildup in prototype capsules at EGCR operating temperatures. Rosenthal and Cantor⁸ have shown that the yield of the alkali metals is high (about 62% of that of the noble gases) and have

⁸M. W. Rosenthal and S. Cantor, "Some Remarks on the Contribution of Fission Product Cesium to the Pressure Buildup in UO₂ Fuel Elements," ORNL CF-60-3-81 (March 18, 1960).

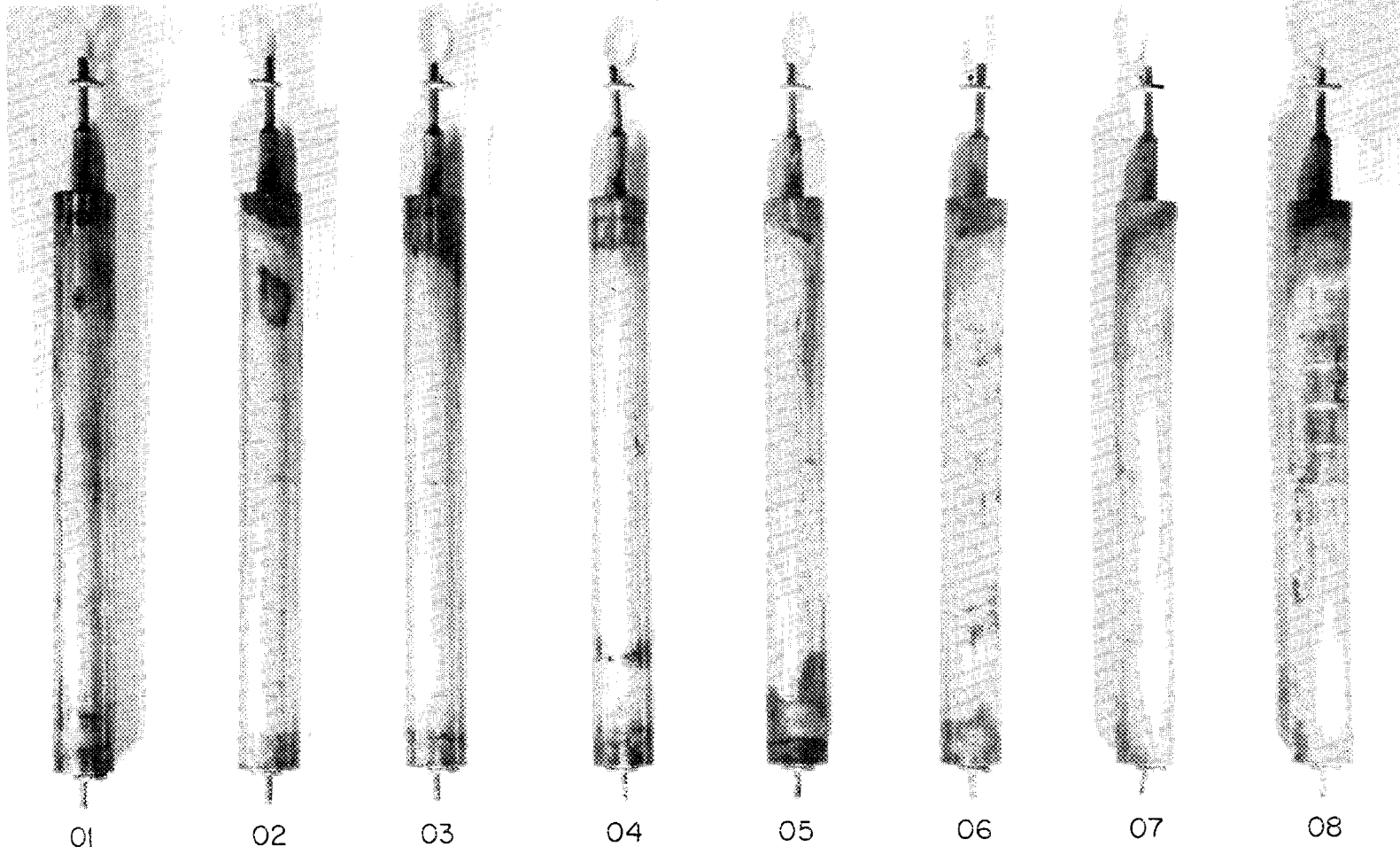


Fig. 5.4. Group II ORR-Irradiated Capsules After Removal from NaK Container and Cleaning.

cited evidence that cesium, the primary alkali-metal product, is mobile in hot UO_2 . The vapor pressures of metallic cesium and rubidium are less than 1 atm at temperatures below 1250°F , and since the vapor pressure will be controlled by the lowest temperature in the fuel element, which is expected to be below 1250°F , they conclude⁸ that the pressure contribution from this source will not be significant. A measurement of the pressure buildup in an EGCR prototype fuel capsule (O-6) has supported this conclusion.

The pressure in capsule O-6 was measured at temperatures up to 1700°F , and no significant contribution from high-temperature vaporization was noted. The capsule was heated to 1650°F , cooled, and reheated to 1700°F . A plot of the pressure data versus temperature shows (Fig. 5.5) a deviation from a straight line of about 4 psi at 1650°F (about 3.5% of the total pressure). Since the cooling curve and the second heating curve follow a straight line, it may be assumed that the slight pressure increase during the first heatup was due to additional noble gases being released.

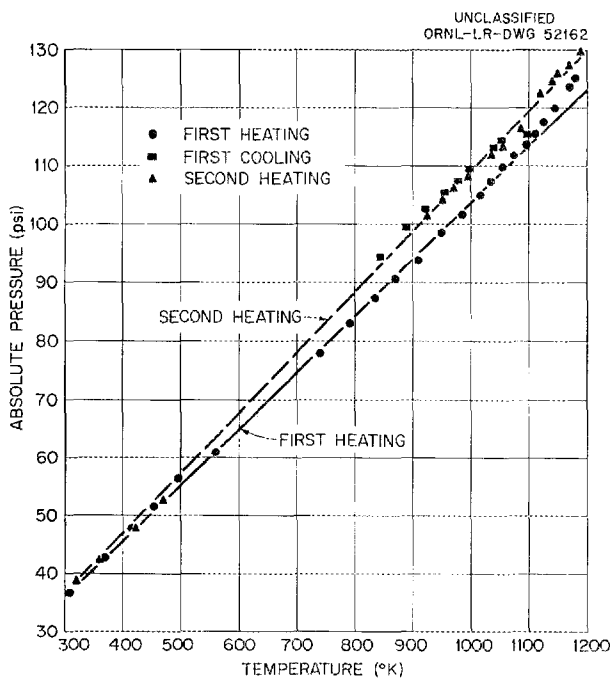


Fig. 5.5. Pressure Buildup in Capsule O-6 at High Temperatures.

ORR Closed-Cycle-Loop Experiments

Irradiation of two UO_2 samples encased in siliconized silicon carbide-coated graphite⁹ in the ORR-B9 closed-cycle loop was terminated after 790 hr at 1800°F. During the last 46 hr of the irradiation the flux was 1.0×10^{14} neutron/cm²·sec because the ORR power level was increased to 30 Mw. Postirradiation examination of these specimens has not yet begun.

In order to determine whether the fission-product activity in the coolant gas was from the samples being tested or was from contamination remaining in the in-pile tubes from a previous experiment, gas samples were taken with the test samples withdrawn from the reactor flux zone. The gas samples taken while the experimental assembly was withdrawn yielded a count rate for the detectable isotopes that was approximately the same as that of the gas collected during full flux irradiation. It is therefore concluded that the fission-product leakage, if any, from the graphite-clad UO_2 samples was small compared with the residual background activity.

The next samples scheduled for irradiation are UO_2 cylinders encased in uncoated low-permeability graphite. These samples were assembled and sealed by the National Carbon Company. The Si-SiC seal at the top of the graphite lid is shown in Fig. 5.6. The two samples have been encapsulated in Inconel, with thermocouples inserted between and beneath the samples. The Inconel capsule was weld sealed in a dry box purged with helium.

Instantaneous Fission-Gas-Release Experiment

An increase by two orders of magnitude over the initial fission-gas-release rate of the thin-plate high-density UO_2 sample being used for studies of instantaneous fission-gas release led to the conclusion that the UO_2 had been oxidized by trace quantities of oxygen in the sweep gas.

⁹"GCR Quar. Prog. Rep. June 30, 1960," ORNL-2964, pp. 166-7.

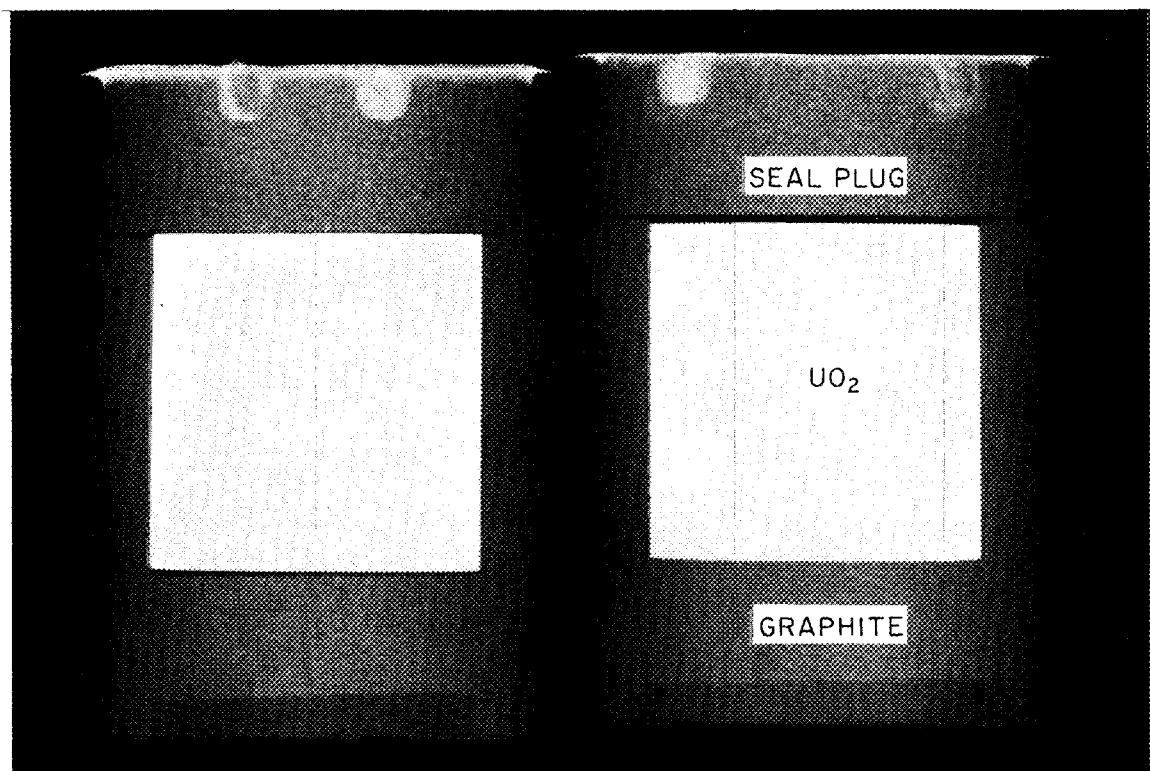


Fig. 5.6. X-ray Photograph of UO_2 Cylinders in Low-Permeability Graphite Sealed with Siliconized Silicon Carbide.

This conclusion was strengthened by the observation of stored energy in the UO_2 , since stored energy has been observed only in UO_2 with an oxygen-to-uranium ratio of 2.08 or greater.¹⁰

In order to assure an oxygen-free sweep gas, a new system was installed for using argon or helium containing 3% hydrogen. Oxygen in the sweep gas is removed by catalyzing the reaction between hydrogen and oxygen. The gas stream is then dried and passed through a column of high temperature (1400°F) copper turnings. The excess hydrogen in the sweep gas reduces the fuel to UO_2 rather than allowing oxidation.

¹⁰"GCR Quar. Prog. Rep. June 30, 1960," ORNL-2964, pp. 167-74.

The effectiveness of the reducing atmosphere was demonstrated by operating for one week with the new sweep-gas system. The fission-gas-release rate was reduced by a factor of 3, demonstrating that excess oxygen was responsible for the earlier increased fission-gas-release rate. When the hydrogen-helium mixture first contacted the UO_2 there was a burst of fission gas that gradually subsided over a period of about 8 hr. There was no temperature change at the time of this burst, and this was the only burst observed which was not caused by a variation of temperature. Gamma energy spectra showed that the relative composition of the fission gas did not change as the activity level decreased with time.

During the time the fuel was in the reducing atmosphere it became obvious, from temperature relations, that the thin-plate sample had broken and perhaps crumbled. The fuel capsule has been removed from the reactor and will be examined in the hot cell. An oxygen-to-uranium ratio measurement will be attempted.

The fuel for the next experiment is now being prepared. It will also be in the form of thin plates of high-density UO_2 , and, in addition to the fission-gas-release studies, thermal and electrical conductivity measurements will be made during irradiation.

6. OUT-OF-PILE TESTING OF MATERIALS AND COMPONENTS

Compatibility Tests of Graphite, Structural Materials, and Helium

Low-pressure thermal-convection loop No. 12, which contained AGOT graphite and specimens of structural materials in a helium environment, and which operated with a hot-leg temperature of 1100°F, was terminated after 1000 hr. This loop was the third in a series¹ in which the impurity content in the helium was maintained in the range tentatively specified for the EGCR. As shown in Table 6.1 the CO content of the helium in loop No. 12 was controlled at a value of 0.18 vol % by injection of a measured amount of pure carbon monoxide. The helium used was essentially free of all other impurities, except for 0.15 vol % CO₂, which was present by virtue of the CO-graphite equilibrium.

Table 6.1. Maximum Impurity Concentration of Helium Environment in Low-Pressure Thermal-Convection Loop No. 12 Compared with EGCR Helium Specification

| Impurity | Impurity Concentration in Helium (vol %) | |
|------------------|---|--------------------|
| | In Loop No. 12 | EGCR Specification |
| CO ₂ | 0.15 | 0.2 |
| CO | 0.18 | |
| O ₂ | 0.0005 | |
| CH ₄ | 0.0005 | |
| H ₂ O | 0.002 | 0.1 |
| H ₂ | 0.003 | 0.1 |

The extent of oxidation of the steel specimens exposed in this loop is indicated in Table 6.2. As may be seen, the weight gains of the

¹"GCR Quar. Prog. Rep. June 30, 1960," ORNL-2964, pp. 186-8.

Table 6.2. Oxidation of Low-Alloy Steels Exposed to Helium and to Air for 1000 hr at 1100°F

| Environment | Specimen Description | Weight Gain (mg/cm ²) | Weight of Film (mg/cm ²) | Weight of Metal That Reacted (mg/cm ²) |
|---------------------|-----------------------|-----------------------------------|--------------------------------------|--|
| Helium (loop 12) | T-1 steel | 2.0 | 7.3 | 5.3 |
| | 2.25% Cr, 1% Mo steel | 1.5 | 5.5 | 4.0 |
| | 3% Cr, 1% Mo steel | 1.3 | 4.9 | 3.5 |
| | 5% Cr, 0.5% Mo steel | 1.6 | 5.7 | 4.1 |
| Air ^{a,b} | Carbon steel | 27 | 98 | 71 |
| | 2.25% Cr, 1% Mo steel | 15 | 54 | 39 |
| | 5% Cr, 0.5% Mo steel | 5.0 | 18 | 13 |

^aH. H. Uhlig, "The Corrosion Handbook," pp. 644-7, Wiley and Sons, Inc., New York, 1948.

^b"Steels for Elevated Temperature Service," pp. 21-25, United States Steel Company, 1949.

chromium-containing steel specimens were only slightly less than the weight gain of the T-1 steel specimen; however, the oxide films appeared to be considerably more adherent on the chromium-containing materials. The representative, published oxidation data that are included in Table 6.2 for plain carbon and chromium steels tested in air at 1100°F show trends similar to those observed for comparable specimens tested in loop No. 12. The addition of 2.25% chromium reduced the weight gains of steel specimens exposed to helium by a factor of 1.3 to 1.6 and of those exposed to air by a factor of approximately 1.8. Increasing the chromium addition to 5% (comparable to AISI 502 steel) effected a further decrease in the oxidation rate in air, the rate being five times lower than for plain carbon steels. In helium, however, the oxidation of specimens containing 5% chromium was comparable to that of the specimens containing 2.25 to 3% chromium.

The fourth in the series of controlled-impurity tests (No. 13) was terminated after 740 hr of loop operation with a heated specimen temperature of 1500°F and a graphite temperature of 1100°F. The test atmosphere during the run was impure helium containing 400 to 600 ppm of both CO

and CO₂. Disassembly of the facility in preparation for test No. 14 is in progress.

Evolution of Gases from Graphite

Experimental studies of the degassing behavior of selected grades of graphite have been continued with the use of the techniques described previously.² Several graphite specimens prepared from needle coke by the National Carbon Co., the Great Lakes Carbon Corp., and the Speer Carbon Co. have been degassed at various temperatures. Studies have also been made of graphite specimens obtained from the Speer Carbon Co. in an attempt to ascertain the effect on the gas content of the graphite of manufacturing variables such as type of purification and the atmosphere used during the final cooling. Rate data have been collected for various graphite specimens at 600 and 1000°C, in addition to the data on volume and composition of gas evolved at the different temperatures of interest.

The following graphite specimens were studied during this quarter:

1. NCN - a 16 × 16-in. extrusion prepared by the National Carbon Co. from needle coke.

2. Speer TP - a Speer Carbon Co. 6 × 6-in. extrusion that was prepared from needle coke having a maximum particle size of 0.0328 in. A thermal purification process was applied to this graphite.

3. Speer GP - a specimen identical with Speer TP except that a gas purification process was used instead of the thermal purification process.

4. Speer NC - a 4 1/4 × 4 1/4-in. extrusion of Moderator 2 grade graphite prepared by the Speer Carbon Co. from Texas coke having a maximum particle size of 0.0328 in. A gas purification process was used, along with final cooling in a nitrogen atmosphere. (This graphite is comparable with that designated Moderator 2 except for the atmosphere present during the final cooling.)

²"GCR Semiann. Prog. Rep. June 30, 1959," ORNL-2767, p. 190.

5. Speer AC -- a specimen identical with Speer NC except that an argon atmosphere was used during final cooling instead of nitrogen.

6. AGOT-LS -- a 4 x 5-in. extrusion prepared by the National Carbon Co. from Continental needle coke using a graphitization temperature of 2800°C. This and the following graphite are samples of NPR reflector graphite supplied by Hanford. They are comparable to the graphite to be supplied for the EGCR except for the extrusion size and the particle size of the coke mix.

7. GLC -- a 4 x 5-in. extrusion that was prepared by the Great Lakes Carbon Corp. to the same specifications as those used for AGOT-LS; however, D or J cokes were used.

The data obtained by degassing the various graphite specimens at a maximum temperature of 1000°C (external resistance heating) are reported in Table 6.3. The temperatures recorded are the temperatures of gas collection, and the corresponding gas volume represents the volume of gas evolved between that temperature and the next lower temperature. It should be noted, however, that a large fraction of the gas is collected at the recorded temperature. (The volume corresponding to 300°C is the volume collected between room temperature and 300°C.)

A comparison of the data given in Table 6.3 for the different specimens prepared from needle cokes reveals some striking differences. The total volumes of gas evolved by National Carbon NCN and AGOT-LS specimens are not only larger than those reported for Speer TP, Speer GP, and Great Lakes GLC, but the ratio of H₂ to CO and CO₂ in the gas evolved by the National Carbon graphite is smaller than for the other specimens. The release of gas as a function of temperature also shows some differences for the various needle coke specimens. In general, the Speer TP, Speer GP, and GLC specimens evolved only small amounts of gas between room temperature and 600°C; at least two-thirds of the total volume was evolved in the 600 to 1000°C range. The NCN and AGOT-LS graphites evolved at least half of the total volume between room temperature and 600°C. These observations are in general agreement with the results given previously³

³"GCR Quar. Prog. Rep. June 30, 1960," ORNL-2964, pp. 193-4.

Table 6.3. Volume and Composition of Gas Evolved by 1 1/2-in.-diam and 2-in.-Long Graphite Specimens at 300, 600, and 1000°C

| Graphite Sample | Temperature (°C) | Time (hr) | Gas Volume (cm ³ /100 cm ³ of graphite) | Gas Constituents | | | | | | | | | | | | |
|----------------------------|------------------|-----------|---|------------------|-----------------|--------------|-----------------|------------------|-----------------|-----------------|-----------------|----------------|-----------------|-------|-----------------|-------|
| | | | | H ₂ | | Hydrocarbons | | H ₂ O | | CO ₂ | | N ₂ | | CO | | Other |
| | | | | vol % | cm ³ | vol % | cm ³ | vol % | cm ³ | vol % | cm ³ | vol % | cm ³ | vol % | cm ³ | |
| National Carbon NCN C-1 | 300 | 11 | 0.6 | 13 | 0.1 | 9 | 0.1 | 56 | 0.3 | 7 | | 12 | 0.1 | 2 | | |
| | 600 | 22 | 14.8 | 17 | 2.5 | 10 | 1.5 | 6 | 0.9 | 55 | 8.2 | 1 | 0.1 | 11 | 1.7 | |
| | 1000 | 21 | 11.7 | 56 | 6.6 | 1 | 0.1 | 0.2 | | 0.2 | | 2 | 0.2 | 41 | 4.8 | |
| | Total | | 27.1 | | 9.2 | | 1.7 | | 1.2 | | 8.2 | | 0.4 | | 6.5 | |
| NCN O-1 | 300 | 15 | 0.6 | 15 | 0.1 | 12 | 0.1 | 55 | 0.3 | 6 | | 9 | 0.1 | 3 | | |
| | 600 | 23 | 14.4 | 20 | 2.9 | 13 | 1.8 | 8 | 1.2 | 46 | 6.6 | 1 | 0.1 | 12 | 1.8 | |
| | 1000 | 21 | 11.0 | 55 | 6.0 | 1 | 0.1 | 0.5 | 0.1 | 0.3 | | 2 | 0.2 | 42 | 4.6 | |
| | Total | | 26.0 | | 9.0 | | 2.0 | | 1.6 | | 6.6 | | 0.4 | | 6.4 | |
| NCN O-2 | 300 | 11 | 0.5 | 15 | 0.1 | 18 | 0.1 | 42 | 0.2 | 10 | | 12 | 0.1 | 3 | | |
| | 600 | 22 | 14.6 | 23 | 3.4 | 9 | 1.3 | 12 | 1.8 | 42 | 6.1 | 2 | 0.3 | 12 | 1.8 | |
| | 1000 | 21 | 14.9 | 55 | 8.2 | 1 | 0.1 | 0.4 | 0.1 | 0.1 | | 5 | 0.7 | 38 | 5.7 | |
| | Total | | 30.0 | | 11.7 | | 1.5 | | 2.1 | | 6.1 | | 1.1 | | 7.5 | |
| Speer TP 2 | 300 | 6 | 0.6 | 8 | 0.1 | 11 | 0.1 | 37 | 0.2 | 4 | | 32 | 0.2 | 6 | | |
| | 600 | 22 | 2.6 | 16 | 0.4 | 32 | 0.8 | 24 | 0.6 | 7 | 0.2 | 7 | 0.2 | 14 | 0.3 | |
| | 1000 | 23 | 6.5 | 75 | 4.9 | 2 | 0.1 | 0.3 | | 0.1 | | 1 | 0.1 | 21 | 1.5 | |
| | Total | | 9.7 | | 5.4 | | 1.0 | | 0.8 | | 0.2 | | 0.5 | | 1.8 | |
| TP 4 | 300 | 4 | 0.5 | 4 | | 11 | 0.1 | 52 | 0.3 | 8 | | 21 | 0.1 | 3 | | |
| | 600 | 18 | 2.7 | 24 | 0.7 | 40 | 1.1 | 12 | 0.3 | 5 | 0.1 | 6 | 0.1 | 12 | 0.3 | |
| | 1000 | 13 | 6.3 | 67 | 4.2 | 4 | 0.3 | 1 | 0.1 | 1 | 0.1 | 2 | 0.1 | 25 | 1.6 | |
| | Total | | 9.5 | | 4.9 | | 1.5 | | 0.7 | | 0.2 | | 0.3 | | 1.9 | |
| Speer GP 1 | 300 | 19 | 0.6 | 8 | 0.1 | 33 | 0.2 | 37 | 0.2 | 7 | | 11 | 0.1 | 4 | | |
| | 600 | 23 | 2.4 | 19 | 0.4 | 21 | 0.5 | 12 | 0.3 | 13 | 0.3 | 4 | 0.1 | 31 | 0.8 | |
| | 1000 | 20 | 5.1 | 74 | 3.8 | 1 | 0.1 | 0.3 | | 0.2 | | 1 | 0.1 | 23 | 1.2 | |
| | Total | | 8.1 | | 4.3 | | 0.8 | | 0.5 | | 0.3 | | 0.3 | | 2.0 | |

Table 6.3 (continued)

| Graphite Sample | Temperature (°C) | Time (hr) | Gas Volume (cm ³ /100 cm ³ of graphite) | Gas Constituents | | | | | | | | | | | | |
|-----------------|------------------|-----------|---|------------------|-----------------|--------------|-----------------|------------------|-----------------|-----------------|-----------------|----------------|-----------------|-------|-----------------|-------|
| | | | | H ₂ | | Hydrocarbons | | H ₂ O | | CO ₂ | | N ₂ | | CO | | Other |
| | | | | vol % | cm ³ | vol % | cm ³ | vol % | cm ³ | vol % | cm ³ | vol % | cm ³ | vol % | cm ³ | |
| Speer GP 2 | 300 | 18 | 0.4 | 22 | 0.1 | 26 | 0.1 | 30 | 0.1 | 3 | | 12 | 0.1 | 7 | | |
| | 600 | 19 | 1.6 | 29 | 0.5 | 24 | 0.4 | 20 | 0.3 | 6 | 0.1 | 10 | 0.2 | 11 | 0.2 | |
| | 1000 | 20 | 4.0 | 79 | 3.2 | 2 | 0.1 | 2 | 0.1 | 0.1 | | 1 | | 16 | 0.6 | |
| | Total | | 6.0 | | 3.8 | | 0.6 | | 0.5 | | 0.1 | | 0.3 | | 0.8 | |
| Speer NC 1 | 300 | 20 | 0.5 | 19 | 0.1 | 29 | 0.1 | 20 | 0.1 | 7 | | 12 | 0.1 | 12 | 0.1 | |
| | 600 | 22 | 1.9 | 15 | 0.3 | 25 | 0.5 | 9 | 0.2 | 16 | 0.3 | 2 | | 33 | 0.7 | |
| | 1000 | 22 | 3.8 | 69 | 2.6 | 1 | | 2 | 0.1 | 0.5 | | 1 | | 27 | 1.0 | |
| | Total | | 6.2 | | 3.0 | | 0.6 | | 0.4 | | 0.3 | | 0.1 | | 1.8 | |
| NC 2 | 300 | 12 | 0.5 | 10 | 0.1 | 26 | 0.1 | 35 | 0.2 | 6 | | 16 | 0.1 | 7 | | |
| | 600 | 8 | 1.9 | 13 | 0.2 | 24 | 0.5 | 17 | 0.3 | 13 | 0.2 | 5 | 0.1 | 28 | 0.5 | |
| | 1000 | 15 | 3.7 | 74 | 2.8 | 1 | | 0.2 | | 0.5 | | 1 | | 23 | 0.9 | |
| | Total | | 6.1 | | 3.1 | | 0.6 | | 0.5 | | 0.2 | | 0.2 | | 1.4 | |
| Speer AC 1 | 300 | 17 | 0.6 | 8 | | 10 | 0.1 | 38 | 0.2 | 3.7 | | 36 | 0.2 | 4 | | |
| | 600 | 20 | 1.3 | 22 | 0.3 | 38 | 0.5 | 15 | 0.2 | 3.4 | | 10 | 0.1 | 12 | 0.2 | |
| | 1000 | 22 | 3.4 | 83 | 2.8 | 3 | 0.1 | 0.6 | | 0.1 | | 1 | | 12 | 0.4 | |
| | Total | | 5.3 | | 3.1 | | 0.7 | | 0.4 | | | | 0.3 | | 0.6 | |
| AC 2 | 300 | 12 | 0.4 | 5 | | 7 | | 31 | 0.1 | 4.3 | | 44 | 0.2 | 4 | | |
| | 600 | 9 | 1.5 | 24* | 0.4 | 36* | 0.5 | 15* | 0.2 | 3* | | 6* | 0.1 | 7* | 0.1 | |
| | 1000 | 18 | 4.3 | 83 | 3.6 | 4 | 0.2 | 0.2 | | 0.3 | | 1 | | 11 | 0.5 | |
| | Total | | 6.2 | | 4.0 | | 0.7 | | 0.3 | | | | 0.3 | | 0.6 | |

*Mass spectrometer sample lost; value from gas chromatograph.

Table 6.3 (continued)

| Graphite Sample | Temperature (°C) | Time (hr) | Gas Volume (cm ³ /100 cm ³ of graphite) | Gas Constituents | | | | | | | | | | | | |
|------------------------------|------------------|-----------|---|------------------|-----------------|--------------|-----------------|------------------|-----------------|-----------------|-----------------|----------------|-----------------|-------|--------------------|----------------------|
| | | | | H ₂ | | Hydrocarbons | | H ₂ O | | CO ₂ | | N ₂ | | CO | | Other |
| | | | | vol % | cm ³ | vol % | cm ³ | vol % | cm ³ | vol % | cm ³ | vol % | cm ³ | vol % | cm ³ | |
| National Carbon AGOT-LS-1 | 300 | 17 | 0.7 | 7 | 0.1 | 20 | 0.1 | 54 | 0.4 | 4 | | 10 | 0.1 | 3 | | |
| | 600 | 20 | 11.2 | 15 | 1.7 | 10 | 1.1 | 20 | 2.2 | 42 | 4.6 | 3 | 0.3 | 10 | 1.1 | |
| | 1000 | 27 | 11.0 | 57 | 6.3 | 1 | 0.1 | 0.4 | | 0.5 | 0.1 | 1 | 0.1 | 40 | 4.4 | |
| | Total | | 22.9 | | 8.1 | | 1.3 | | 2.6 | | 4.7 | | 0.5 | | 5.5 | |
| AGOT-LS-2 | 300 | 11 | 0.6 | 9 | 0.1 | 16 | 0.1 | 55 | 0.3 | 6 | | 10 | 0.1 | 4 | | |
| | 600 | 23 | 9.4 | 8 | 0.7 | 14 | 1.3 | 20 | 1.9 | 47 | 4.4 | 3 | 0.3 | 9 | 0.8 | |
| | 1000 | 21 | 11.0 | 55 | 6.1 | 1 | 0.1 | 0.4 | | 2 | 0.2 | 1 | 0.1 | 40 | 4.4 | |
| | Total | | 21.0 | | 6.9 | | 1.5 | | 2.2 | | 4.6 | | 0.5 | | 5.2 | |
| Great Lakes GLC 3A | 300 | 10 | 0.4 | 8 | | 11 | | 60 | 0.2 | 3.6 | | 10 | | 4 | 4% SO ₂ | |
| | 600 | 21 | 1.5 | 11 | 0.2 | 25 | 0.4 | 33 | 0.5 | 9 | 0.1 | 6 | 0.1 | 13 | 0.2 | 2% SO ₂ |
| | 1000 | 22 | 8.6 | 54 | 4.7 | 2 | 0.2 | 1 | 0.1 | 5 | 0.4 | 1 | 0.1 | 35 | 3.0 | 0.8% SO ₂ |
| | Total | | 10.5 | | 4.9 | | 0.6 | | 0.8 | | 0.5 | | 0.2 | | 3.2 | |
| GLC 2A | 300 | 11 | 0.4 | 7 | | 13 | 0.1 | 52 | 0.2 | 5.3 | | 13 | 0.1 | 8 | 5% SO ₂ | |
| | 600 | 12 | 1.5 | 12 | 0.2 | 25 | 0.4 | 31 | 0.5 | 9 | 0.1 | 3 | | 19 | 0.3 | 0.4% SO ₂ |
| | 1000 | 10 | 8.6 | 53 | 4.6 | 5 | 0.4 | 3 | 0.3 | 4.2 | 0.4 | 1 | 0.1 | 33 | 2.9 | 1% SO ₂ |
| | Total | | 10.5 | | 4.8 | | 0.9 | | 1.0 | | 0.5 | | 0.2 | | 3.2 | |

for other needle coke specimens prepared by these three graphite producers.

The results reported for Speer TP and GP show that the thermally purified graphite (Speer TP) released only slightly more gas when heated to 1000°C than did the gas-purified material (Speer GP). Similarly, no marked difference was found between the volume of gas evolved by the nitrogen-cooled graphite (Speer NC) and the argon-cooled graphite (Speer AC). The gas released by the latter contained very little CO₂ or CO at any temperature up to 1000°C. The results are to be compared with those of a previous test⁴ of Speer Moderator 2 graphite, which was manufactured under conditions identical with those used for Speer NC and AC, except for the atmosphere during final cooling, and which evolved ~10 cm³ of gas per 100 cm³ of graphite when degassed to 1000°C.

Rate data obtained for various specimens are given in Figs. 6.1 through 6.5. Data reported for 600°C were collected from samples previously degassed at 300°C, and, similarly, the 1000°C data came from samples previously degassed at 600°C. If appreciable volumes of gas are released, little reliance should be placed on the volumes measured during at least the first hour, because gas is evolved while the specimen is coming up to temperature and rapid gas evolution may result in a buildup of pressure

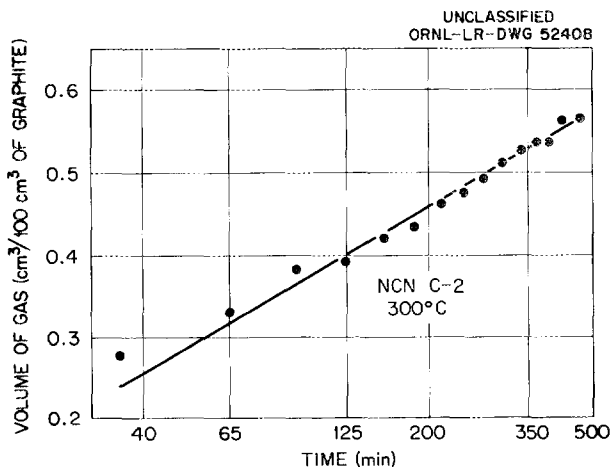


Fig. 6.1. Volume of Gas Evolved by NCN Graphite Plotted Against Log of Time.

in the tube if the pump is unable to remove the gas as rapidly as it is evolved.

Figure 6.1 shows that a plot of the volume of gas evolved by NCN graphite at 300°C against the log of time gives an essentially linear relationship. These data are presented because the gas released at 300°C consists

⁴"GCR Quar. Prog. Rep. Sept. 30, 1959," ORNL-2835, p. 135.

predominantly of water vapor and various hydrocarbons. These components appear only at low concentrations in the gas collected at 600 and 1000°C.

The rate data given in Figs. 6.2, 6.3, and 6.4 show that at 1000°C

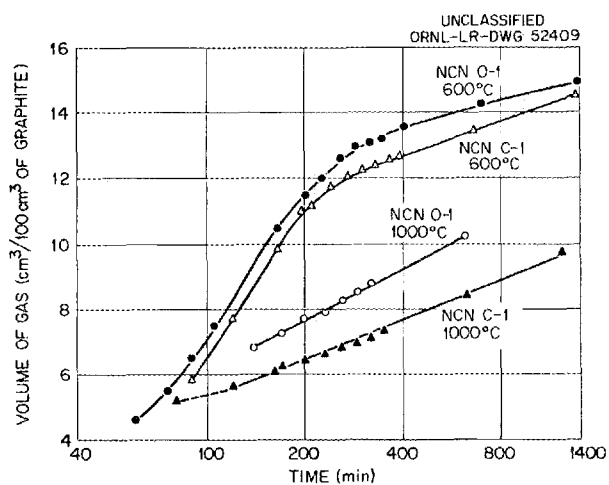


Fig. 6.2. Volume of Gas Evolved by NCN Graphite Plotted Against Log of Time.

a plot of the volume of gas evolved against the log of time gives a straight line for all the specimens examined if the short-time measurements are ignored. Similar treatment of the data obtained at 600°C, however, fails to give such consistent results. Two of the specimens, namely, NCN and AGOT-LS, either fail to give a linear relationship in the period of time used or attain linearity only after about 6 hr of heating.

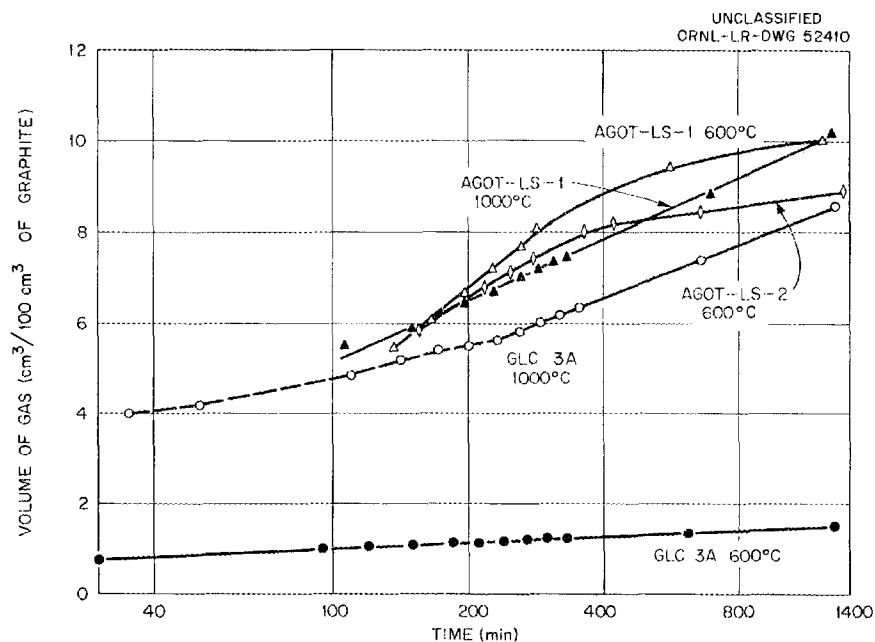


Fig. 6.3. Volume of Gas Evolved by GLC and AGOT-LS Graphite Plotted Against Log of Time.

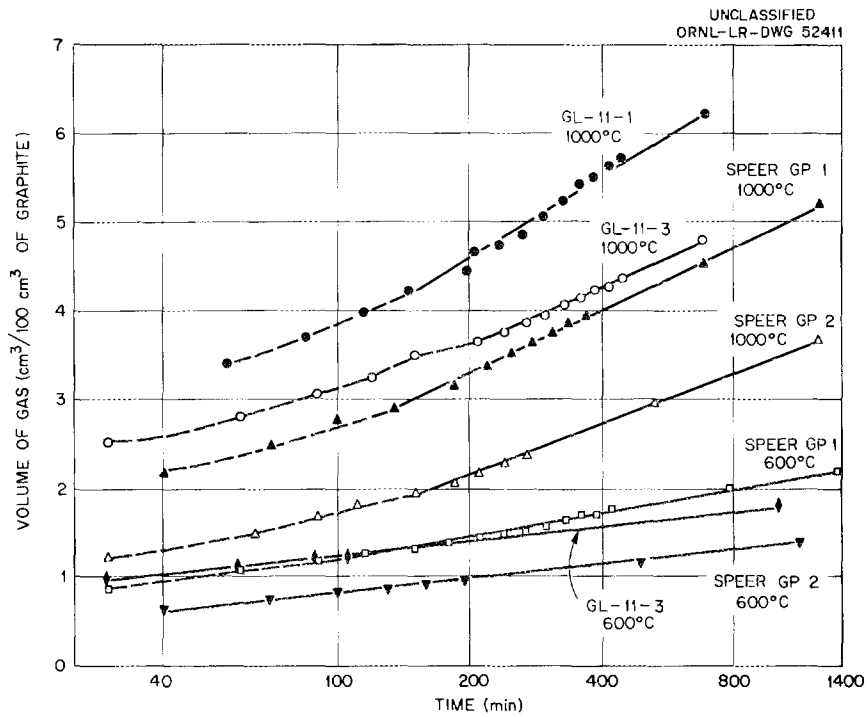


Fig. 6.4. Volume of Gas Evolved by GL-11 (HPDA) and Speer-GP Graphites Plotted Against Log of Time.

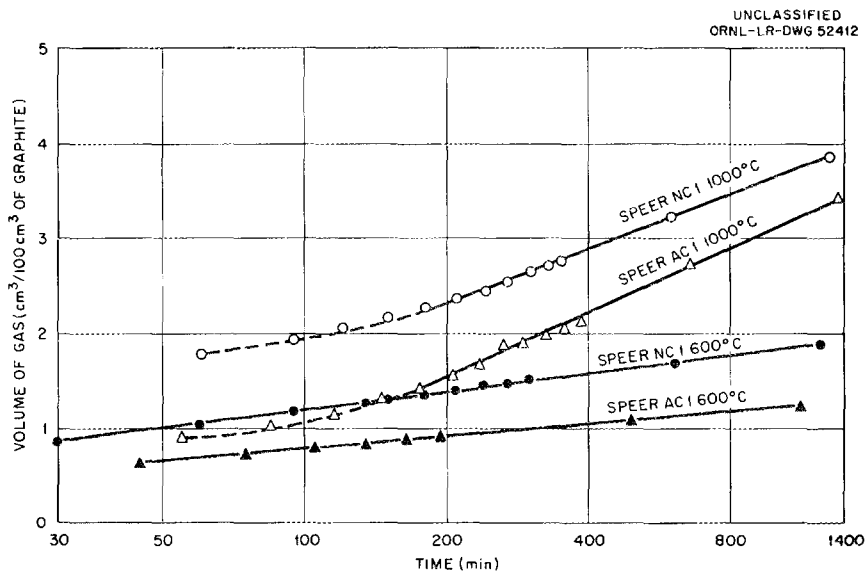


Fig. 6.5. Volume of Gas Evolved by Speer-AC and Speer-NC Graphite Plotted Against Log of Time.

The NCN graphite also gives a 600°C curve that lies well above the 1000°C line; the AGOT-LS 600°C curve lies above the 1000°C line for 20 hr and then appears to cross it. This general behavior is in agreement with that reported earlier³ for AGOT-VCB graphite, also prepared by National Carbon Co. from needle coke. It is believed that the large volume of gas released at 600°C containing a large fraction of CO₂ is responsible for the curvature at 600°C. No satisfactory explanation can be offered, however, for the release of this large volume of gas at about 600°C by these particular specimens. The differences in the degassing behavior of AGOT-LS and GLC graphite are shown in Fig. 6.3. These two types of graphite were presumably prepared to similar specifications by two producers using different needle cokes. Data obtained for other needle coke specimens, GL-11 or HPDA (previously described³) and Speer GP, are given in Fig. 6.4. The plots of these data, as well as those for Speer NC and AC in Fig. 6.5, are similar to the plots for GLC graphite.

Data obtained by degassing the various types of graphite at 1800°C by induction heating are given in Table 6.4. Where data are given only for 1800°C, the specimen was heated to 1700°C for approximately 30 min while the gas was held in contact with it; the temperature was then lowered, the gas pumped off, and the temperature raised to 1800°C. Pumping was continued and the specimen was held at 1800°C until gas evolution was essentially complete. In all other runs, the specimen was heated to 1000°C without pumping, held at 1000°C for 1 hr, and cooled. The gas was then pumped out and the temperature was returned to 1000°C while pumping. The specimen was then held at 1000°C until the gas collection was complete. The gas collected at 1400°C includes the gas pumped off while raising the temperature from 1000 to 1400°C, plus that removed during a holding period at 1400°C. Similarly, the 1800°C fraction was collected while raising the temperature to 1800°C, as well as while heating at 1800°C.

The data given in Tables 6.4 and 6.5 show that NCN graphite evolved a considerably larger volume of gas than any of the other needle coke specimens (Speer TP, Speer GP, and GLC) listed here or described

Table 6.4. Volume and Composition of Gas Evolved by 1 1/4-in.-diam and 1-in. Long Graphite Specimens at 1000, 1400, and 1800°C

| Graphite Sample | Temperature (°C) | Time (hr) | Gas Volume (cm ³ /100 cm ³ of graphite) | Gas Constituents | | | | | | | | | | | | |
|-----------------|------------------|-----------|---|------------------|-----------------|--------------|-----------------|------------------|-----------------|-----------------|-----------------|----------------|-----------------|-------|-----------------|------------|
| | | | | H ₂ | | Hydrocarbons | | H ₂ O | | CO ₂ | | N ₂ | | CO | | Ar (vol %) |
| | | | | vol % | cm ³ | vol % | cm ³ | vol % | cm ³ | vol % | cm ³ | vol % | cm ³ | vol % | cm ³ | |
| National Carbon | 1000 | 7 | 62.0 | 64 | 39.4 | 1 | 0.5 | 0.2 | 0.1 | 0.1 | 0.1 | 1 | 0.5 | 35 | 21.4 | |
| NCN C-3 | 1400 | 12 | 26.1 | 60 | 15.7 | 1 | 0.3 | 0.2 | 0.1 | 0.1 | | 7 | 1.9 | 31 | 8.1 | |
| | 1800 | 12 | 16.2 | 73 | 11.9 | 1 | 0.1 | | | 0.1 | | 5 | 0.8 | 21 | 3.4 | |
| | Total | | 104.3 | | 67.0 | | 0.9 | | | 0.2 | | 0.1 | | 3.2 | 32.9 | |
| NCN O-3 | 1800 | 6 | 96 | 75 | 72 | 0.4 | 0.4 | 0.2 | 0.2 | 0.3 | 0.3 | 3 | 3 | 22 | 21 | |
| NCN C-4 | 1800 | 7 | 98 | 66 | 65 | 0.4 | 0.4 | 0.1 | 0.1 | 0.1 | 0.1 | 1 | 1 | 32 | 31 | |
| Speer | 1000 | 5 | 25.0 | 70 | 17.5 | 3 | 0.7 | 1 | 0.3 | 2 | 0.5 | 2 | 0.5 | 23 | 5.8 | |
| TP 1B | 1400 | 11 | 22.7 | 65 | 14.8 | 1 | 0.2 | 1 | 0.2 | 0.2 | | 2 | 0.4 | 31 | 7.1 | |
| | 1800 | 11 | 20.6 | 59 | 12.1 | 1 | 0.1 | | | 0.1 | | 2 | 0.4 | 38 | 7.7 | |
| | Total | | 68.3 | | 44.4 | | 1.0 | | | 0.5 | | 0.5 | | 1.3 | 20.6 | |
| TP 1A | 1800 | 23 | 61 | 59 | 36 | 0.6 | 0.4 | | | 0.4 | 0.2 | 2 | 1 | 38 | 23 | |
| GP 3C | 1000 | 6 | 18.8 | 78 | 14.6 | 1 | 0.2 | 1 | 0.2 | 1 | 0.2 | 0.3 | 0.1 | 18 | 3.4 | |
| | 1400 | 11 | 14.3 | 65 | 9.3 | 0.5 | 0.1 | 0.6 | 0.1 | 0.7 | 0.1 | 2 | 0.3 | 32 | 4.5 | |
| | 1800 | 15 | 15.3 | 47 | 7.2 | 0.4 | 0.1 | | 0.1 | 0.2 | | 3 | 0.4 | 49 | 7.5 | |
| | Total | | 48.4 | | 31.1 | | 0.4 | | | 0.4 | | 0.3 | | 0.8 | 15.4 | |
| GP 3B | 1800 | 10 | 56 | 75 | 42 | 0.5 | 0.3 | 0.2 | 0.1 | 0.1 | 0.1 | 0.8 | 0.5 | 24 | 13 | |

Table 6.4 (continued)

| Graphite Sample | Temperature (°C) | Time (hr) | Gas Volume (cm ³ /100 cm ³ of graphite) | Gas Constituents | | | | | | | | | | | | |
|-----------------------|------------------|-----------|---|------------------|-----------------|--------------|-----------------|------------------|-----------------|-----------------|-----------------|----------------|-----------------|-------|-----------------|------------|
| | | | | H ₂ | | Hydrocarbons | | H ₂ O | | CO ₂ | | N ₂ | | CO | | Ar (vol %) |
| | | | | vol % | cm ³ | vol % | cm ³ | vol % | cm ³ | vol % | cm ³ | vol % | cm ³ | vol % | cm ³ | |
| Speer | 1000 | 5 | 15.7 | 56 | 8.7 | 1 | 0.1 | 1 | 0.1 | 1.8 | 0.3 | 3 | 0.4 | 38 | 6.0 | |
| NC 4 | 1400 | 5 | 6.7 | 66 | 4.5 | 0.2 | | 2 | 0.1 | 0.1 | | 10 | 0.7 | 22 | 1.4 | |
| | 1800 | 3 | 1.9 | 62 | 1.2 | | | | 0.1 | 0.1 | | 20 | 0.4 | 15 | 0.3 | |
| | Total | | 24.3 | | 14.4 | | 0.1 | | 0.3 | | 0.3 | | 1.5 | | 7.7 | |
| NC 5 | 1000 | 8 | 14.7 | 77 | 11.4 | 1 | 0.1 | 1 | 0.1 | 0.5 | 0.1 | 1 | 0.1 | 20 | 2.9 | |
| | 1400 | 6 | 6.6 | 73 | 4.8 | 0.3 | | 1 | 0.1 | 0.1 | | 14 | 0.9 | 10 | 0.7 | |
| | 1800 | 2 | 1.5 | 60 | 0.9 | 0.2 | | | | 0.1 | | 23 | 0.3 | 14 | 0.2 | |
| Total | | 22.8 | | 17.1 | | 0.1 | | 0.2 | | 0.1 | | 1.3 | | 3.8 | | |
| NC 6 | 1800 | 6 | 25.2 | 74 | 18.8 | 0.4 | 0.1 | 0.7 | 0.2 | 0.2 | 0.1 | 5 | 1.2 | 19 | 4.8 | |
| AC 4 | 1000 | 8 | 12.6 | 93 | 11.7 | 1 | 0.1 | 0.2 | | 0.1 | | 0.5 | 0.1 | 6 | 0.7 | 0.2 |
| | 1400 | 6 | 5.4 | 78 | 4.2 | 0.5 | | 1 | 0.1 | 0.1 | | 5 | 0.3 | 10 | 0.5 | 6 |
| | 1800 | 4 | 1.8 | 50 | 0.9 | 0.3 | | | | 0.1 | | 7 | 0.1 | 27 | 0.5 | 16 |
| Total | | 19.8 | | 16.8 | | 0.1 | | 0.1 | | | | 0.5 | | 1.7 | | |
| AC 3 | 1800 | 5 | 21.4 | 93 | 19.9 | 0.5 | 0.1 | 0.1 | | 0.1 | | 0.5 | 0.1 | 3 | 0.6 | 3 |
| Great Lakes GLC 2C | 1000 | 7 | 9.5 | 63 | 6.1 | 1 | 0.1 | 1 | 0.1 | 1.4 | 0.1 | 1 | 0.1 | 32 | 3.0 | |
| | 1400 | 7 | 9.9 | 55 | 5.5 | 1 | 0.1 | 0.3 | | 0.1 | | 4 | 0.4 | 40 | 3.9 | |
| | 1800 | 3 | 1.2 | 55 | 0.6 | 1 | | | | | | 47 | 0.6 | 1 | | |
| Total | | 20.6 | | 12.2 | | 0.2 | | 0.1 | | 0.1 | | 1.1 | | 6.9 | | |
| GLC 2B | 1700 | 9 | 20.9 | 83 | 17.3 | 0.7 | 0.1 | 0.1 | | 0.2 | | 3 | 0.6 | 13 | 2.7 | |

Table 6.5. Comparison of EGCR Fuel Assembly Sleeves
Fabricated from Various Grades of Graphite

| Vendor | Sleeve No. | Grade of Graphite | Permeability at 2 atm (millidarcys) |
|-------------------------|---------------|-------------------------|---|
| Great Lakes Corporation | 148 | R-1HLM | 9.2 |
| | 135 | R-1HLM | 10.0 |
| | 113 | R-1HLM | 14.1 |
| Speer Carbon Company | 60 | Nuclear | 12.3 |
| National Carbon Company | A | AGOT | 45.8 |
| | R | AGOT | 270.0 |
| | 19 | AGOT | 297.0 |

previously.³ The values for GIC are preliminary, but they indicate a low gas content. Very rough estimates of the gas content of AGOT-LS suggest a potential gas volume 2 to 3 times that of GIC. A comparison of the data for Speer TP and Speer GP, which differ only in the purification process applied, show the gas content of the gas-purified graphite (Speer GP) to be somewhat lower than that of the thermally purified graphite (Speer TP), with the main difference being in the CO released. Similarly, the total gas volumes released by Speer NC (nitrogen cooled) and Speer AC (argon cooled) are not very different; the latter evolved very little CO, however. The release of argon by Speer AC above 1400°C suggests that this gas was trapped by closure of small pores during cooling and escaped after these pores were reopened at high temperatures.

The fractions of the total gas released at the different temperatures vary for some of the specimens. For example, Speer NC, Speer AC and GIC evolved only small amounts of gas above 1400°C, whereas Speer TP and Speer GP released about one-third of the total gas above 1400°C. Variations in the fractions released by various specimens at 1000 and 1400°C are also evident from the data. With one exception, the volume evolved at 1000°C by induction heating was at least twice as great as that found using external resistance heating. The two volumes reported

for GLC graphite are comparable, but, as indicated previously, the GLC data obtained by induction heating are preliminary. If these data are verified, it will be the first time the volumes evolved at 1000°C by the two heating methods are at all in agreement.

Transport of Gases Through Graphite

Permeability Studies

Analyses of possible pressure distributions in the EGCR core have revealed that the helium coolant will tend to flow laterally through the various graphite components, as well as vertically along the intended flow paths. For a fixed helium exit temperature, the average fuel element surface temperature will increase as the magnitudes of the lateral flow components increase. The amount of lateral flow depends, in part, on the over-all permeability of the graphite. This over-all permeability includes contributions from fuel-element sleeves, sleeve joints, sleeve coatings, and the large 16-in. × 16-in. × 20-ft graphite moderator columns.

A series of room-temperature permeability determinations were made to obtain the Darcy constant (a measure of permeability) for typical, uncoated, EGCR sleeve graphite, with and without joints. The materials used in this investigation were representative of the types of graphite available and under consideration for EGCR use. Additional plug specimens were obtained from two AGOT bars to simulate the moderator columns. The relationship which is applicable to the graphite studied and which relates the variables measured to a permeability constant, k , is

$$k = \frac{Q_a P_a \mu L}{A(\Delta P) P_m},$$

where Q_a is the volumetric flow rate of gas (measured at a pressure P_a) which passes through a graphite specimen of cross sectional area A , and thickness L under a pressure drop ΔP of $(P_{x=0} - P_{x=L})$; P_m is the mean pressure $[0.5 (P_{x=0} + P_{x=L})]$; and μ is the gas viscosity.

For the experimental measurements, the test gas (helium) flow path was arranged so that the gas passed through a regulator, the graphite sleeve, and a back-pressure valve, where the gas was throttled to atmospheric pressure, P_a . The throttled gas was then passed through a wet test meter to obtain Q_a . The pressure drop across the graphite was measured directly with a butyl phthalate manometer. The mean pressure, P_m , was obtained by averaging the readings of two Bourdon gages. The A/L ratio for the sleeve was obtained from the expression

$$\frac{A}{L} = \frac{2\pi h}{\ln \frac{d_o}{d_i}},$$

where h is the total length of the cylinder plus any short sections, and d_o and d_i are the inner and outer diameters, respectively, of the graphite sleeve.

A modified Hassler apparatus⁵ was used in the determinations of the permeability of the graphite plugs. The test results for the AGOT plug specimens⁶ show that the permeability varies slightly with pressure as a result of deviations from Darcy's law or "slip-effect."⁷ This deviation requires that the pressure be specified when a permeability value is tabulated. All EGCR sleeve materials studied to date have, however, followed Darcy's law in the viscous flow region, with only a small degree of pressure dependence. Permeability values obtained from two different AGOT bars indicated relatively good agreement (20 to 50 millidarcy) when the specimens were of similar dimensions and subjected to similar test procedures. Large differences were encountered, however, when the specimen shapes and flow patterns were varied. Two cylinders

⁵G. L. Hassler et al., Trans. Am. Soc. Mech. Engrs. 118, 116 (1936).

⁶J. Truitt et al., "Transport of Gases Through Ceramic Materials," ORNL-2931 (April 29, 1960).

⁷P. C. Carman, "Flow of Gases Through Porous Media," Academic Press, New York, 1956.

gave a value of 6.5 md, which is to be compared with an average value of 45.5 md for five plugs. Since all the specimens were obtained from adjacent sites within the same bar, these variations must be attributed to either the anisotropic internal structure of the graphite⁸ or surface damage induced during specimen fabrication.

Plugs taken from Great Lakes sleeve 133 were used to determine a reference value for subsequent tests of large specimens. Radially cut plugs showed an average value of 6.5 md compared with an average value of 11.6 md for vertically cut plugs. Since the average permeability value should not vary more than $\pm 10\%$, a definite effect of orientation on permeability is shown by these data. The direction of the gas flow and the specimen thickness were similar for the radially cut plugs and the full-size sleeves. Therefore, the 6.5-md value for the radially cut plugs should be a representative value for Great Lakes Corporation materials.

All full-size sleeves were machined so that each sleeve had a male and a female end. Sleeve 133, from which the short sections and plugs used for the tests described above were fabricated, was therefore used as a large cylindrical specimen with squared, or flat, ends to check the effectiveness of the rubber-gasket seal to the brass plates of the test apparatus. This specimen gave a value of 6.9 md as compared with 6.5 md for the radial plugs and thus demonstrated that the seals were effective and that small, properly oriented specimens tend to give average permeability values for the source material.

The results of tests on the remaining full-length Great Lakes sleeves are given in Table 6.5. If it is assumed that the permeability of sleeve 133 was not lower than the permeabilities of the remaining sleeves, the data show that the thin-walled sections at the machined ends of the remaining sleeves led to slightly higher over-all permeability values. Further, it appears that the Spear Carbon Company and Great Lakes Corporation materials are comparable. National Carbon Company sleeve A

⁸P. L. Walker, Nature 176, 1167-8 (1955).

gave the same value as that obtained previously with specimens from AGOT-grade bars. The other AGOT sleeves (R and 19) appeared to be cracked.

Tests were also performed to evaluate the sealing effectiveness of the Allis-Chalmers joint design. The joint sections of Great Lakes sleeve 133 were placed on each Great Lakes sleeve, in turn, and a standard flow test was carried out. The results are presented in Table 6.6. Each joint had a squared end, which, as shown by tests with sleeve 133, improved the efficiency of the brass plate-to-rubber gasket seal, particularly on the female end of the long section. The first section used covered the female end and, in general, the over-all permeability decreased. Addition of the female short section to the male end of the main sleeve neither increased nor decreased the over-all permeability. It is concluded therefore that a graphite-to-graphite joint is as effective as the brass plate-to-rubber gasket closure. The foregoing tests were performed with an approximate 1500-lb closure force on the seals. Since it was felt that a force of this magnitude was much higher than would be

Table 6.6. Evaluation of Graphite-to-Graphite Joints

| Sleeve No. | Permeability at 2 atm (millidarcy) | | |
|------------|------------------------------------|--------------------------------|---------------------------------|
| | Joint Specimen I ^a | Joint Specimen II ^b | Joint Specimen III ^c |
| 148 | 9.2 | 9.5 | 9.6 |
| 135 | 10.0 | 8.3 | 8.3 |
| 113 | 14.1 | 11.4 | 12.9 |

^aJoints formed by rubber gaskets and brass plates at both ends of sleeve.

^bSpecimen included one joint formed with short male-end section from sleeve 133.

^cSpecimen included two joints formed with short male- and female-end sections from sleeve 133.

encountered under actual conditions, a series of tests with various other closure forces were run. The results of these tests are presented in Table 6.7. The complete test section consisted of sleeve 113 and a short male-end section from sleeve 133. The Allis-Chalmers joint design appears to be reasonable from the standpoint of closure effectiveness for these graphite materials; however, as the permeability of the sleeve material is reduced, the effect of the joint on flow will increase markedly.

Table 6.7. Effect of Closure Force on Permeability of Graphite-to-Graphite Joint

| Closure Force (lb) | Permeability at 2 atm (millidarcy) |
|--------------------|------------------------------------|
| 200 | 14.3 |
| 400 | 14.0 |
| 650 | 12.8 |
| 900 | 12.6 |
| 1150 | 12.7 |
| 1500 | 11.4 |

Low-Temperature Diffusion Experiments

Measurements of the mutual diffusion coefficient, D_{12} , of argon and helium in AGOT graphite have been made at room temperature, 0°C, and -65°C. All data fit the equation

$$D_{12} = 4.22 \times 10^{-3} D_{12}^* ,$$

where D_{12}^* is the classical "free-space" diffusion coefficient of helium and argon in cm²/sec. It is concluded therefore that the diffusion mechanism is classical and that if mechanisms such as surface diffusion which might result from an adsorbed (liquid) layer exist their effects must be less than the experimental error (~8%).

Supporting theoretical evidence that surface diffusion (flow of molecules in the adsorbed state) is negligible has been found. Based on thermodynamic principles⁹ and available adsorption data for argon on AGOT graphite,¹⁰ it was found that, under the experimental conditions used, the maximum argon flow rate through the graphite as a result of surface diffusion would be less than 10^{-8} cm³ (STP)/sec. Since the flow rates measured in the diffusion experiment were of the order of 0.1 cm³ (STP)/sec, it was not expected that surface diffusion could be detected.

Diffusion of Fission Products in Graphite

An analysis of the data on diffusion of fission products in porous graphite matrices has indicated that the migration mechanism is a complex, multistep, transfer process. In addition to migration of the particles by diffusion, chemical reactions with the graphite can immobilize some of the released fission products. Studies have been made of surface-migration mechanisms and surface reactions in order to evaluate their role in fission-product transport through porous reactor-grade graphite matrices.

In a series of experiments at temperatures between 1400 and 2200°K, the rates of diffusion of BaO, SrO, Y₂O₃, and ZrO₂ in reactor graphite were studied. As the results summarized in Table 6.8 indicate, the rates of diffusion and activation energies increase with the melting point of the oxide above the Tammann temperature of $0.5 T_M$ in the range where surface migration can take place. The free-energy values for carbide formation by reaction between graphite and the metal oxide indicate that this is most likely to take place for yttrium and zirconium or, in general, for rare earth and hard-metal ions. An additional possibility under consideration is the formation of loosely held addition compounds with surface defects in the graphite lattice.

⁹E. R. Gilliland, R. F. Baddour, and J. L. Russell, AIChE Journal, March 1958, pp. 90-96.

¹⁰M. C. Cannon, W. T. Ward, G. M. Watson, and W. R. Grimes, "Adsorption of Xenon and Argon on Graphite," ORNL-2955 (in press).

Table 6.8. Mass-Transfer and Thermodynamic Properties of Oxides of Fission-Product Elements

| Fission-Product Compound | Coefficient of Diffusion at 1773°K (cm ² /sec) | Energy of Activation (kcal/mole) | Free Energy for Carbide Formation Reaction at 1773°K (kcal/mole) | Melting Point (°K) |
|-------------------------------|---|----------------------------------|--|--------------------|
| | × 10 ⁻⁵ | | | |
| BaO | 3.72 | 16.4 | +49.1 | 2196 |
| SrO | 0.32 | 119.8 | +37.2 ^a | 2703 |
| Y ₂ O ₃ | 0.62 ^b | c | +26.2 ^a | 2683 |
| ZrO ₂ | 0.024 | 136.8 | -11.2 | 2950 |

^aBased on ΔH_f and ΔS_f values derived from a semitheoretical correlation.

^bValue for 1623°K.

^cValue not available.

The data presented indicate that, unlike the situation in noble-gas transfer (see preceding section) surface-diffusion and carbide-formation reactions might be significant contributing mechanisms in the diffusion of fission products through porous graphite matrices at reactor operating temperatures.

Chemical Analyses of Reactor Materials

Automatic Continuous Analysis of Helium

A second process-gas chromatograph has been purchased because of increased demand for automatic continuous gas analyses. The new instrument is a Greenbrier Chroma-matic 312, which is identical in function to the Chroma-matic 112 described previously.¹¹ Model changes by the manufacturer include rearrangement of components for convenience, the substitution of

¹¹"GCR Quar. Prog. Rep. Dec. 31, 1959," ORNL-2888, pp. 178-84.

improved valves, and provision for external adjustment of carrier gas flow rates.

Because of the extreme range in the concentrations of contaminants to be measured in gas-cooled reactor development samples (from several per cent to a few parts per million), additional modifications have been carried out at the Laboratory to permit changes in the sample size and consequent changes in sensitivity without opening the temperature-controlled compartment. An additional modification permits the analysis of "grab samples" from sources other than the systems on which process analyses are carried out.

These modifications were made by using a valve designed for chromatographic applications by the Phillips Petroleum Corporation and manufactured by the Greenbrier Instrument Company. The Phillips valve has six ports equally spaced on a 1-in. circle. Connections between adjacent ports can be closed by the application of air pressure to a flexible (Teflon) diaphragm at a point between the ports. These valves offer the advantages of small size, rapid action, and negligible volume and dead space.

In the unmodified Phillips valve, the control air is directed to close connections between alternate pairs of ports simultaneously. Such a valve is shown in the center of Fig. 6.6 installed to provide a means for analyzing "grab samples." A bulb containing the pressurized sample is connected to the system by means of a standard taper joint, and the sample lines and loop are evacuated and isolated. The sample loop is then filled by opening the stopcock on the sample bulb, closing the stopcock, and bleeding excess pressure to the atmosphere. The control solenoids are actuated by a signal from the control unit to direct the flow through the sample valve. Vacuum is applied to the diaphragm at open connections to reduce pressure drops and permit complete evacuation of the sample loop.

A second Phillips valve, which is shown on Fig. 6.6 and in more detail on Fig. 6.7, has been modified to permit closing of connections between ports individually. The control air is directed to inject a

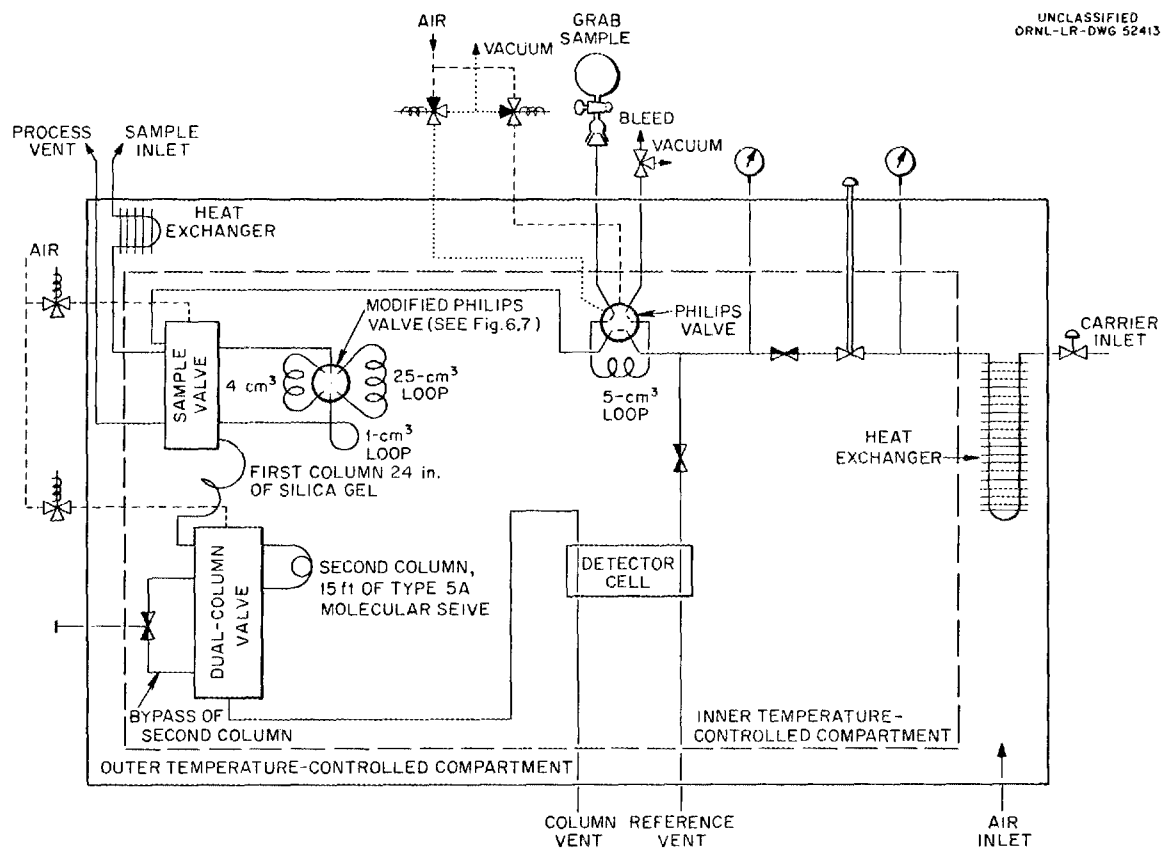


Fig. 6.6. Schematic Flow Diagram of Chroma-Matic-312 Process Chromatograph.

total sample volume of 25 cm^3 . By appropriate selection of solenoids, sample volumes of 5 and 1 cm^3 can be injected. Thus five-fold increases and decreases in sensitivity over that of the Chroma-matic 112 can be obtained.

All the modifications indicated in Fig. 6.6 have been completed, and the system has been leak-tested. Sample loops which have been fabricated from calculated lengths of $3/16$ -in. tubing are being calibrated with standard samples of CO_2 in helium. Any adjustment required in the volumes of the samples loops will be accomplished by crimping the tubing.

Determination of Helium in Air

A procedure has been developed for the measurement of small increments in the concentration of helium in air. Such measurements were performed

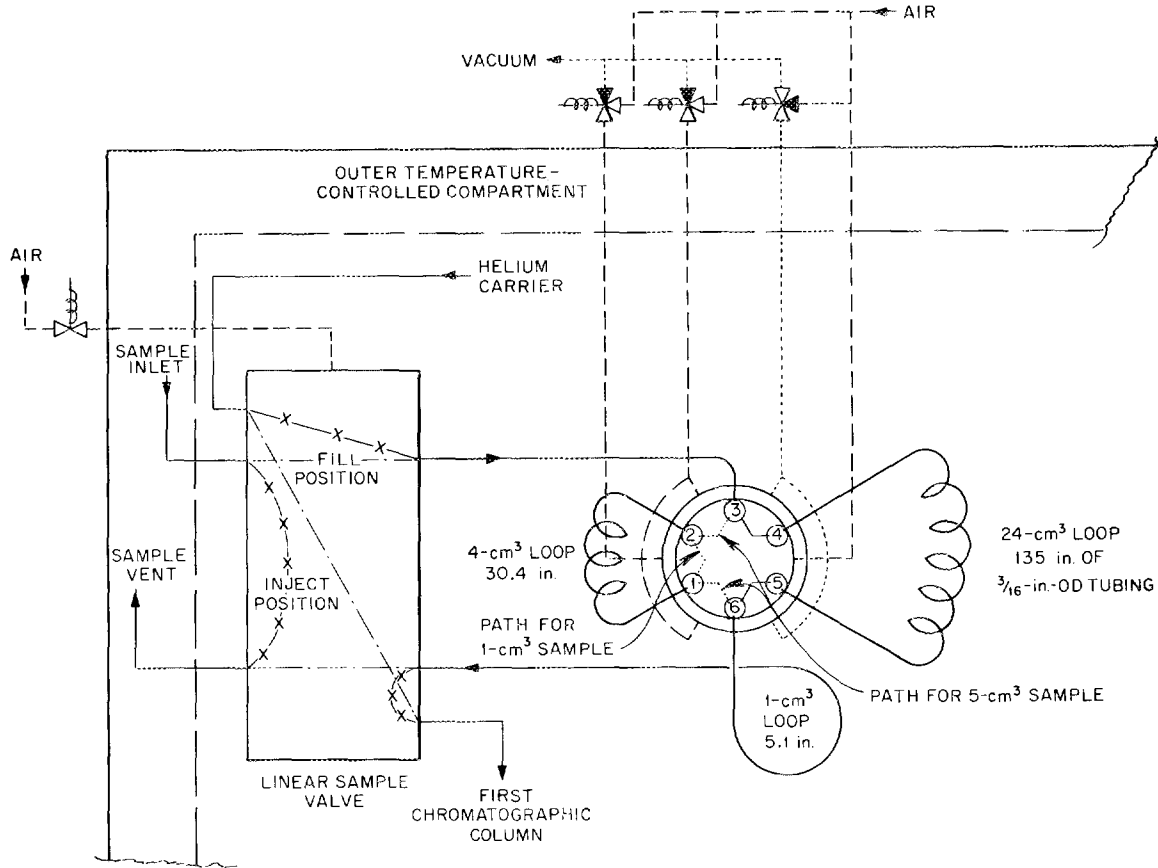


Fig. 6.7. Valving System for Multiple Sample Volumes.

in a study of the radiation hazard which would result from the rupture of an EGCR in-pile test loop. The determinations were carried out with a Greenbrier Chroma-Lab 950 chromatograph, which was used primarily as a thermal-conductivity apparatus to achieve the necessary sensitivity of 1 to 2 ppm. In this method a 25-cm³ sample was injected into a 40 cm³/min stream of air as a carrier gas. The carrier gas was routed directly through 1/8-in. tubing to the detector, a thermal conductivity bridge with 8-K thermistor elements. Bridge output was measured with a 1-mv recorder. For maximum sensitivity the instrument was not temperature controlled but operated at room temperature, which varied from 20 to 24°C. Standard samples were prepared by the dilution of calculated

pressures of helium with bottled breathing air, which was also used as a carrier gas. The injection of a standard generated a peak of distorted rectangular shape, corresponding to an increase in thermal conductivity. Full-scale recorder deflection was produced by a concentration of about 70 ppm of helium.

Because no chromatographic column was used in the system, the measurement was not specific for helium. Accordingly, increases in the concentration of helium rather than absolute concentration values were reported. At each of four sampling points, a reference sample was taken immediately before the release of helium, and then additional samples were taken at preselected time intervals after release. Increments in helium concentration were calculated from increases in conductivity over that of the reference samples. On the basis of duplicate determinations, increments of helium from 8 to 400 ppm were measured with a coefficient of variation of 2%. On an absolute basis the average difference between ten duplicate determinations was 1.4 ppm.

Investigation of Adsorbers for Removing Fission-Product Gases from Helium

Measurements of adsorption of krypton from flowing helium and other carrier gases were extended to cover additional types of charcoal and a wider range of adsorber operating conditions. These measurements are being made to obtain data on the operation of adsorbers for general gas-cooled reactor application and for GC-ORR loop No. 2.

The data obtained in this study from elution curves for radiotracer krypton are presented in Table 6.9. Values for the dynamic adsorption coefficient k , a quantity proportional to retention time, are based on the volumetric flow rate measured at the adsorber pressure and at 24°C. As the data of Table 6.9 indicate, helium is not appreciably adsorbed on charcoal at these temperatures and has little adverse effect on k and N , the number of theoretical plates per foot, at pressures up to 300 psi. The deleterious effect of exposure of the adsorber to gases containing

Table 6.9. Dynamic Adsorption of Krypton by Activated Carbon

| Type of Activated Carbon and Mesh Size | Adsorber Temperature (°C) | Carrier Gas | | | k, Adsorption Coefficient (cm ³ /g) | N, No. of Theoretical Plates per Foot |
|--|---------------------------|------------------------------|-----------------|-------------------------------|--|---------------------------------------|
| | | Type | Pressure (psia) | Superficial Velocity (ft/min) | | |
| Columbia HCC, 12/28X | 24 | He | 14.5 | 1.6 | 57 ^a | 72 |
| | 0 | He | 14.5 | 1.6 | 112 | 79 |
| | -33 | He | 14.5 | 1.6 | 520 ^a | 103 |
| | 24 | He | 14.5 | 0.07 | 36 ^a | 10 |
| | 24 | He | 325 | 1.6 | 53 ^a | 81 |
| | 24 | He | 325 | 0.5 | 48 ^a | 151 |
| | -33 | He | 330 | 1.6 | 480 | 155 |
| | -33 | He | 330 | 0.4 | 440 | 97 |
| | 25 | Air (R.H. = 51) ^b | 14.5 | 0.07 | 29 | 20 |
| | 25 | Air (R.H. = 59) ^b | 14.5 | 0.07 | 16 | 18 |
| Columbia ACC, 6/14X | 25 | He | 14.5 | 1.6 | 57 | 59 |
| | 0 | He | 14.5 | 1.6 | 119 | 65 |
| Pittsburgh PCB, 12/30 | 25 | He | 14.5 | 1.6 | 52 | 58 |
| | 0 | He | 14.5 | 1.6 | 122 | 65 |

^aReported previously but included for comparison.

^bCharcoal was in adsorption equilibrium with water concentrations corresponding to the estimated relative humidities (R.H.) indicated.

appreciable quantities of water vapor is evident, however, from the two runs using wet air.

Low values for k and N are evident at low flow velocities of carrier gas. The low value for N is caused by the longitudinal diffusion of krypton becoming important, and the low k value is probably due to the elution curve not having a well defined peak (the location of which is used to calculate k). For purposes of interpolation and extrapolation, a plot of $\log k$ vs T^{-1} , where conditions other than temperature are constant, gives a nearly straight line. All three of the activated carbons tested appear to be useful adsorbents for radioactive fission-product gases.

In a proposed design for a purge trap for GC-ORR loop No. 2, the helium velocity was to have been approximately 0.0035 ft/min. A krypton elution curve was obtained in a laboratory test for this velocity but at a pressure of 1 atm, whereas the trap was to operate at 250 psia. The charcoal used was Columbia HCC 12/28X at 24°C with an effective length of 10 in. This trap gave the very low breakthrough time of 1.8 hr, which is to be compared with the calculated average holdup time of about 100 hr for the hypothetical case of large N . The effect of diffusion is even more strikingly indicated here than in the case mentioned above. Accordingly, since transport of krypton and xenon by longitudinal diffusion is highly important for adsorbents operating at low helium-carrier-gas velocities, an experimental and theoretical study of fission-gas diffusion in charcoal has been initiated. Measurements are being made of the diffusion of krypton through charcoal for a variety of experimental conditions. Data thus far obtained correspond to the charcoal being in 2-in.-i.d. pipes, with static helium at 1 atm as the predominant component of the gas phase. A pulse of natural krypton with Kr^{85} tracer is injected at one end of the charcoal column, and the rate of migration of krypton is determined by means of a G-M counter tube located at the other end of the column. The scope of measurements made thus far is indicated in Table 6.10, where breakthrough time represents the time at which Kr^{85} is first observable.

Table 6.10. Diffusion of Krypton Through Charcoal

| Type of Charcoal and Mesh Size | Length of Charcoal Column (in.) | Charcoal Temperature (°C) | Approximate Breakthrough Time (min) |
|--------------------------------|---------------------------------|---------------------------|-------------------------------------|
| Columbia HCC, 12/28X | 10.2 | 25 | 70 |
| | 10.2 | 0 | 140 |
| Pittsburgh PCB, 12/30 | 10.2 | 25 | 50 |
| | 21.5 | 25 | 360 |
| Pittsburgh PCB, 6/16 | 10.2 | 25 | 45 |
| Empty pipe* | 10.2 | 25 | ~0.2 |

*Helium filled; length and temperature refer to the helium in this case.

In conjunction with these measurements, an Oracle program has been written for evaluating the applicable solution of the diffusion equation. The solution, which is an infinite series, relates the krypton concentration to time and position in the adsorber. By comparison of experimental and calculated data, effective diffusion coefficients will be determined for use in estimating adsorber performance.

In connection with observed heating during high-pressure tests on the GC-ORR loop charcoal traps, a few laboratory-scale tests were performed under simulated conditions. Temperature rises of about the same magnitude were observed; e.g., a temperature rise of the charcoal of 25°C was observed when the laboratory trap was pressurized with nitrogen from 0 to 580 psig over a period of a few seconds. From experimental and theoretical considerations, the observed heating appeared to be explained satisfactorily by the heats of adsorption and compression; in addition, its localized nature in the tests of the loop trap appeared to be consistent with the geometry of the loop traps. On the other hand, bulging of a loop trap, which also was associated with the pressurization, does not seem to have been due to the heating but rather to the high pressure alone.

Measurement of High Temperatures

Drift Studies of Chromel-P-Alumel Thermocouples in Various Atmospheres

An investigation of the large negative drifts in emf noted with Chromel-P-Alumel thermocouples in a stagnant helium atmosphere has been continued. Previously reported drifts were obtained using quartz thermocouple-protection tubes. Because of the possibility of quartz reactions which might result in contamination of the thermocouple materials, a series of measurements was made using 0.375-in.-o.d., 0.25-in.-i.d., 18-in.-long alumina tubes as the protection tubes. Within the limits of the experiment, no differences were noted between the use of alumina and quartz tubes. The emf measurements, electrical resistances, and profile measurements were checked to detect inhomogeneities, and no appreciable differences were found. It is concluded that quartz is not necessary for obtaining the negative emf drifts.

As previously reported, the negative emf drift in these experiments is due to changes occurring in the Chromel-P wire. The Alumel wire always has a slight positive drift without showing appreciable lack of homogeneity at any point in the wire. In addition, Chromel-P-platinum thermocouples were found to drift negatively without exposure to Alumel wire. Therefore, much of the study has been concentrated on the Chromel-P wire alone. The emf-drift tests showed that bright-annealed and dull (oxidized) Chromel-P wire gave the same general results. Some differences were noted, but the differences were mainly rate effects which did not alter the major mechanism. All but special tests have been carried out with the dull wire.

In order to study the sequence of changes during the emf-drift tests, Chromel-P wires were exposed to stagnant helium at 1000°C for various periods of time. The results of these tests showed that the following changes in the wire occurred during the time of rapid negative drift. The first noticeable change was a brightening of the surface of the wire in the hottest zone of the furnace. This brightening started within minutes after insertion of the wire into the furnace and spread during

the exposure time throughout the entire heated portion of the wire. The bright section of the wire was attracted weakly by a magnet. With increasing time, the wire in the hottest part of the furnace gradually became dull gray and lost its magnetism. After several days, all the wire except that in the sharp thermal-gradient region had an oxidized appearance. The wire in the gradient retained its bright film. The bright film was rather easily peeled off the wire, and a black oxidized layer was exposed. Fluorescent x-ray analysis showed the film to be at least 99% nickel. As expected, the bright section of the wire was strongly attracted by a magnet and even retained appreciable magnetism after removal of the bright film.

As previously reported, profile measurements showing inhomogeneous sections along the length of thermocouple wires have been made by withdrawing the couples from the furnace in 1-in. increments and measuring the emf error at each position. In order to detect the inhomogeneous sections of the single wires treated in the above experiments, it was necessary to set up a unilateral gradient furnace.¹² The wires to be tested were silver-soldered into a long length between two leaders of untreated Chromel-P wire. One leader of untreated Chromel-P wire was fed into the furnace through a hole in the door, around a takeup reel in the heated zone, and out through the wall of the furnace. In operation the wire was driven into or out of the furnace (400°C) at constant speed while any emf developed between the two untreated leaders was being recorded. In effect, the emf was the difference between that developed in an untreated wire by a fixed gradient and that developed in the treated wire by a moving gradient. The emf output was dependent upon inhomogeneous sections of the wire. In the tests it was shown that physical inhomogeneities (cold-work, etc.) and variations in chemical composition of the original wire were insignificant in comparison with the inhomogeneities that caused the large negative drifts.

¹²D. L. McElroy and J. F. Potts, "Thermocouple Research, Final Report," ORNL-2773 (in press).

The results of a series of measurements made on single Chromel-P wires treated at 1000°C in a stagnant helium atmosphere for various times are summarized in Table 6.11. Profiles were obtained for the wires, and then the bright film was removed with an abrasive air blast. The profiles were then remeasured, assuming that the previous measurement had no effect on the wire. Repeated measurements on the same wire showed this assumption to be valid.

The results indicate that the initial, small, negative drift along the wire is removed by abrasion. However, the more slowly developing positive drift in the isothermal (hot) zone and the negative drift in the temperature-gradient zone are relatively unchanged by removal of the bright nickel film. It appears that the nickel film is not the major cause of the large negative drifts.

One sample of Chromel-P wire was treated in stagnant helium at 1000°C for 72 hr in a tube containing a titanium wire. The titanium prevented most of the negative drift usually expected.

Table 6.11. Results of Measurements of Single Chromel-P Wires Treated at 1000°C in a Stagnant Helium Atmosphere

| Duration of Wire Heat Treatment | EMF Peak (mv) | | | |
|---------------------------------|-------------------|-----------------------------|-------------------|-----------------------------|
| | Before Abrasion | | After Abrasion | |
| | Isothermal Region | Temperature-Gradient Region | Isothermal Region | Temperature-Gradient Region |
| 10 min | -0.3 | 0 | -0.1 | 0 |
| 30 min | -0.3 | 0 | -0.1 | 0 |
| 5.5 hr | -0.3 | 0 | | |
| 48 hr | +0.2 | -4.8 | +0.2 | -4.6 |
| 96 hr* | +0.3 | -0.1 | | |

*In vacuum.

As previously reported, the thermocouples failed to drift negatively when under vacuum. This effect is shown in Table 6.11. The wire tested under vacuum showed practically no negative drift.

Exposure of thermocouples made of Geminol-P versus Alumel versus platinum to stagnant helium at 1000°C for 1006 hr resulted in only a slight positive drift. The Geminol leg showed a +0.2-mv change, with a total change of +0.9 mv for the Geminol-Alumel couple. This is in contrast to the results for a series of Chromel-P-Alumel couples, which drifted negatively 8 to 11 mv during the same time. The Geminol wires showed slight oxidation, in contrast to the Chromel-P wires, which were almost completely oxidized in the temperature-gradient region.

Tungsten-Rhenium Thermocouples

Two tungsten-rhenium thermocouples were maintained in a pure helium atmosphere at 1000 to 1100°C for 675 hr. During this period, the temperature was cycled four times between 500 and 1100°C without increased error in the thermocouple emf. The indicated temperatures agreed to within 5°C and were approximately 10°C lower than calibration data reported by Lachman.¹³ The thermocouples were prepared by the ORNL Metallurgy Division from stainless steel sheathed 0.025-in. tungsten-rhenium wires. The junctions were formed by using a helix of 0.010-in. rhenium wire around the tungsten wire and were welded to the 0.025-in. tungsten and rhenium wires. A spot-welded couple and a Heliarc-welded couple were tested. The Heliarc-welded couple failed after about 650 hr by developing a high-resistance junction that gave erratic results. Investigation showed a partial break in the 0.010-in. rhenium wire adjacent to the weld joining it to the 0.025-in. rhenium wire. The sheath of the spot-welded couple failed during the test. The sheath separated with a gap of about 1/8 in. between parts, without damage to the wires. This break occurred 3 in. from the junction and apparently resulted in more oxidation of the metals than was noted in the Heliarc-welded specimen.

¹³J. C. Lachman, General Electric Company, personal communication.

7. DEVELOPMENT OF TEST LOOPS AND COMPONENTS

ORR Gas-Cooled In-Pile Loops

Loop No. 1

The in-pile section and transfer station of loop No. 1 were installed during the reactor shutdown of August 8. This work completed the installation of the main loop and the major auxiliary equipment, except the emergency power supply and the sweep gas system. Leak testing of mechanical joints is complete, and shakedown of the loop is in progress. The system pressure is limited to 45 psig, pending operational and hazards committee approval of the loop. Operation of the compressors, heater, cooler, and water pumps appears to be satisfactory, and the entire system is being run on automatic control for extended periods.

Fabrication of the primary system sample box is nearly complete. A preliminary test indicated the feasibility of the foam-plastic method of sealing contaminated pipe for removal from the pool, and preparations are being made for a full-scale test. Further developmental work on the underwater manipulation of flange bolts has been found to be necessary, and the use of impact wrenches for this service is being tested. A cartridge type of electric heater is being developed for calibration of the in-pile gas-stream thermocouple, and a simplified transfer-station loading tube is being fabricated that will eliminate the plastic sleeves and shearing of the instrument lead tube underwater. A revised operational and hazards report has been prepared for review by the committees which must approve the loop prior to full-scale operation.

Loop No. 2

Fabrication of the primary components of loop No. 2 is nearing completion. The side-stream molecular sieve and cooler were redesigned to facilitate shielding. Fabrication has been initiated on these items.

It was decided to use a chloride-free material, such as Amsco 125-82 or triethylphosphate, instead of Freon 11 as the coolant for the side-stream carbon trap. The design drawings for this trap were completed.

Fabrication of the south facility plug was completed, and the unit was installed on schedule in the ORR during the extended reactor shutdown in July. Drawings of the containment cell for the loop were completed and transmitted to the construction contractor.

Components in the primary helium coolant circuits which have large surface areas and/or large temperature gradients are to be lead shielded because of probable fission-product deposition during operation. Design and detailing of these shields are approximately 70% complete.

On the basis of satisfactory test results at temperatures up to 1300°F, it has been decided to use Marman Conoseal flanged joints for the 2 1/2- and 5-in. IPS applications in this loop. These joints, as modified for this use, have double gaskets and a buffer zone which will be maintained at a pressure 50 psi above that in the loop.

Detail drawings of a positioning fixture for the removable elbow are complete, and design and detail drawings have been completed for an electrically operated device for applying torque to the bolts on the 5-in. removable-elbow clamp. A design for forcing apart the slip joints of the removable elbow and a design for retaining the gaskets in position during remote assembly of the elbow have been completed. Design of a cover for the retention of contaminated products in the removable elbow and in the mating nozzles has been made. An investigation of sampling and analytical requirements for loop 2 was made, and a draft of criteria for gas-sampling was prepared.

Construction and assembly of the evaporator and condenser are complete and the heater is partially assembled. These components are to be tested out-of-pile, as described in a later section of this chapter. Dye-penetration and helium-leak-detection tests were made on a shipment of 84 of the heater cartridges. The dye-test indicated numerous sheath penetrations, but the cartridges passed the helium leak tests. Additional cartridges have been ordered to tighter specifications.

The test stand for the remotely operated crane and single-arm manipulator was designed and is being fabricated. This test stand will be used to develop and demonstrate equipment and techniques for the remote removal of the in-pile test section.

Under conditions of zero fission power and no coolant flow, it was calculated that the fuel element temperature would rise a maximum of approximately 400°F due to gamma-ray afterheat. This will not produce fuel melt-down. However, preliminary results from an analog computer study of the loop indicate that the test section will require modification and that the critical component, temperature-wise, will probably be a baffle between the main coolant stream and the shell coolant stream. Data from analog computer runs simulating the graphite-jacketed fuel element operating at a fission-power generation rate of 150 000 Btu/hr.ft with a jacket temperature of 2500°F are being analyzed.

An analysis of the temperature distribution in the metal of the ob-round section of the south-facility nose plug indicated that the reactor setback controls should be set for activation at a minimum flow rate of 60 gpm of cooling water to prevent flashing of the cooling water. An analysis was made of the possibility of damage to the loop 2 containment cell by postulated missiles resulting from equipment failure. Although the analysis is not complete, the missile hazard appears to be very small and wall penetration will not occur.

EGCR In-Pile Loops

Through-Tube Design

Three design layouts have been prepared for the 5 1/2-in.-o.d. through tubes, and the preferred design is shown in Fig. 7.1. This design eliminates an expansion joint required in the other two designs by allowing the loop tee in the bottom nozzle to move downward to compensate for the differential thermal expansion between the loop tube and the reactor. The nozzle load to the reactor vessel was reduced by connecting the breech closure to the primary loop containment.

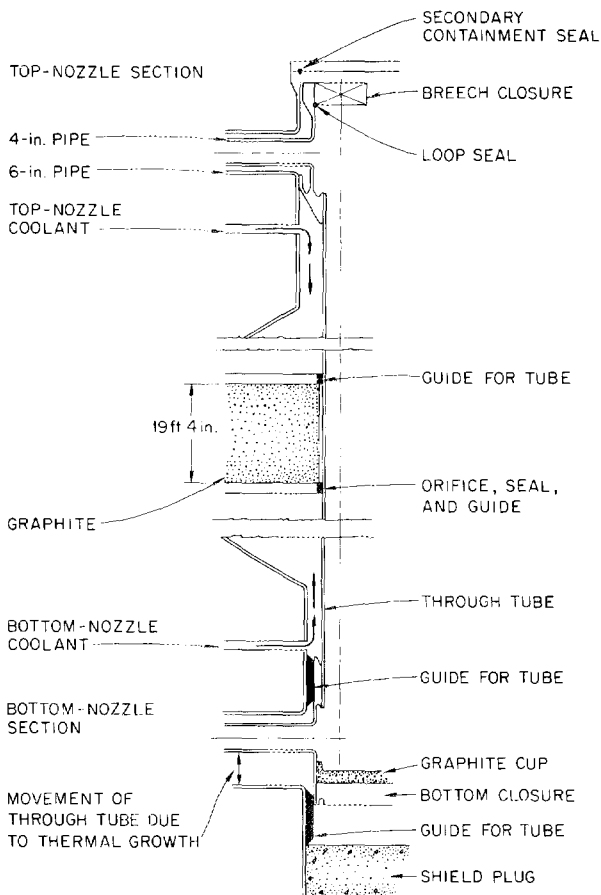


Fig. 7.1. Design of 5 1/2-in.-o.d. EGCR Core Through Tube.

of the tube proper, the axial load on the tube will be a tensile load under normal conditions. Again, depressurization of the loop will cause a compressive axial load that will be considerably smaller than the critical load for the tube.

Component Designs

Gas Filters. New pressure-drop data require that the diameter of the main loop-gas filter be increased from 12 to 18 in. Under the most severe operating condition, the calculated pressure drop through the primary filter element is 7 in. H₂O. In addition to the primary absolute

An evaluation of the axial loads on the through tubes and reactor nozzles was made for the current preliminary designs with and without expansion bellows. A compressive load greater than the critical column-buckling load was found for the 5 1/2-in.-o.d. through tube with an expansion bellows. Without the bellows, the through tube will normally operate with a tensile load; hence, there will be no column-buckling problem. With the loop depressurized, the reactor pressure will cause a compressive load, but this will be considerably less than the critical load for the tube.

Since the effective diameter of the bellows for the 9 1/2-in.-o.d. through tube can be made smaller than the inside diameter

filter, a prefilter and postfilter are to be included in the filter vessel to protect the primary filter from the larger of the incident particles. The postfilter is designed to protect the compressor impeller from the large particles in case the primary filter becomes overloaded and ruptures.

The type 347 stainless steel filter vessel will be approximately 20 in. in diameter and will be surrounded by insulation and lead shielding. The filter system will give an efficiency of at least 99.9% for 0.3 μ particles and larger and will operate with a total pressure drop of about 15 in. of H₂O.

Gas Heater. An evaluation was made of alternate designs for the loop process gas heater.^{1,2} Difficulties in procuring leak-tight seals for heater leads and insulation suitable for use in high-pressure helium have led to the choice of resistance-heated pipe sections. It is now intended to provide heat to the loop gas by passing a large electric current through a section of the loop pipe in the experimenters' cell. The pipe which will be heated will be in the form of a U-tube; i.e., two 20-ft sections of straight pipe will be joined by a standard 180-deg turn fitting. No electric current will pass through the turn or through the welds at the ends of the straight pipe sections.

Diversion Valve. The following specifications were prepared for a diversion valve and were submitted to vendors for bids:

Helium System

| | | |
|--|------|------|
| System pressure, psi | 500 | 1000 |
| Maximum flow through valve, lb/hr | 9190 | 9190 |
| Temperature, °F | 1050 | 1050 |
| Maximum pressure drop across valve from inlet to outlet through either discharge port, psi | 2.1 | 2.1 |

¹"GCR Quar. Prog. Rep. March 31, 1960," ORNL-2929, pp. 239-42.

²"GCR Quar. Prog. Rep. June 30, 1960," ORNL-2964, p. 239.

CO₂ System

| | | |
|--|--------|--------|
| System pressure, psi | 500 | 1000 |
| Maximum flow through valve, lb/hr | 41 000 | 41 000 |
| Maximum pressure drop across valve from inlet to outlet through either discharge port, psi | 3.9 | 2.0 |

Sniffer-Gas System. The criteria for the sniffer-gas system for detecting a helium or carbon dioxide leak to the annulus between the loop piping and the secondary containment piping were established. A small flow of air will be passed through the annulus via an inlet and an outlet orifice, and leakage into or out of the annulus will modify the annulus pressure by unbalancing the flow rates. Radiation measurements will be used to back up the pressure measurement for detection of leakage into the annulus.

Buffer-Gas System. The buffer-gas system is designed to detect helium or carbon dioxide leakage at mechanical joints by sensing a drop in the pressure between double seals. The buffer gas will be maintained at a pressure greater than the loop operating pressure. The system will not be capable of determining which joint is leaking until the loop has been shut down and the cell can be entered for manual valve operation.

Gas-Transfer System. The gas-transfer system will consist of the transfer pump, storage tanks, and a safety surge tank. The transfer pump is to be a multiple-stage diaphragm pump capable of transferring gas from the loop to the storage tanks or from the storage tanks to the loop in less than 5 hr. The maximum discharge pressure is 1100 psia, and the minimum suction pressure is 8 psia.

The gas-storage system will consist of six 24-in.-o.d., 12 1/2-ft-long tanks connected with headers. The total system volume will be approximately 200 ft³.

The safety surge tank is designed to add a measured volume of gas to the loop in the event of loss of one compressor when the loop is operating with helium at 500 psia. The tank will hold approximately 5 1/2 lb of helium at 1000 psia for release into the loop upon demand. This addition of helium will increase the loop pressure from 500 to 646 psia at the rate of 4 psi/sec.

Cooler. The loop coolers have been redesigned to bring the steady-state thermal stresses within the limits specified by the ASME Boiler Code for Unfired Pressure Vessels. The original cooler design consisted of heavy concentric pipes separating the loop gas and the demineralized cooling water. The steady-state thermal stresses in the pipe separating the hot gas (up to 1050°F) and cold water (150°F) was approximately 100 000 psi. The current design employs a shell-and-tube arrangement with the gas flowing inside the tubes. By employing a larger gas flow area and thin-walled tubes, the steady-state thermal stresses are below those permitted by the Code.

Demineralized-Water System

The demineralized-water cooling system has been modified to provide secondary containment in the event of a rupture of the primary loop gas into the water system. Such a rupture could occur either at the loop coolers or at the water-cooled compressor casings. The demineralized-water system is not designed for high pressures. Consequently, in the event of a gas leak into the cooler, automatic valving on the cooler water-feed lines will seal the cooler from the rest of the water system. The cooler is designed for an allowable pressure of 500 psia. Any overpressure will open a pressure-relief valve which will vent the cooler to the experimental cell serving the loop. Both the cooler and the compressor demineralized-cooling-water supply systems are provided with means for detecting and containing both small gas leaks and major system ruptures. Provision is also made for emergency cooling of the compressors and the loop cooler.

Cell Ventilation System

A brief study was made of the cell ventilation system to be provided by Kaiser Engineers in order to evaluate its adequacy. It was found that the ventilation rate was about an order of magnitude higher than that required for any anticipated occupancy of the cell. Consequently, it was recommended that the ventilation rate be reduced by a factor of 10. The

lower flow rate will reduce the size of the ventilation duct blowers and associated piping, permit easier monitoring of the cell radiation level, and reduce the probability of large-scale fission-product release to the stack in the event of a major system rupture in the cell.

Hazard Studies

Natural-Convection Cooling. An analysis has indicated that natural convection will be a significant heat-removal process in the experimental loops. When the flow characteristics of the final loop piping layouts are known, convection calculations will be made to determine accurately the rate at which heat can be removed from the test element by this process.

Transient Thermal Stresses. In order to evaluate transient thermal stresses in loop piping, calculations were made to determine temperature vs time and position for the concentric piping from the cooler to the cell wall after a rapid drop of cooler outlet temperature. The calculations were based on 6-in. sched.-80 stainless steel pipe inside 8-in. sched.-40 stainless steel pipe with air in the annulus. For a 60-ft length, it was found that a step change in the inlet temperature would lower the inner pipe temperature rapidly before any appreciable change occurred in the outer pipe temperature. The greatest difference between mean temperatures of the inner and outer pipes was approximately 85% of the initial step change. This occurred after about 4.5 min.

Thermal Expansion. During investigation of certain emergency conditions, it was found that cooling characteristics of the process and containment piping between the through-tube nozzles and the cell-wall anchor point would result in considerable differential contraction. The changes required to provide the necessary freedom of movement for the process piping within the containment piping are being studied.

Kinetic Study. The dynamic behavior of the EGCR loop is being investigated with the use of the ORNL Reactor Controls Analog Facility. The preliminary analog simulation was based on the loop design as of mid-June. Four cases were studied; two of these were helium-cooled

systems and two were carbon dioxide-cooled systems. All four cases were based on proposed test specimens.³ Two of the cases considered required attemperation in the fuel element section and two did not. The calculations considered normal changes in power, scram conditions, loss of one of three and loss of one of two compressors, loss of pressure, and compressor speed-control failure. The loss of compressor and loss of pressure accidents were considered both with and without corrective action.

The primary conclusion to be drawn from the results of this preliminary analog study is that, in general, the dynamic behavior of the loop is essentially the same for helium and carbon dioxide and for attemperated and nonattemperated conditions. The system appeared stable, without overshoots or oscillations in temperature and flow rate upon changes in power. The loss of compressor accidents were found to cause fairly rapid changes in specimen surface temperature and gas temperatures which would probably result in loop failure if uncorrected. Upon loss of one of three compressors, however, corrective actions, such as compressor speedup and increasing the loop pressure, brought the loop back to normal operating conditions quite rapidly, with minimum excursions, as shown in Fig. 7.2. Reactor shutdown would be required upon the loss of one of two operating compressors. The analog simulation indicated an orderly shutdown could be accomplished without major excursions in temperature. Typical curves for both scram and orderly shutdown are shown in Fig. 7.3. The study confirmed that loss of loop pressure even from a fast leak was a serious accident and, in most cases, would cause substantial temperature excursions, even with a scram. Typical results are presented in Fig. 7.4. The failure of a compressor speed controller that resulted in a minimum speed would be a serious problem only if the compressor minimum speed were set at a value considerably below the normal operating point.

³R. B. Kormeyer et al., "Comparison of Fuel Assembly Tests Prognosticated for EGCR Loops," ORNL CF-60-1-1.

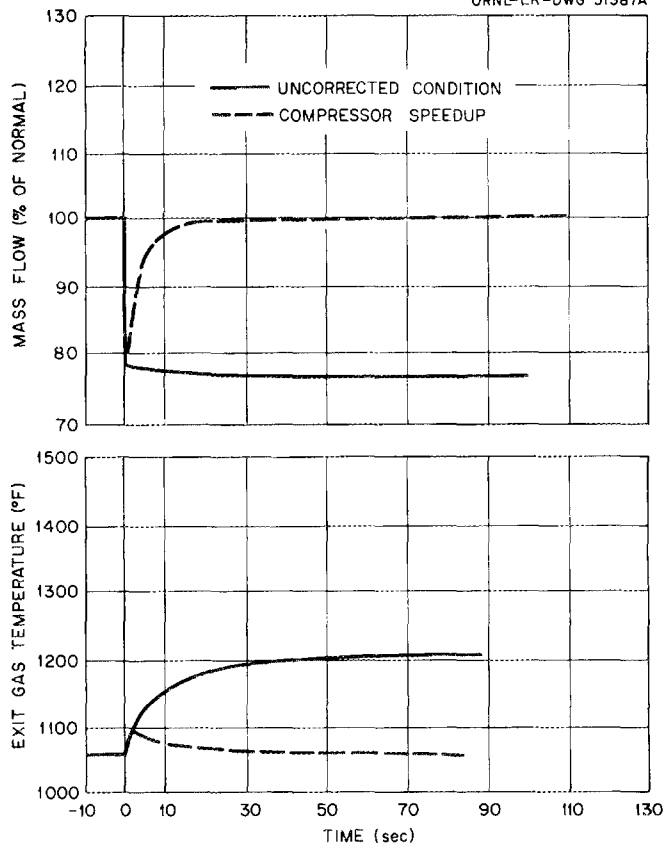


Fig. 7.2. Typical Curves for Instantaneous Loss of One of Three Operating Compressors of an EGCR Loop System.

necessary to remove the shielding from between adjacent coolers and, in some locations, from between adjacent pipe runs. A 10-ft section of removable shielding will be available to provide shielding in case diverter valve maintenance is required.

The ORNL designs of the experimental crane shed and the cell personnel air lock are essentially complete, and a single-line diagram for the cell electrical system has been prepared. The diagram shows two separate power supplies, one from the EGCR 13.8-kv substation and the other a 13.8-kv transmission line from the Y-12 area. The system has four transformers, rated at 13.8 kv/4.8 kv and 1500 kva each, serving two main busses and one auxiliary bus. Each loop will have two compressors, a loop heater, and a transfer pump fed from the EGCR source. One compressor per cell will be fed from the Y-12 source.

Supporting Facilities

The loop supporting facilities are being designed by Kaiser Engineers. Structural drawings which affect the experimental loop pipe runs within the containment vessel have been received. It was necessary to modify the Kaiser design slightly in order to have adequate room within the reactor biological shield for installation and maintenance of the loop cooler and the cooler diverter valve and also to have adequate space for installation of the upper and lower horizontal pipe runs. In order to provide this additional space within the pipe chase, it was

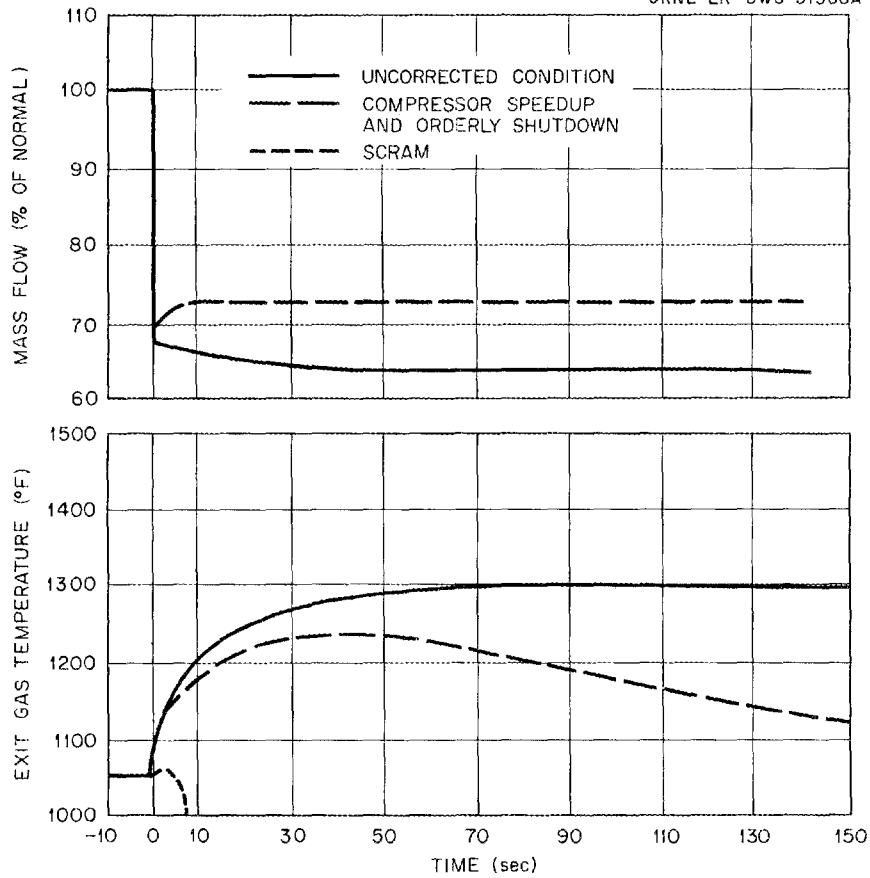


Fig. 7.3. Typical Curves for Instantaneous Loss of One of Two Operating Compressors of an EGCR Loop System.

Hydrogen-Cooled Loop Design Study

A preliminary study was made of the proposed hydrogen-cooled in-pile loop, and it was found that the potential hazards were more extensive than first anticipated. Extensive additional study will be required to fully evaluate these hazards. Present plans call for the hydrogen loop to be located in a modified version of one of the large core through tubes. Since high performance is not considered to be essential in acquiring experience with the use of hydrogen gas as a coolant, the loop performance specification will be relaxed both as to operating pressure and test fuel element power. The basic design criteria now being

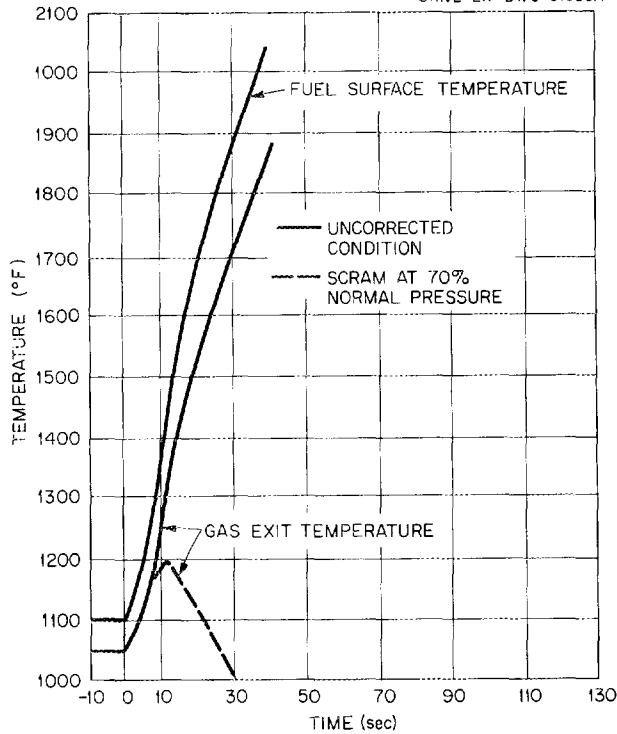


Fig. 7.4. Typical Curves for EGCR Core Through-Tube Failure Where Loop Pressure Drops from 1000 psia to Reactor Pressure in 10 sec.

The experimenters' cell will contain all the principal loop components, and it too will be filled with an inert-gas atmosphere that will be continuously processed to remove hydrogen and oxygen.

considered specify a loop pressure of 300 psi, hydrogen temperature of 600 to 1050°F, and test fuel element power levels of up to 500 kw.

The explosive hazard of the hydrogen loop will be controlled by surrounding all hydrogen-filled pipes and components with an inert gas that will be continuously processed to maintain an ever-safe hydrogen and oxygen content. In order to accomplish this it will be necessary to place a small core through tube inside the large core through tube. Outside the reactor pressure vessel, the annulus of a concentric pipe arrangement will provide space for the inert gas. The experi-

Loop Component Tests

Heater, Evaporator, and Condenser for GC-ORR Loop No. 2

An out-of-pile test loop is being assembled for testing the performance of the GC-ORR loop No. 2 heater, evaporator, condenser, and heater power and control equipment. The test loop is to provide a helium flow of 500 lb/hr at 300 psig and 600°F, heater gas outlet temperatures up to 1470°F, heater element skin temperatures up to 1700°F, evaporator gas inlet temperatures up to 905°F, and evaporator gas outlet temperatures

not to exceed 600°F. The maximum flow capacity (500 lb/hr at design conditions) of the only compressor available for this test, an HECT-II compressor, makes it impossible to achieve the design flow rate of 1000 lb/hr. It will be possible, however, to extrapolate the data obtained from the test loop at the lower flow to full flow conditions.

The test loop will contain two closed circuits, a 300-psig helium loop and a steam and condensate loop, and two open circuits, a demineralized-water makeup system and a cooling water system. The helium loop is composed of a HECT-II compressor, the heater, the evaporator, a bypass around the heater, and the necessary 2 1/2-in. pipe and fittings. Remotely operated control valves in the bypass and heater inlet lines permit diverting a portion of the helium flow around the heater. This will permit testing of the heater at the maximum gas outlet temperature without exceeding the evaporator gas inlet design temperature of 905°F.

The steam and condensate loop is made up of a 2 1/2-in. steam line from the top shell side of the evaporator to the top shell side of the condenser and a 1-in. condensate line from the bottom shell side of the condenser to the bottom shell side of the evaporator. A manually operated valve and a vent line are provided at the highest point of the steam line to permit purging the system of air when starting up. A pressure-relief valve is also provided in the steam line.

The demineralized-water makeup system is composed of two 50-gal stainless steel drums, a continuously operated positive-displacement pump, a bypass around the pump, an automatically operated flow-control valve, a manually operated flow-control valve, and the necessary 1/4-in. pipe and fittings. The valving arrangement at the drums permits either drum to be removed and refilled while the second drum is in use. An in-line pressure-relief valve in the pump bypass maintains a preset pressure on the system. The cooling water system consists of a 1-in. pipe to a process-water header, manual throttling valve, a flowmeter, the tube side of the condenser, and an outlet pipe to the waste-water system.

Orifices are provided in the compressor return and heater bypass lines for determining the helium flow through any portion of the helium

loop. The temperature is sensed with thermocouples at several critical points inside the heater, at the orifices, and at the inlet and outlet of the compressor, the heater, the evaporator, and the condenser. Temperatures from the critical locations are recorded continuously on a multipoint recorder, while those from less critical locations and from backup thermocouples are indicated by means of a selector switch. Pressure taps are provided for measuring the helium loop pressure, the steam pressure, the demineralized-water makeup system pressure, and the pressure drops across the heater, evaporator, and condenser. Reflex sight gages indicate the water level in the evaporator and the condensate level in the condensate return line. An automatic level controller maintains the water level in the evaporator between preset limits. The cooling-water flow through the condenser is measured with a flowmeter. An electrical interlock cuts the power to the heater and a time-delay switch stops the compressor when the evaporator gas-outlet design temperature is exceeded.

Ceramic-Metal Seal for Heater Leads

A heater-lead seal developed by the Hynes Electric Heating Division, Turbine Equipment Company, has been tested. The design of the seal, which combines metallic and ceramic components, is shown in Fig. 7.5. The central electrode is of type 316 stainless steel, and the insulating material is Super Mica 500, which has a coefficient of expansion of 10×10^{-6} in./in. $^{\circ}$ C, a compressive strength of 27 000 to 30 000 psi, and a tensile strength of 5000 to 7000 psi. Super Mica 500 is rated for use at 900 $^{\circ}$ F. The clearance between the central electrode and the Super Mica is filled with Fiberfrax impregnated with epoxy resin. There are two gaskets, each of Fiberfrax impregnated with epoxy resin; one is between the shoulder of the central electrode and the Super Mica, and the other is between the Super Mica and the flange. The flange is type 347 stainless steel. An electrical lead and seal of this type was tested by the Hynes Company at a 3000-v potential, and it exhibited no electrical leakage.

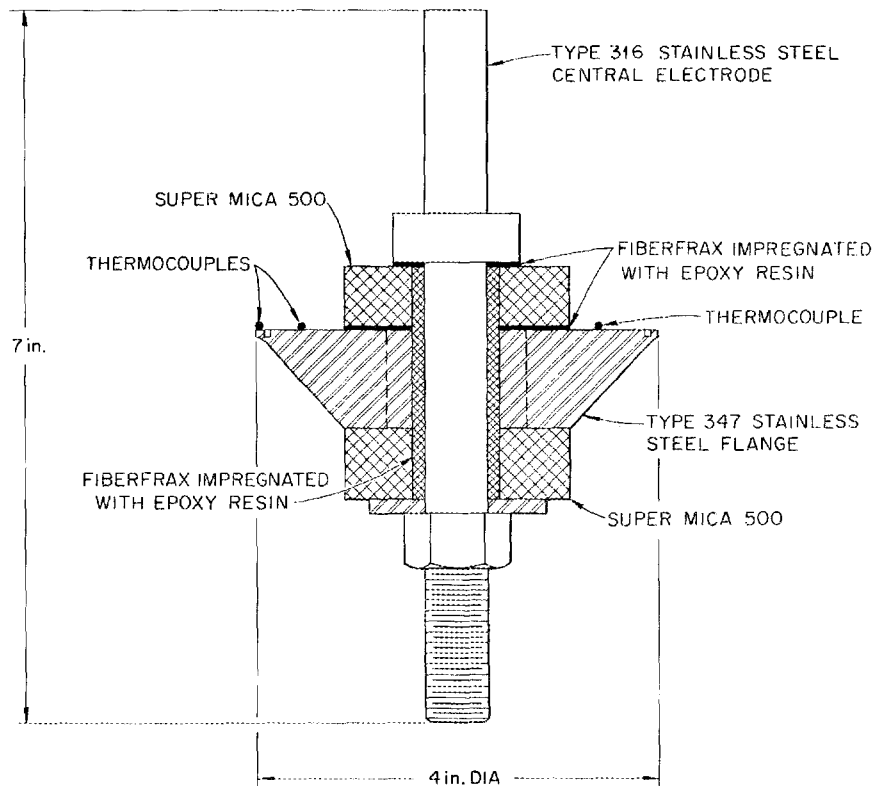


Fig. 7.5. Hynes Heater Lead With Metal-Ceramic Seal.

The ORNL test program consisted of mounting the seal element in a special fixture and exposing it to the pressure gradient range of interest (0 to 1000 psi) at increasing temperatures. Testing of the heater lead seal was terminated when a helium leakage rate of $10 \text{ cm}^3/\text{min}$ was obtained with a pressure difference across the seal of 20 psig and with the seal at a temperature of 600°F . When the pressure container was opened, it was observed that some of the epoxy resin used in the seal construction had melted and had been forced out of the seal. In order to further confirm by visual inspection that the seal leaked, a helium pressure of 20 psig was applied to the bottom side of the seal and water was sprayed on the top side. Gas bubbles leaked through the seal and appeared at the interfaces of the ceramic and metal parts.

The initial low-temperature leakage rates of the seal, as measured with the use of a mass spectrograph helium leak detector, are summarized in Table 7.1. Following these tests, data were obtained on helium leakage rates through the Hynes Seal with the seal at 285 to 290°F and at five test pressures ranging from 200 to 1000 psig. A water-filled glass manometer was used to measure the leakage. The data obtained in these tests are presented in Fig. 7.6.

Heater Electrical Breakdown Test

Chromalox tubular heating elements in hairpin form inserted through and welded into a single header plate are being investigated for gas heating. The header plate separates the process helium from a higher pressure zone of buffer helium. Because of the possibility of electrical breakdown of the helium buffer gas in the zone between the sheaths and terminals of the tubular heaters, tests of the configuration of interest are to be made to define its operating characteristics in helium at pressures up to 1000 psig and temperatures up to 950°F when exposed to electrical potentials in the range 0 to 1000 volts. The high-pressure

Table 7.1. Results of Leakage Tests of Heater-Lead Seal

| Pressure Above Seal (psig) | Temperature of Seal (°F) | Duration of Pressure Differential (min) | Helium Leak Rate (cm ³ /sec) |
|----------------------------|--------------------------|---|---|
| 990 | Room | 10 | 0 |
| 200 | 303 | 10 | <1.1 × 10 ⁻⁶ |
| 400 | 303 | 10 | <1.1 × 10 ⁻⁶ |
| 200 ^a | 300 | 10 | 0 |
| 400 ₁ | 300 | 10 | 0 |
| 600 ^b | 300 | 2 to 3 | >10 ⁻⁵ |

^aBefore this and subsequent tests, the volume immediately beneath the seal was purged with nitrogen to reduce the helium background for more accurate readings with the helium leak detector.

^bAt this test pressure, the leak detector suddenly indicated off-scale.

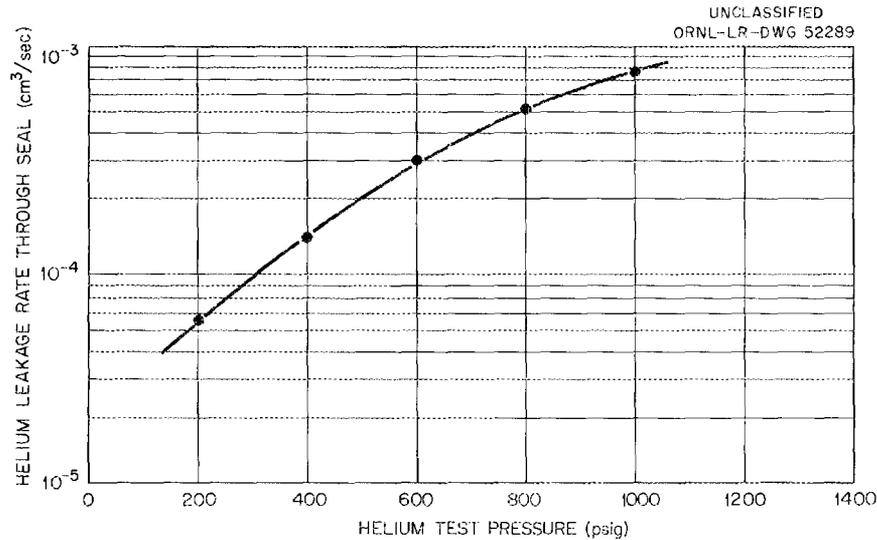


Fig. 7.6. Leakage of Heater-Lead Seal as a Function of Helium Pressure at a Seal Temperature of 290°F.

test chamber, the high-pressure piping system, the electrical power supply, and the instrumentation have been designed, fabricated, and assembled. The test chamber, including the modified Conax seals for the high-voltage leads, has been tested and approved. The resistance to ground of the electrodes in the Conax seals was in excess of 200 megohms in air at room temperature. A potential of 500 v was applied between the electrode and body of each Conax seal, and no indications of electrical breakdown were noted. A full-length Chromalox tubular heater will be tested for electrical breakdown in this test system.

EGCR Loop Valves

A test facility has been designed and constructed for screening tests of valves for the EGCR loops. The valves selected for testing are a Y-type globe valve with a Limatorque operator manufactured by the Wm. Powell Company, a ball valve with a Limatorque operator manufactured by General Kinetics Corporation, and a gate valve with a hermetically sealed actuator manufactured by Darling Valve and Manufacturing Company.

Each valve will be tested at 1050°F and 1000 psig to demonstrate compliance with specifications as to seal-plug leakage, stem-seal

effectiveness, and valve-actuator reliability. The valves will be automatically cycled 100 times between atmospheric pressure and 1000 psig of helium and between 200 and 1050°F during the course of the test program.

Special Compressors

Regenerative Compressors

Two regenerative compressor units have been installed in the twin-turbine vessel of the GC-ORR loop No. 1. During the loop shakedown and instrumentation checkout period, the compressors have operated satisfactorily as a single unit and in series over a range of speeds (6 000 to 12 000 rpm) and temperatures (up to 600°F) at limited pressure, pending approval of operation at design pressures.

The two defective compressor housings mentioned previously were successfully repaired by nickel plating the coolant passageways. The repair work was accomplished by the GATX Kanigen process. A mechanical repair technique that provides a shrink fit between the shell and the spiral drum is being investigated by the A-Tool and Gage Company.

Compressors with Gas-Lubricated Bearings

The delivery of the Bristol Siddeley compressor has been delayed because of inability to eliminate bearing metal-to-metal contact that is probably due to high-speed whirl. The compressor has been rebuilt 19 times in pragmatic attempts to solve the problems.

In an effort to determine possible causes for the bearing rubbing being experienced in the test runs, a bearing study was initiated at ORNL. The thrust and impeller end-bearing loads were determined to be 22 and 24 lb, respectively. The analysis indicated that the 2.25-in.-diam, 6-in.-long bearings are lightly loaded, and, as a result, the attitude angle is nearly 90 deg. This renders the bearing unstable. The results of computer solutions for other bearing designs indicate that a 180-deg partial bearing should offer the required load capacity with an attitude angle small enough to insure stability of operation.

High-Temperature Gas-Bearing-Compressor Test System

A test system for high-temperature performance checks of gas-bearing compressors has been completed. The compressor to be tested in this system has been received and is undergoing final acceptance inspections.

Compressors for GC-ORR Loop No. 2 and EGCR Loops

Contracts for three compressors for loop No. 2 and 16 compressors for the EGCR loops, all with gas bearings, were awarded to Bristol Siddeley Engines Limited during the last report period.

Mechanical Joint Service Testing

Elevated temperature thermal-cycling and load-cycling tests of mechanical pipe joints were continued in the three mechanical joint test stands described previously.⁴ The current tests have indicated that the 10-in.-IPS standard Conoseal joints will remain leaktight within acceptable limits under both thermal cycling and mechanical load cycling with internal gas temperatures up to 1050°F. Although the flange-sealing surfaces of these units were as much as 0.010 in. out of round because of warpage which occurred during welding of the units into the test fixture, satisfactory seals were obtained by limiting the torque applied to the clamp studs to 150 ft-lb. Repeated closures of these joints have demonstrated that the joints can be resealed if new gaskets are installed for each closure.

The test results also indicate that the 2 1/2-in.-IPS gas-buffered Conoseal joints utilizing N-155 high-temperature alloy clamps will remain leaktight under mechanical load cycling with internal gas temperatures up to 1500°F. However, these units have exhibited a tendency to leak under thermal-cycling conditions at maximum operating temperatures of 1400°F and above.

Five-in.-IPS gas-buffered Conoseal and six-in.-IPS gas-buffered Grayloc mechanical joints have been received for testing and evaluation.

⁴"GCR Quar. Prog. Rep. June 30, 1960," ORNL-2964, p. 243.

Initial room-temperature leak tests of these units gave a leakage rate of $<1 \times 10^{-10}$ cm³ (STP)/sec for the inner seals of both units and 4×10^{-8} and $<1 \times 10^{-10}$ for the outer seals of the Conoseal and Grayloc units, respectively.

Previous reports in this series are:

ORNL-2500 Parts 1-4, issued April 1, 1958
ORNL-2505 Issued June 19, 1958
ORNL-2510 Issued September 18, 1958
ORNL-2676 Period Ending December 31, 1958
ORNL-2767 Period Ending June 30, 1959
ORNL-2835 Period Ending September 30, 1959
ORNL-2888 Period Ending December 31, 1959
ORNL-2929 Period Ending March 31, 1960
ORNL-2964 Period Ending June 30, 1960

INTERNAL DISTRIBUTION

- | | |
|--------------------------|-------------------------|
| 1. G. M. Adamson | 44. T. Hikido |
| 2. S. A. Beall | 45. M. R. Hill |
| 3. R. J. Beaver | 46. H. W. Hoffman |
| 4. M. Bender | 47. A. Hollaender |
| 5. D. S. Billington | 48. A. S. Householder |
| 6. E. P. Blizzard | 49. H. Inouye |
| 7. A. L. Boch | 50. W. H. Jordan |
| 8. C. J. Borkowski | 51. P. R. Kasten |
| 9. W. F. Boudreau | 52. G. W. Keilholtz |
| 10. G. E. Boyd | 53. C. P. Keim |
| 11. E. J. Breeding | 54. M. T. Kelley |
| 12. J. C. Bresee | 55. J. J. Keyes |
| 13. R. B. Briggs | 56. R. B. Korsmeyer |
| 14. W. E. Browning | 57. P. Lafyatis |
| 15. C. E. Center (K-25) | 58. J. A. Lane |
| 16. R. A. Charpie | 59. S. A. Levin (K-25) |
| 17. R. S. Cockreham | 60. R. S. Livingston |
| 18. T. W. Cole | 61. H. G. MacPherson |
| 19. J. H. Coobs | 62. W. D. Manly |
| 20. J. A. Conlin | 63. E. R. Mann |
| 21. W. B. Cottrell | 64. R. W. McClung |
| 22. J. A. Cox | 65. H. E. McCoy |
| 23. F. L. Culler | 66. H. C. McCurdy |
| 24. H. N. Culver | 67. H. F. McDuffie |
| 25. J. H. DeVan | 68. C. J. McHargue |
| 26. D. A. Douglas | 69. F. R. McQuilkin |
| 27. L. B. Emlet (K-25) | 70. H. J. Metz |
| 28. E. P. Epler | 71. A. J. Miller |
| 29. R. B. Evans | 72. R. S. Miller |
| 30. D. E. Ferguson | 73. J. G. Morgan |
| 31. J. Foster | 74. K. Z. Morgan |
| 32. J. L. Fowler | 75. J. P. Murray (Y-12) |
| 33. A. P. Fraas | 76. F. H. Neill |
| 34. J. H. Frye, Jr. | 77. M. L. Nelson |
| 35. G. A. Garrett (K-25) | 78. L. G. Overholser |
| 36. A. E. Goldman | 79. N. Ozisik |
| 37. J. M. Googin (Y-12) | 80. P. Patriarca |
| 38. B. L. Greenstreet | 81. F. S. Patton (Y-12) |
| 39. W. R. Grimes | 82. A. M. Perry |
| 40. E. Guth | 83. D. Phillips |
| 41. J. P. Hammond | 84. C. A. Preskitt |
| 42. W. O. Harms | 85. M. E. Ramsey |
| 43. R. F. Hibbs (Y-12) | 86-87. P. M. Reyling |

- | | |
|----------------------|--|
| 88. T. K. Roche | 108. W. C. Thurber |
| 89. M. W. Rosenthal | 109. D. B. Trauger |
| 90. A. F. Rupp | 110. E. Von Halle (K-25) |
| 91. G. Samuels | 111. C. S. Walker |
| 92. H. W. Savage | 112. J. L. Wantland |
| 93. A. W. Savolainen | 113. G. M. Watson |
| 94. J. L. Scott | 114. A. M. Weinberg |
| 95. O. Sisman | 115. M. E. Whatley |
| 96. E. D. Shipley | 116. J. R. Weir |
| 97. M. J. Skinner | 117. J. C. White |
| 98. G. M. Slaughter | 118. E. A. Wick |
| 99. A. H. Snell | 119. G. C. Williams |
| 100. I. Spiewak | 120. C. E. Winters |
| 101. E. Storto | 121. J. Zasler |
| 102. R. D. Stulting | 122-125. ORNL - Y-12 Technical Library Document Reference Section |
| 103. J. C. Suddath | 126-195. Laboratory Records Department |
| 104. C. D. Susano | 196. Laboratory Records Department, ORNL R. C. |
| 105. J. A. Swartout | 197-199. Central Research Library |
| 106. E. H. Taylor | |
| 107. D. F. Toner | |

EXTERNAL DISTRIBUTION

- 200-202. W. F. Banks, Allis-Chalmers Mfg. Co.
203-205. P. D. Bush, Kaiser Engineers
206. E. Creutz, General Atomic
207-209. R. B. Duffield, General Atomic
210. D. H. Fax, Westinghouse Atomic Power Division
211. T. Jarvis, Ford Instrument Co.
212. Richard Kirkpatrick, AEC, Washington
213-214. H. Lichtenburger, General Nuclear Engineering Corp.
215. J. P. McGee, Bureau of Mines, Appalachian Experiment Station
216. S. G. Nordlinger, AEC, Washington
217. H. B. Rahner, Savannah River Operations Office
218. Corwin Rickard, General Atomic
219. S. T. Robinson, Sanderson & Porter
220. M. T. Simnad, General Atomic
221. Donald Stewart, AEC, Washington
222. G. W. Tompkin, Mallinckrodt Nuclear Corporation
223. Philip L. Walker, Pennsylvania State University
224. R. E. Watt, Los Alamos Scientific Laboratory
225-226. W. L. Webb, East Central Nuclear Group, Inc.
227. Division of Research and Development, AEC, ORO
228-804. Given distribution as shown in TID-4500 (15th ed.)
under Reactors - Power category (75 copies - OTS)